ELSEVIER

Coordination Chemistry Reviews
178–180 (1998) 1313–1405

COORDINATION CHEMISTRY REVIEWS

Conformations and coordination schemes of carboxylate and carbamoyl derivatives of the tetraazamacrocycles cyclen and cyclam, and the relation to their protonation states

M. Meyer [a], V. Dahaoui-Gindrey [b], Claude Lecomte [b], Roger Guilard [a,*]

[a] *Laboratoire d'Ingénierie Moléculaire pour la Séparation et les Applications des Gaz (LIMSAG), UMR 5633, Université de Bourgogne, Faculté des Sciences, 6 Boulevard Gabriel, 21100 Dijon, France*

[b] *Laboratoire de Cristallographie et Modélisation des Matériaux Minéraux et Biologiques* (LCM^{3}B), *UPRESA 7036, Université Henri Poincaré, Nancy I, Faculté des Sciences, BP 239, 54506 Vandoeuvre-lès-Nancy, France*

Received 8 April 1998; accepted 16 June 1998

Contents

Abstract 1314
1. Introduction 1315
2. Conformational properties of the 12- and 14-membered tetraazamacrocycles 1317
3. 1,4,7,10-Tetraazacyclododecane (cyclen) derivatives 1320
   3.1. Protonation scheme of cyclen 1320
   3.2. Protonation schemes of carboxylate derivatives 1322
   3.3. Metal complexes of monosubstituted carboxylate derivatives 1325
   3.4. Metal complexes of disubstituted carboxylate derivatives 1325
   3.5. Metal complexes of tri- and tetrasubstituted carboxylate derivatives 1327
      3.5.1. Synthesis of the metal complexes 1327
      3.5.2. Structural characteristics of tricarboxylate complexes 1328
      3.5.3. Structural characteristics of DOTA complexes 1336
         3.5.3.1. Six- and seven-coordinated transition metals 1336
         3.5.3.2. Eight-coordinated metals 1339
         3.5.3.3. Nine-coordinated yttrium and lanthanide metals 1340
      3.5.4. Structural characteristics of other tetracarboxylate complexes 1346
   3.6. Tetrasubstituted carbamoylmethyl derivatives 1350
      3.6.1. Primary amides 1350
      3.6.2. Secondary amides 1353
      3.6.3. Tertiary amides 1354
   3.7. Tetrasubstituted 2-carbamoylethyl derivatives 1356
4. 1,4,8,11-Tetraazacyclotetradecane (cyclam) derivatives 1357
   4.1. Protonation scheme of cyclam 1357
   4.2. Monosubstituted carboxylate derivatives 1360

* Corresponding author. Tel.: +33 3 80396111; Fax: +33 3 80396117;
e-mail: roger.guilard@u-bourgogne.fr

0010-8545/98/$ – see front matter © 1998 Elsevier Science S.A. All rights reserved.
PII S0010-8545(98)00169-6

4.3. Disubstituted carboxylate derivatives 1364
4.4. Trisubstituted acetate derivatives 1369
4.5. Tetrasubstituted acetate derivatives 1369
4.5.1. Protonation scheme 1369
4.5.2. Structural characteristics of earth-alkaline-metal complexes 1371
4.5.3. Structural characteristics of transition metal complexes 1372
4.5.4. Structural characteristics of lanthanide metal complexes 1377
4.6. Tetrasubstituted propionate derivatives 1379
4.6.1. Protonation scheme 1379
4.6.2. Structural characteristics of lanthanide metal complexes 1385
4.7. Carbamoyl derivatives 1388
4.7.1. Structural characteristics of disubstituted carbamoyl metal complexes 1389
4.7.2. Tetrasubstituted carbamoyl derivatives 1390
4.7.2.1. Protonation scheme of TETPA 1390
4.7.2.2. Structural characteristics of transition metal complexes 1392
5. The use of molecular electrostatic potentials in predicting the coordination mode 1392
5.1. Molecular modeling and molecular electrostatic potentials 1392
5.2. Cyclen and cyclam 1394
5.3. DOTA and TETA 1395
5.4. TETP 1396
6. Conclusions 1398
Acknowledgments 1398
References 1399

Abstract

This paper discusses and rationalizes the metal coordination pattern of 12- and 14-membered tetraazamacrocyclic carboxylate and carbamoyl ligands based on the cyclen and cyclam framework in light of their acido–basic properties. Structural and protonation data are reviewed in order to illustrate the influence of the free ligand's protonation state and of the pH conditions during the complexation reaction on the final coordination mode of the metallic cations. © 1998 Elsevier Science S.A. All rights reserved.

Keywords: Coordination scheme; Cyclam; Cyclen; Electrostatic potential; Protonation; Tetraazamacrocycles; X-ray crystal structures

List of abbreviations

a.u.	atomic units
α_{twist}	twist angle
BM	Bohr magneton
CN	coordination number
DFT	density functional theory
DMF	dimethylformamide
DMSO	dimethylsulfoxide
DO1A	1-carboxymethyl-1,4,7,10-tetraazacyclododecane

DO2A	1,7-bis(carboxymethyl)-1,4,7,10-tetraazacyclododecane
DO3A	1,4,7-tris(carboxymethyl)-1,4,7,10-tetraazacyclododecane
DOTA	1,4,7,10-tetrakis(carboxymethyl)-1,4,7,10-tetraazacyclododecane
EDDA	*N*,*N*′-ethylenediaminediacetic acid
EDTA	*N*,*N*,*N*′,*N*′-ethylenediaminetetraacetic acid
DO3AHP	1,4,7-tris(carboxymethyl)-10-(2-hydroxypropyl)-1,4,7,10-tetraazacyclododecane
IR	infrared
ISA	inverted-square-antiprismatic
LIS	lanthanide-induced shift
Ln	lanthanide
MEP	molecular electrostatic potential
MM	molecular mechanics
MRI	magnetic resonance imaging
RMS	root mean squares
SA	square-antiprismatic
τ	torsion angle
tet a	*meso*-5,5,7,12,12,14-hexamethyl-1,4,8,11-cyclotetradecane
TETA	1,4,8,11-tetrakis(carboxymethyl)-1,4,8,11-tetraazacyclotetradecane
TETP	1,4,8,11-tetrakis(carboxyethyl)-1,4,8,11-tetraazacyclotetradecane
TETPA	1,4,8,11-tetrakis(2-carbamoylethyl)-1,4,8,11-tetraazacyclotetradecane

1. Introduction

The field of coordination chemistry of polyazamacrocycles (of which the first example was reported as early as 1937 by van Alphen [1]) has undergone spectacular growth since the publication of seminal articles by Curtis [2] and Thompson and Curtis [3] in the early 1960s. Two cyclic tetraamines have played a key role in this field: the 12-membered tetraazacyclododecane and the 14-membered tetraazacyclotetradecane, commonly named cyclen (**1**) and cyclam (**2**), respectively.

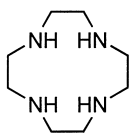

1 cyclen

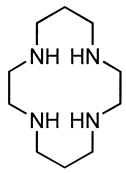

2 cyclam

Efficient synthetic methods for these two easily functionalized ligands [4–13] and the original properties exhibited by their metal complexes have provoked widespread interest in cyclen and cyclam, encompassing medicine [14–17], enzyme mimics [18–22], catalysis (peroxidation [23,24], oxidation [25], epoxidation [26–32], O_2 reduction [33–35], CO_2 reduction [36,37], H_2O_2 reduction [38], NO_3^- and NO_2^- reduction [39–43], inhibition of oxidation [44]), separation and transport of gases [45–55], analytical chemistry [56–60], and extraction of metal cations [56,61–64]. Hence, these cyclic systems behave differently from open-chain analogs.

Furthermore, functionalization of the parent macrocycles has opened new directions in fields ranging from fundamental coordination chemistry to diagnostic and nuclear medicine. These latter ligands are involved in numerous applications as selective complexing agents of transition and heavy metals, lanthanides and actinides

in biomedicine [65–69], hydrometallurgy [70] and waste-water treatment [71]. Of particular importance are the *N*-substituted tri- and tetraacetate cyclen ligands $H_3DO3AHP$ and H_4DOTA.

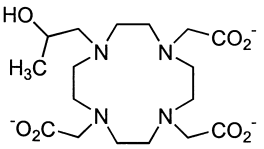

3 $DO3AHP^{3-}$

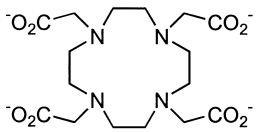

4 $DOTA^{4-}$

$[Gd(DOTA)H_2O]^-$ is one of the most stable and inert gadolinium complexes known today [72,73]. Its *N*-methyl-D-glucamine salt is sold under the trade name DOTAREM® by the French company Guerbet. Since 1989, this pharmaceutical has gained considerable clinical and commercial significance as an efficient contrast agent for magnetic resonance imaging (MRI) [65,66,74,75], in spite of the mild osmotic shocks caused to the patients by intravenous administration of gram amounts of this negatively charged complex. More recently, a neutral triacetic analog, $[Gd(DO3AHP)H_2O]$, has been introduced on the market under the name PROHANCE® by Squibb Co., which circumvents the major drawback of $[Gd(DOTA)H_2O]^-$. Monoclonal antibody conjugates of macrocyclic polyaminocarboxylate complexes have also been used as effective tumor targeting agents in β^- radiotherapy (^{67}Cu, ^{90}Y) or in positron imaging (^{64}Cu, ^{67}Ga, ^{68}Ga, ^{111}In) [67–69].

From a fundamental point of view, a complete understanding of the various factors inherent to the ligands which influence the physicochemical properties of the resultant complexes has not yet been achieved. In particular, structural prediction based on conformational, sterical or electronical parameters is of prime importance for the rational design of new macrocyclic ligands possessing tuned metal affinities, selectivities or formation–dissociation kinetics. The main criteria which determine the stereochemistry and coordination mode of metallic cations by tetraazamacrocycles are: (1) the ring size; (2) the degree of substitution at the *N*-atoms; (3) the electronic and steric properties of the *N*-substituents; (4) the coordination number of the metal cation; (5) the metal-to-ligand ratio and the nature of the salt used in the complexation reaction (i.e. the nature of the counter anion); and (6) the reaction's pH conditions (i.e. protonation state of the free ligand, buffering conditions, etc.). Aspects (1)–(5) have been discussed extensively in the literature [76–78] and will not be covered in the present review. However, recent results have pointed out the role of aspect (6) [79–81]. The aim of this article is to correlate the protonation state and the structure of the free macrocycles with the coordination scheme observed in the corresponding metal complexes, and to explore some of the predictive capabilities of the molecular electrostatic potential (MEP). The following review deals with *N*-substituted carboxylate and carbamoyl derivatives of 12- and 14-membered tetraazamacrocycles. The synthesis of the ligands has been comprehensively reviewed by several authors [79,82–85] and lies beyond the scope of this article. The literature has been covered up to the spring of 1998. As far as possible, the protonation constants reported are taken from the compilation by Martell and Smith [73] and

the ionic radii are those given by Shannon [86]. The atomic coordinates were retrieved from the Cambridge Structural Database, and the program ORTEP [87] was used to generate the molecular structures. Particular attention has been paid to reporting structural parameters. When inconsistencies with the original literature have been noticed, the data indicated were calculated from the positional parameters deposited with the Cambridge Crystallographic Data Centre, 12 Union Road, Cambridge, UK.

2. Conformational properties of the 12- and 14-membered tetraazamacrocycles

The conformation of macrocyclic alkanes can conveniently be described by Dale's nomenclature [88–90] based on the torsion-angle sequences between the *anti* and *gauche* bonds. The conformation is designated by a series of numbers, each digit representing the number of chemical bonds between two consecutive "genuine corners". The central atom of an *anti–gauche–gauche–anti* ($ag^{\pm}g^{\pm}a$) bond sequence defines a "genuine corner" when both consecutive *gauche* torsion angles are of the same sign, or as a "pseudocorner" when they are of opposite sign, as shown below (pseudocorners are marked in bold):

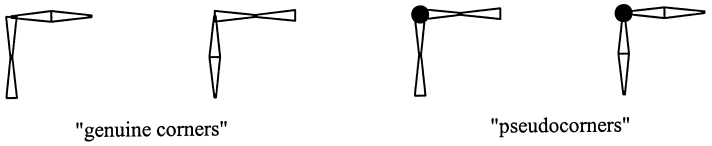

A positive value of the torsion angle is assigned to a *gauche* bond if the rear bond is rotated clockwise with respect to the front bond when looking along the bond axis [91]. The starting point and direction followed around the ring are chosen so as to give the smallest number. Two successive *gauche* torsion angles of same sign allow an efficient bending of the chain and both sets of 1,4-hydrogen atoms essentially do not interact. When the torsion angles are of opposite sign, their absolute values are higher than those found for a "genuine corner" due to larger steric interactions. Other bond arrangements are less favorable for ring closure. Macrocycles smaller than cyclooctadecane cannot accommodate an isolated *gauche* bond (i.e. an *anti–gauche–anti* sequence) because of the small chain-bending induced by this arrangement. A sequence of three or more *gauche* bonds of equal sign generates a helix, whereas a sequence of more than two *gauche* bonds of alternating sign leads to severe steric 1,6-interactions. However, a sequence of four *gauche* bonds, such as two are of equal sign and are followed by two of equal but opposite sign, is encountered in strained ring conformations. Indeed, the strain due to the 1,5- and 1,7-steric interactions is sufficiently relieved in medium-sized cycles by a systematic deviation of the dihedral angles from $\pm 60^{\circ}$. Cyclododecane, cyclotetradecane, and the related crown ethers are helpful models to aid understanding of the stereochemistry inherent to free or metal-bonded cyclen and cyclam derivatives. However, for macrocycles containing heteroatoms the nomenclature is ambiguous, and conformers

which possess the same torsion angle sequences but which differ by the position of the heteroatoms, have to be distinguished. Some conformations of the 12- and 14-membered scaffolds are depicted in Fig. 1, where the pseudocorners are marked in bold.

For cyclododecane, several force-field calculations have shown that the D_4 symmetric (3,3,3,3) conformation is the less strained, although it is not of the diamond lattice type, and that distortions which lower the symmetry to D_2 are barely significant [88,92–96]. Each vertex corresponds to a "genuine corner" and all *anti* torsion angles are located along the sides. All hydrogen atoms belonging to the ethylenediamine groups are staggered. Thus, the four five-membered chelate rings of the cyclododecane scaffold are constrained to adopt the same skew conformation as well as the same configuration in order to avoid steric interactions, leading to a pair of enantiomers denoted (λ,λ,λ,λ) and (δ,δ,δ,δ) according to Corey's nomenclature [97]. The next three conformations in order of increasing total strain energy are the (2,3,3,4), the (2,3,4,3) and the (2,4,2,4) of C_1, C_s and C_2 symmetry, respectively [88,96]. In agreement with the computational studies, cyclododecane adopts the (3,3,3,3) square conformation in the crystalline and liquid state [98,99] as well as in solution [100]. The same ring conformation has also been found in 1-hydroxydodecyldimethylphosphonate [101], 2,12-dibromocyclododecanone [102], *trans*-13,13-dimethyl-13-azoniabicyclo[10.1.0]tridecane iodide [103], azacyclododecane hydrochloride [104] and 2,5,8,11-tetraethyl-1,4,7,10-tetraazacyclododecane [105]. Conformational studies of crown ethers [90] have shown that crystalline 1,4,7,10-tetraoxacyclododecane adopts a centrosymmetric biangular (6,6)-B conformation containing only two "genuine corners" located *trans* to each other, while the two other vertices are "pseudocorners" [106,107]. Below $-160\,^{\circ}C$, IR and NMR spectroscopic studies carried out in freon solutions revealed a slow exchange equilibrium between the biangular (6,6)-B and the square (3,3,3,3)-B conformations [108,109]. The latter ring conformation predominates for metal-coordinated macrocycles with the oxygen atoms in a square-planar arrangement [110], as in the alkaline and earth–alkaline metal complexes [111,112]. Early molecular mechanics calculations have shown that the (6,6)-B arrangement is $7.5\,kJ\,mol^{-1}$ higher in energy compared with the (3,3,3,3)-B conformation [113]. Recently, the potential due to the lone pairs on the oxygen atoms has been included in the force field, and energy differences of less than $5\,kJ\,mol^{-1}$ were calculated between the (3,3,3,3)-B, (6,6)-B and (4,8) conformers of 1,4,7,10-tetraoxacyclododecane [110].

For cyclotetradecane, the diamond-lattice type quadrangular (3,4,3,4) conformation has been reported both in the solid state [114,115] and in solution [100], in agreement with the lowest calculated strain energy, which follows the order (3,3,3,3)<(3,3,4,4)<(3,3,3,5)<(2,4,4,4) [88,89,116]. The 14-membered rings of 1,8,-diazacyclotetradecane dihydrobromide [117], and 1,8-bis(hydroxy)-1,8,-diazacyclotetradecane [118] also adopt a (3,4,3,4) conformation in the crystalline state. Force-field calculations carried out on 1,4,8,11-tetraoxacyclotetradecane indicate that the biangular (7,7)-C conformation is stabilized with respect to the quadrangular (3,4,3,4)-C conformation by $2.55\,kJ\,mol^{-1}$ [113]. In spite of higher torsional strain about the C–O bonds at the "pseudocorners", the (7,7)-C arrangement gives rise to a lower angular strain than the (3,4,3,4)-C conformation, and reduces the repulsive

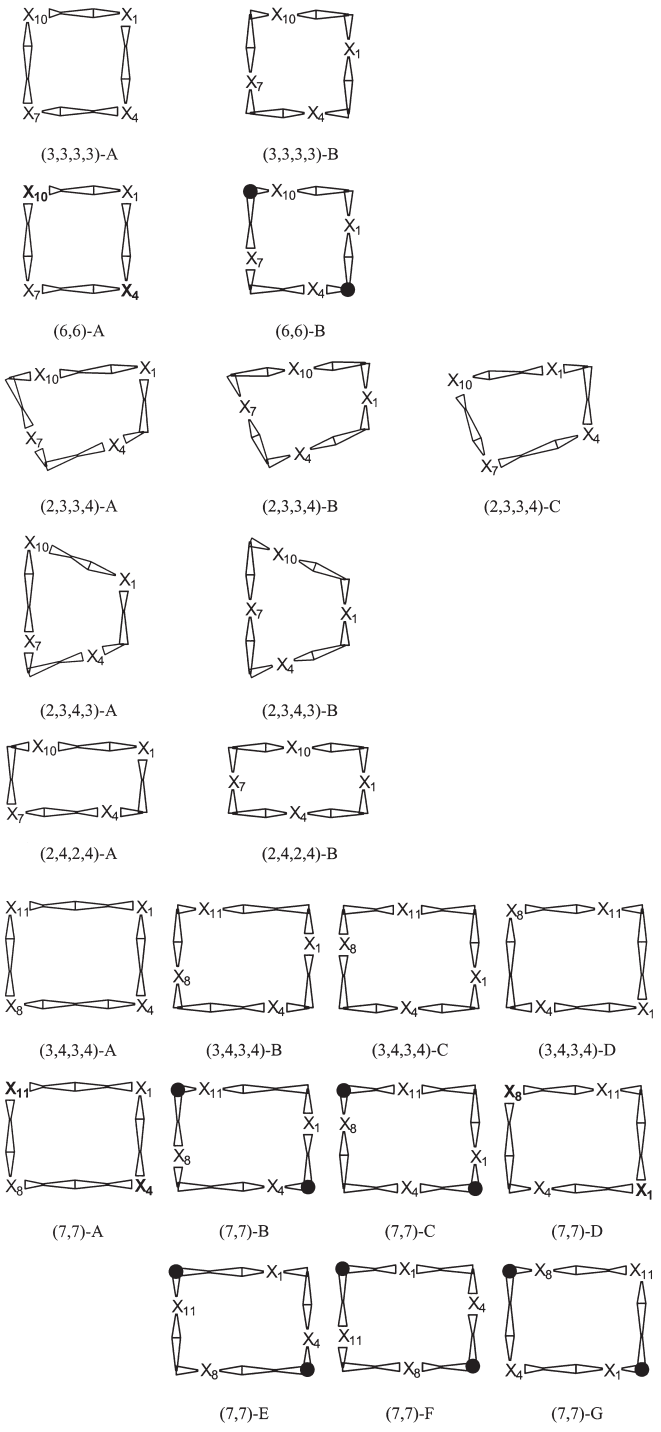

Fig. 1. Wedge-type representation of some possible conformations of 12- and 14-membered macrocycles containing four identical heteroatoms following Dale's conventions [88,89]. ''Pseudocorners'' are marked in bold or visualized by a black dot. The unmarked corners correspond to ''genuine corners''. The indices indicate the atoms' positions along the cycle.

transannular non-bonded *gauche* CH···CH interactions at both "pseudocorners". The low energy barrier allows facile interconversion between both conformers, giving rise to limited atomic displacements. The biangular (7,7)-C conformation has been observed in the solid state [119], and in CS_2 and CCl_4 solutions [120]. However, in the polar $CHCl_2F$ solvent, the quadrangular conformation becomes increasingly populated as the temperature is lowered [120]. In addition, anangular conformations with four pseudocorners are common in the cyclam series. This contrasts with the behavior of 12-membered macrocycles for which high torsional strain and short ($\sim$2.0 Å) exo CH···HC contacts are expected [110].

A nomenclature describing metal-ion cyclam complexes in an octahedral coordination scheme has been proposed by Bosnich et al. [5]. Relying on the N–H bond direction relative to the four nitrogen atom plane, five energetically distinct nonenantiomeric *cis* and *trans* isomers are conceptually possible, since each coordinated nitrogen atom is chiral. The five forms, commonly denoted I–V or alternatively by the chirality of the four nitrogen atoms according to the (R,S)-nomenclature are represented in Fig. 2. This stereochemical description, initially proposed for cyclam-containing complexes, can also be applied to the metal-free ligands and extended to cyclen. However, the four nitrogen atoms are achiral as a result of the four-fold symmetry of the 12-membered skeleton, and obviously conformers III and IV become identical (Fig. 2).

3. 1,4,7,10-tetraazacyclododecane (cyclen) derivatives

3.1. Protonation scheme of cyclen

The X-ray structures of cyclen.$3H_2O$ and of $[H_4cyclen]Cl_4$ (Fig. 3) have been reported by Reibenspies et al. [121,122]. In both structures, the 12-membered rings

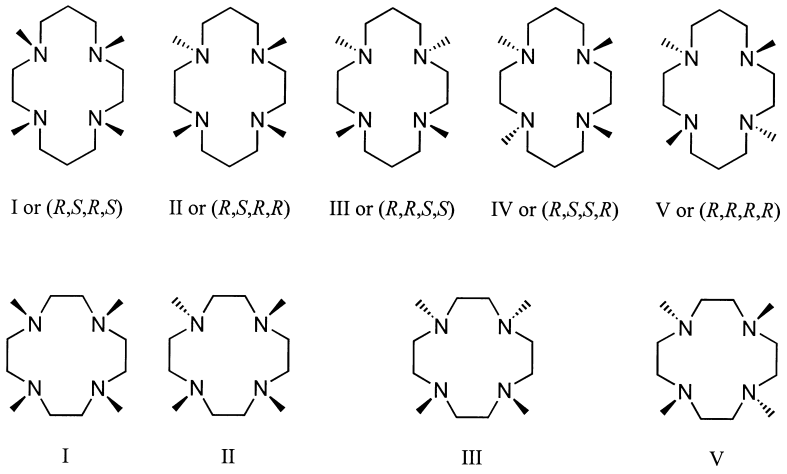

Fig. 2. Schematic representation of the possible configurations of cyclam and cyclen according to Bosnich's nomenclature [5]. The chirality of one enantiomer only is indicated.

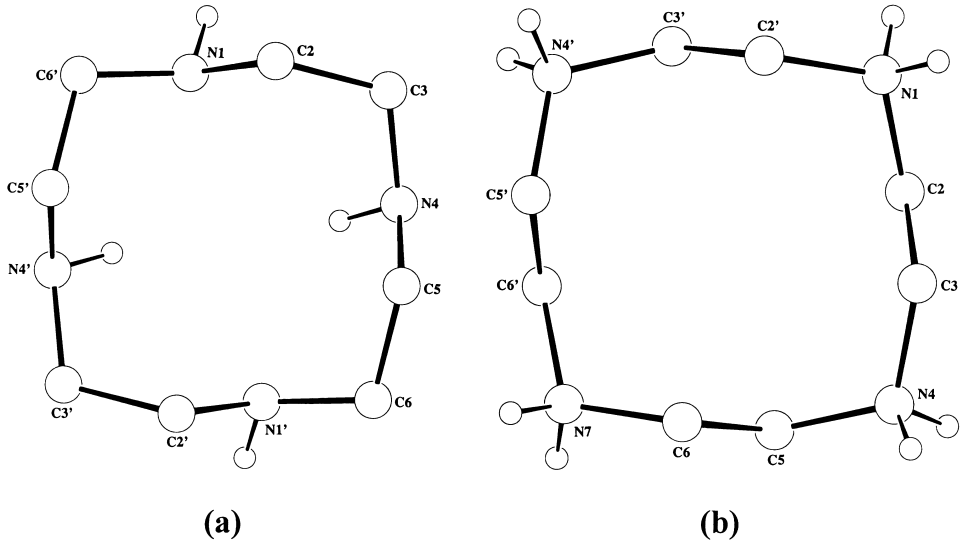

Fig. 3. Molecular views of (a) deprotonated cyclen [121] and (b) tetra-protonated cyclen [122].

are folded in a (3,3,3,3) conformation, but differ in the distribution of the nitrogen atoms with respect to the side and corner positions. For the neutral molecule, the corners are occupied by carbon atoms [(3,3,3,3)-B conformation], with an average C–N distance of 1.464(3) Å, and each nitrogen atom is hydrogen-bonded to a water molecule. The protons linked to N1 and N1′[1] are directed away from the center of the cycle, while those bound to N4 and N4′ point inside the cavity. In the tetra-protonated state, the four nitrogen atoms are located on the corners of the square giving rise to a (3,3,3,3)-A conformation with a torsion-angle sequence of −71.5(1), 159.1(2), −65.0(2), −63.3(2), 157.6(2), and −72.0(1)° for τ_1–τ_6, respectively. As expected, the average C–N bond length is significantly longer [1.497(3) Å].

Cyclen, and more generally all tetraazamacrocycles, exhibit high basicity in the first two protonation steps and rather low basicity in the last two steps. The critical protonation constants ($\log K^{H}$) for cyclen are reported in Table 1. The significantly higher difference between $\log K_1^{H}$ and $\log K_2^{H}$ compared with the value calculated for a statistical separation of two protonation constants ($\log 4 = 0.60$) [135] reflects electrostatic repulsion between the protonated sites. In order to minimize this repulsion, protonation occurs on *trans*-located nitrogen atoms. The cyclic nature of the ligand induces a dramatic increase in the electrostatic repulsion energy once the second site is protonated, leading to a decrease of about eight orders of magnitude between $\log K_2^{H}$ and $\log K_3^{H}$. This behavior differs markedly from that of open-chain tetraamines [73]: in the noncyclic series, the difference between two consecutive protonation constants is approximately constant, since the flexibility of the chain

[1] The suffix ′ of N1′ indicates that this atom is related to N1 by a crystallographic inversion center, a two-fold axis or a mirror plane. Such a notation is systematically used in the review.

Table 1
Protonation constants for various tetraazmacrocycles

Ligand	Cond.	log K_1^H	log K_2^H	log K_3^H	log K_4^H	log K_5^H	log K_6^H	Ref.
Cyclen	[a]	10.6	9.6	1.5	0.5			[73]
$DO2A^{2-}$	[b]	11.45(2)	9.54(3)	4.00(2)	2.36(3)	<2.3		[123]
$DO2A^{2-}$	[c]	11.38	9.62	3.95	2.62			[124]
$DO3A^{3-}$	[c]	11.59(3)	9.24(3)	4.43(7)	3.48(1)			[125]
$DO3A^{3-}$	[d]	11.96	9.66(2)	4.23(1)	3.51			[126]
$DO3A^{3-}$	[c]	10.72(3)	9.51(3)	4.40(8)				[127]
9	[c]	13.42	9.15	5.30	4.07			[128]
10	[e]	11.91	9.04	4.55				[129]
$DO3AHP^{3-}$	[c]	11.96(2)	9.43(1)	4.30(4)	3.26(1)			[125]
$DO3AHP^{3-}$	[c]	10.89(3)	9.79(3)	4.29(8)				[127]
11	[c]	11.75(5)	9.23(3)	4.13(3)	2.97(4)			[130]
$DOTA^{4-}$	[c]	12.09	9.69	4.54	4.36	1.9(1)[f]	1.7(1)[f]	[73]
$DOTA^{4-}$	[c]	12.6(1)	9.70(1)	4.50(1)	4.14(1)	2.32(1)		[131]
18	[d]	11.81(2)	9.42(7)	4.39(7)	3.43(7)	2.66(8)	<2.5	[132]
Cyclam	[g]	11.29(2)	10.19(1)	1.61(1)	1.91(1)			[133]
$TETA^{4-}$	[c]	10.85(4)	10.13(4)	4.11(4)	3.27(8)	2.17[f]		[73]
$TETP^{4-}$	[g]	>10.8	10.65(2)	4.33(2)	3.60(3)	3.06(4)	2.28(4)	[81]

[a] $I=0.1$, $T=25$ °C.
[b] $I=0.1$ $N(C_2H_5)_4ClO_4$, $T=25$ °C.
[c] $I=0.1$ $N(CH_3)_4Cl$, $T=25$ °C.
[d] $I=0.5$ KNO_3, $T=25$ °C.
[e] $I=0.1$ $N(CH_3)_4NO_3$, $T=25$ °C.
[f] $I=1$ NaCl, $T=25$ °C [134].
[g] $I=0.1$ KCl, $T=25$ °C.

minimizes the electrostatic repulsion between the positively charged nitrogen atoms. The solvation structure of neutral cyclen in aqueous solution has been studied by means of ab initio calculations using the Monte Carlo method [136]: two water molecules are bound to the macrocycle, one above and the other below the ligand plane, while one OH bond is directed towards the cavity. This system is solvated by an average of six additional water molecules in the first hydration shell. The favorable enthalpic and entropic contributions of the solvation term to the overall free energy of complexation account for the so-called "macrocyclic effect".

3.2. Protonation schemes of carboxylate derivatives

Little structural data on free carboxylic cyclen derivatives have been published: Fig. 4 shows the crystal structure of the dihydrate $H_3DO3A.H_2SO_4$ salt [125]. The penta-protonated macrocycle adopts a (3,3,3,3)-B conformation. The secondary nitrogen atom and the *trans*-annular tertiary amine are protonated. The three remaining protons are attached to the three carboxylic pendant arms which are bent over the macrocycle, the carbonyl oxygen atoms being directed towards the cavity. The protons on atoms N4 and N10 point towards the center of the ligand, giving rise to two intramolecular four-center hydrogen bonds: the first concerns the N4–H

donor group and the N1, N7, and O1 acceptors, while the second deals with the N10–H group and the N1, N7, and O5 acceptors. This unusual type of hydrogen bond requires that the three D–H···A angles are greater than 90° [137].

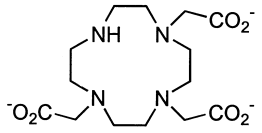

5 $DO3A^{3-}$

No form of the free DOTA ligand has been characterized by X-ray diffraction. The available structural data were gained by IR spectroscopy for H_4DOTA.2HCl, which exhibits in the solid state a typical $\nu_{C=O}$ stretch for COOH groups at 1720 cm^{-1} and a NH^+/OH intercombination band at 2550 cm^{-1} [80]. Thus, it was inferred that all four carboxylic groups and two tertiary amines are protonated.

In solution, the protonation scheme has been elucidated by potentiometry and ^{1}H NMR spectroscopy. The first method provides accurate values of the macroscopic stepwise protonation constants. The selected values reported in Table 1 relate to measurements carried out in the presence of tetraalkylammoniun salts as the background electrolyte. The well-known binding affinity of the polyaminocarboxylates for sodium, and to a lesser extent, potassium, induces lower protonation constants when the ionic strength is adjusted with an alkali salt. This competition effect is particularly pronounced for the first protonation equilibrium [131]. The second technique, NMR spectroscopy, helps to unravel the microscopic protonation scheme

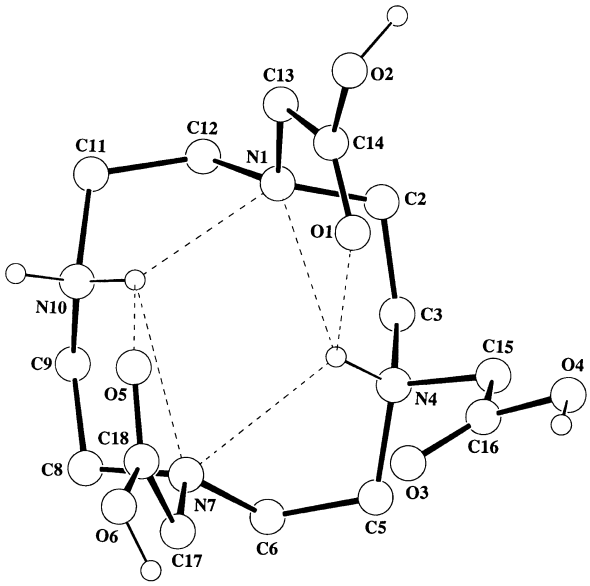

Fig. 4. Molecular view of H_3DO3A [125]. Intramolecular hydrogen bonds are indicated by dashed lines.

by taking advantage of the significant shift in the methylenic proton resonances induced by the protonation of the adjacent nitrogen atoms [134,138].

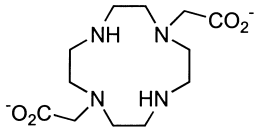

6 $DO2A^{2-}$

The first two protonation constants for the various *N*-substituted carboxylic derivatives (Table 1) are assigned to the protonation of two *trans*-located amino groups, as found for cyclen. For mono-, di- and trifunctionalized ligands, the question is to determine whether the first protonation occurs on a secondary or on a tertiary nitrogen site. ^{1}H NMR measurements for $DO2A^{2-}$ [124] indicates unambiguously the exclusive *trans*-annular protonation of the secondary nitrogen atoms despite the ability of acetate groups to enhance the basicity of tertiary amines through hydrogen bonding [134,139]. For $DO3A^{3-}$, the first protonation also occurs on the secondary amine [126]. These results are supported by a crystallographic study of H_5DO3A^{2-} [125] and by the higher $\log K_2^H$ value for $DO2A^{2-}$ compared with those of $DO3A^{3-}$ and $DOTA^{4-}$, where the second protonation occurs on a tertiary nitrogen atom. The two following constants, $\log K_3^H$ and $\log K_4^H$, which are related to the protonation of both carboxylate functions attached to both unprotonated nitrogen atoms, are thus markedly higher than the third and fourth protonation constants of cyclen. The absence of a positive charge on the two remaining nitrogen atoms accounts for the similarity between $\log K_3^H$ (and $\log K_4^H$ in the case of $DOTA^{4-}$) values and the pK_a of acetic acid, whereas the carboxylate groups in EDTA exhibit a more acidic character. Variable-temperature ^{1}H NMR spectra of $H_nDO2A^{(2-n)-}$ reveal that the cyclododecane scaffold is locked into a rigid conformation at room temperature, probably as a result of hydrogen bonds within the ring, while both acetate arms remain conformationally mobile in H_2DO2A, but become rigid in H_3DO2A^+ and H_4DO2A^{2+} [124]. These experimental features, also documented for other asymmetric macrocycles [139], may support the suggestion by Weeks et al. [123] of the formation of an intramolecular handle-like $O^-\cdots H–O$ hydrogen bond between the *trans*-carboxylate moieties for H_3DO2A^+ and H_4DO2A^{2+}. Such a rigidity has not been observed for DOTA. Referring to the X-ray structure of EDTA [140], Desreux et al. [134] tentatively proposed that both unprotonated carboxylate arms in H_4DOTA might be folded and hydrogen-bonded to the protonated amines, giving rise to two sets of protonation constants. Further support for this cyclic arrangement of the deprotonated acetate groups is provided by the kinetic studies of Kasprzyk and Wilkins [141]. These authors found that the di-protonated H_2DOTA^{2-} form was 4–5 orders of magnitude less reactive than the mono-protonated $HDOTA^{3-}$ species. The following two constants, $\log K_5^H$ (and $\log K_6^H$ for $DOTA^{4-}$) are associated with the protonation of the remaining carboxylate moieties. Since these groups are bonded to protonated nitrogen atoms, $DOTA^{4-}$ exhibits fairly low $\log K_5^H$ and $\log K_6^H$ values, similar to those of EDTA.

Independently of the number of appended carboxylate arms, two nitrogen atoms remain unprotonated even at very low pH.

3.3. Metal complexes of monosubstituted carboxylate derivatives

The copper(II) center in [Cu(DO1A)]Cl, obtained under acidic conditions (pH < 4), is penta-coordinated by the four nitrogen atoms and by a Cl^- anion in a square-pyramidal geometry [142]. The Cu^{2+} ion is located 0.539 Å away from the four nitrogen-atom plane towards Cl^- [Cu–Cl = 2.387(5) Å]. The single carboxylic arm is protonated and does not participate to the copper coordination.

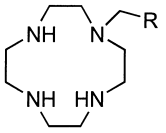

7 DO1A$^-$ R = $-CO_2^-$ [142]

8 [143]

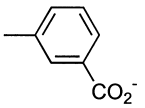

For steric reasons, attachment of the carboxyl group at the *meta* position of a pendant benzyl moiety in ligand **8** also prevents the intramolecular coordination of the fifth chelate ring. However, crystallization from water of the cobalt(III) complex affords a dimer of the general formula $[Co(\mathbf{8})H_2O]_2(C1O4)_4.6H_2O$, where the pendant *m*-toluate group of one ligand is bound to the metal center of an adjacent macrocyclic unit, and vice versa [143]. The crystal contains two independent but essentially identical dimers, each possessing a crystallographic two-fold symmetry (Fig. 5). Each Co^{3+} ion has a distorted octahedral *cis*-II environment made up of the four ring nitrogen atoms, one water molecule, and one carboxylate oxygen atom belonging to the other half of the dimer [Co–W = 1.975(8) and 1.982(8) Å; Co–O = 1.905(8) and 1.899(7) Å in units I and II, respectively]. The distortion is reflected by significant variations in the Co–N bond distances: the longest bond involves the nitrogen atom carrying the side chain [Co–N1 = 2.032(9) and 2.042(9) Å, followed by Co–N7 = 1.96(1) and 1.97(1) Å, Co–N10 = 1.94(1) and 1.93(1) Å, and Co–N4 = 1.914(9) and 1.907(9) Å in units I and II, respectively]. Similarly, the dihedral angles of the four ethylenediamine chelate rings lie between the ideal values for the eclipsed and *gauche* conformations. The chiralities of both rings adjacent to the appended toluate group are λ, while the other two are δ [(2,4,2,4)-B conformation], as in cyclen cobalt(III) [144–146].

3.4. Metal complexes of disubstituted carboxylate derivatives

Glass electrode measurements in an aqueous medium revealed that DO2A generally binds first-raw transition metals either as a penta- or as a hexadentate ligand

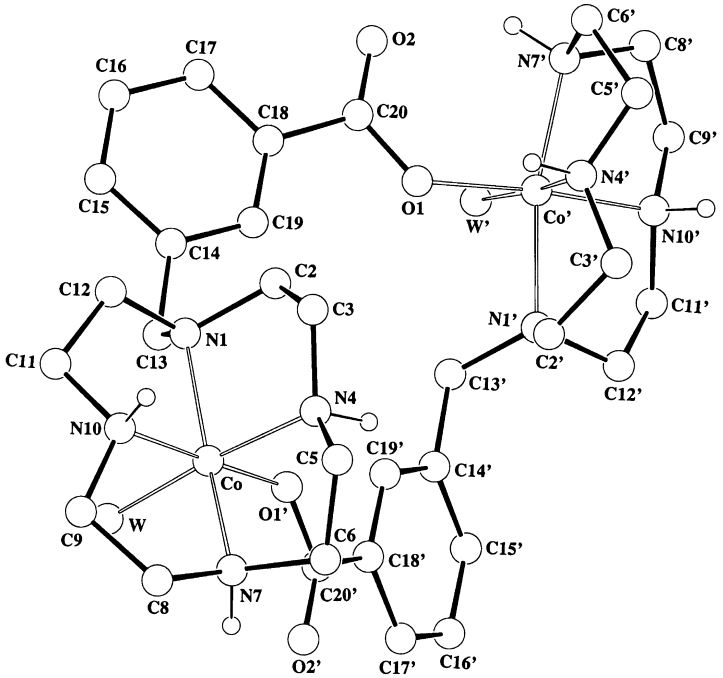

Fig. 5. Molecular view of one of the two dimeric $[Co(\mathbf{8})H_2O]_2^{4+}$ cations [143].

[123,124]. The stabilities of the corresponding complexes are intermediate between those measured for cyclen and DOTA. Currently, only two hexa-coordinated compounds have been characterized. Weeks et al. [123] prepared the nickel(II) complex of DO2A by mixing equimolar amounts of an ethanolic solution of $NiClO_4$ with $H_2DO2A.2H_2O$ dissolved in boiling water without controlling the pH. Recrystallization of the purple precipitate from water yields a dimeric complex, $[Ni(DO2A)].0.5HClO_4.1.5H_2O$ (Fig. 6). Both DO2A units of the dimer are related to each other by a nearly symmetrical hydrogen bond between two uncoordinated carboxylate oxygen atoms. The hydrogen atom is located along the O4A···O4B interatomic axis at equal distances [1.22(4) Å] of the oxygen atoms. As expected for this type of hydrogen bond, the O···O intermolecular contact is very short [2.448(4) Å] (for similar O···O intermolecular contacts, see Section 4.6.1). Consequently, the [Ni(DO2A)] complex is half-protonated here. The hexadentate ligand binds nickel(II) in a distorted *cis*-octahedral fashion of approximate C_{2v} symmetry. The macrocycle is folded along the axis defined by the N4–N10 atoms corresponding to unsubstituted amines, and adopts a *cis*-I (2,4,2,4)-B conformation with all donating groups directed towards the same side. The Ni–N bond lengths range between 2.113(3) and 2.144(3) Å and the equatorial Ni–O bonds between 2.019(2) and 2.068(2) Å. The strongest distortion from the octahedral coordination appears for the axial N4–Ni–N10 [155.4(4)° on average for the two half units] and

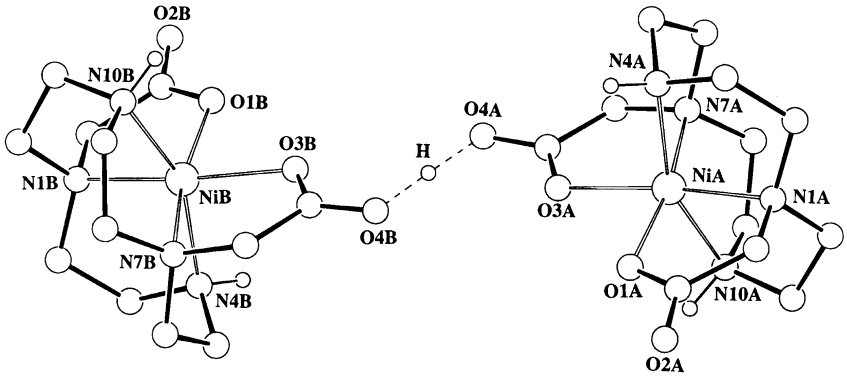

Fig. 6. Molecular view of the $[Ni_2(DO2A)(HDO2A)]^+$ dimer [123]. Intermolecular hydrogen bonds are indicated by dashed lines.

for the equatorial N1–Ni–N7 [109.4(1)°] angles, while the equatorial O1–Ni–O3 [86.5(1)°] angles deviate less severely from the ideal value of 90°.

Following the same synthetic route, the analog zinc(II) complex [Zn(DO2A)]. $1.5HClO_4.2H_2O$ has been prepared [123]. From ^{13}C NMR studies in neutral D_2O, it was concluded that [Zn(DO2A)] also has a time-averaged C_{2v} symmetric *cis*-octahedral structure. In order to ensure fast formation kinetics, mononuclear magnesium, calcium and lanthanide (La^{3+}, Gd^{3+}, Dy^{3+}, Yb^{3+} and Lu^{3+}) complexes have been formed in situ at pH values above 9, and characterized in aqueous solution by potentiometric, NMR and relaxometric techniques [124]. The results agree with an octacoordination of the metal ion by the hexadentate ligand and by two water molecules, as shown for Gd^{3+} and Dy^{3+}. Both enantiomeric (λ,λ,λ,λ) and (δ,δ,δ,δ) square (3,3,3,3) conformations of the cyclen skeleton are involved in a fast interconversion process on the NMR timescale, inducing the chirality change of the four ethylenediamine chelate rings. At room temperature, line broadening of the magnetically inequivalent methylenic ring proton resonances suggests a slower dynamic process. The acetate substituents rearrange quickly and independently of each other as a consequence of limited steric crowding.

3.5. Metal complexes of tri- and tetrasubstituted carboxylate derivatives

3.5.1. Synthesis of the metal complexes

Metal complexes formed with tri- and tetracarboxylate derivatives of cyclen are readily prepared by reacting stoichiometric amounts of the ligand dissolved in water with the corresponding halide, oxide or freshly precipitated hydroxide metal salt (Table 2) [153]. The use of freshly precipitated $Fe(OH)_3$ in the preparation of the Fe(III) complexes is recommended because it circumvents the problems encountered with other iron(III) sources, like the formation of highly insoluble hydrated ferric oxides as the pH is raised during reaction or work-up [148]. Lanthanide oxide

Table 2
Relevant experimental conditions for the synthesis of DO3A and DOTA metal complexes

Compound	Metal salt	pH	Predominant species	Ref.
[Cu(HDO3A)]	$Cu(CH_3CO_2)_2$	4	H_3DO_3A	[147]
[Fe(DO3A)]	$Fe(OH)_3$	?		[148]
[In(DO3A)]	In^{3+}	4		[149]
[Gd(DO3A)]	Gd_2O_3	3.5–7.2		[148]
[Gd(**9**)]	Gd_2O_3	8.0	$H_2\mathbf{9}^-/H_3\mathbf{9}$	[128]
Ca[Ca(DO3AHP)]$_2$	$CaCO_3$	7.95	$H_2DO3AHP^-/H_3DO3AHP$	[147]
Ca[Ni(DOTA)]	$NiCl_2$	10	$HDOTA^{3-}/H_2DOTA^{2-}$	[80]
Ca[Cu(DOTA)]	$CuSO_4$	10	$HDOTA^{3-}/H_2DOTA^{2-}$	[80]
[Ni(H_2DOTA)]	$NiCl_2$	2.5	H_4DOTA	[80]
[Cu(H_2DOTA)]	$CuSO_4$	2.5	H_4DOTA	[80]
[Zn(H_2DOTA)]	$ZnCl_2$	2.5	H_4DOTA	[150]
[Cu(H_3**18**)]ClO_4	$Cu(ClO_4)_2$	3–4	$H_3\mathbf{18}^-/H_4\mathbf{18}$	[132]
Na[Fe(DOTA)]	$Fe(OH)_3$	9 (NaOH)	$HDOTA^{3-}/H_2DOTA^{2-}$	[148]
$Ca(OH_2)_3$[Ca(DOTA)]	$Ca(OH)_2$	?	H_4DOTA	[151]
Na[Ln(DOTA)]	$LnCl_3$	7	H_2DOTA^{2-}	[152]
Na[Y(DOTA)]	$Y(OH)_3$	?	H_4DOTA	[148]

(Ln_2O_3) slurries offer similar advantages when mixed with the free ligand dissolved in water. The reaction mixture is usually heated at $\sim$80 °C for several days until total consumption of the metal hydroxide or oxide because the formation kinetics of most DO3A and DOTA complexes is slow: this is especially the case for the lanthanide complexes [154–157]. As shown in Table 2, the pH conditions during synthesis do not seem to constitute a major factor in determining the final stoichiometry. As a general guideline, seven- or higher-coordinated metal complexes of DO3A or DOTA are readily obtained for a pH range where partially deprotonated forms of the ligand predominate. However, the pH strongly influences the formation kinetics of the complexes and plays an important role in tuning the solubility of the ligand. Hence, in many experimental procedures the neutral H_4DOTA ligand is partially deprotonated prior to the complexation reaction by the addition of one equivalent of base to form H_3DOTA^-, or by controlling the pH to values above 6–7, where the di-protonated species predominates. Crystals suitable for X-ray diffraction studies are generally obtained by slow evaporation of a concentrated aqueous solution of the complex.

3.5.2. Structural characteristics of tricarboxylate complexes

Spurred by the breakthrough of magnetic resonance imaging and the need for low osmolar contrast agents, tricarboxymethyl cyclen derivatives have gained increasing clinical significance since they form neutral gadolinium(III) complexes which cause less pain on injection than the anionic tetraacetate pharmaceuticals. In order to increase their thermodynamic stability and to enhance their hydrophilicity, neutral coordinating hydroxyl groups have been introduced on the fourth nitrogen atom ($DO3AHP^{3-}$ and **11**). Tweedle et al. [158,159] pioneered the coordination

chemistry related to this family of ligands. Currently, a dozen crystal structures have been described in the literature.

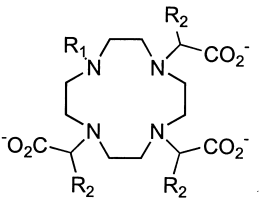

		R_1	R_2
5	$DO3A^{3-}$	-H	-H
9		-H	$-CH_3$
10		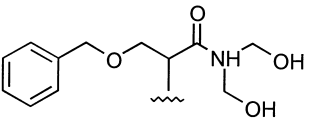	-H
3	$DO3AHP^{3-}$	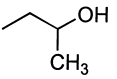	-H
11		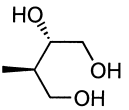	-H

The neutral [Cu(HDO3A)] complex (Fig. 7) was obtained at pH ≈ 4, where H_3DO3A represents the dominant form of the ligand [147]. Among the few structurally characterized transition-metal complexes of tricarboxylate ligands, [Cu(HDO3A)] represents a rare example where the macrocycle adopts a (2,3,3,4)-B rather than the (2,4,2,4) conformation which is found in the C_{2v} symmetric divalent copper, nickel, and zinc complexes of $DOTA^{4-}$ (vide infra). It should be noted that both (2,3,3,4) and (2,4,2,4) ring conformations correspond to the same *cis*-I configuration of the nitrogen atoms. A similar (2,3,3,4) conformation has been observed in the free 1,4,7,10-tetraazacyclododecane-1,4,7,10-tetrakis(methylene phosphonic acid) ligand [160], and in the penta-coordinated copper(II) complexes of 1,4,7,10-tetrabenzyl-2,5,8,11-tetraethyl-1,4,7,10-tetraazacyclododecane [161] and 12,17-dimethyl-1,5,9,17,17-pentaazabicyclo[7.5.5]nonadecane [162]. In [Cu(HDO3A)], one of the three carboxyl groups is protonated and uncoordinated: the metal center is pseudo-octahedrally bound to three nitrogen atoms [Cu–N4 = 2.391(3) Å, Cu–N7 = 2.590(4) Å and Cu–N10 = 2.183(4) Å] and to one oxygen atom [from the acetate group appended to N1, Cu–O1 = 2.077(4) Å] in the equatorial plane. The N1 atom and the O5 atom which belongs to the acetate group appended to N7 occupy the axial positions [Cu–N1 = 2.028(4) Å, and Cu–O5 = 1.923(4) Å and N1–Cu–O5 = 165.7(2)°]. The severe distortion from an octahedral geometry

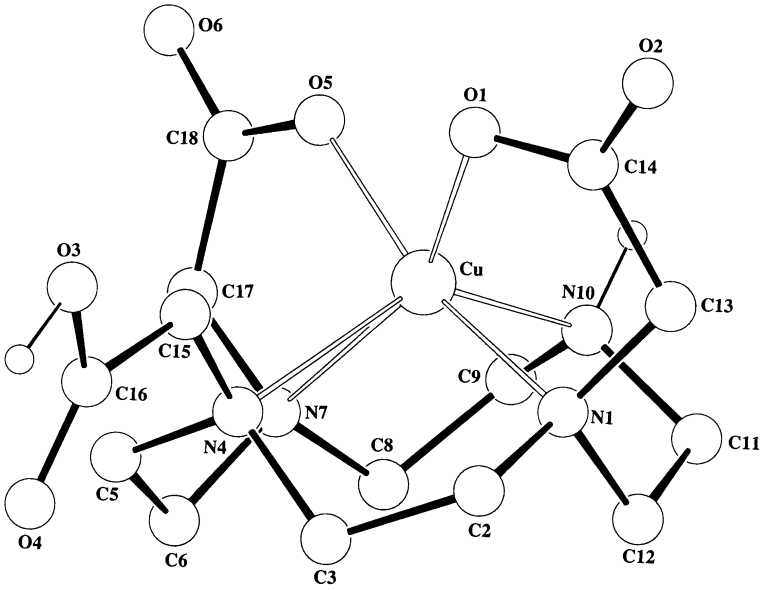

Fig. 7. Molecular view of [Cu(HDO3A)] [147].

is also reflected by the large deviation from the ideal values of the equatorial angles N7–Cu–O1 [158.1(1)°] and N10–Cu–O1 [120.2(1)°]. The single protonated carboxylate chain on N4 points away from the copper atom, as in [Cu(H_2DOTA)] (vide infra).

The neutral hepta-coordinated [Fe(DO3A)].3H_2O [148] and [In(DO3A)] .3H_2O.CH_3OH [149] complexes show a similar face-capped trigonal–prismatic molecular structure, depicted in Fig. 8 for the iron complex. All four nitrogen and three carboxylate oxygen atoms are coordinated to the metal center. Two nitrogen and one oxygen atom lie on the corners of the trigonal faces, while O1 is capping the prism. For the tertiary nitrogen atoms, the average Fe–N and In–N distances are 2.32(5) and 2.37(3) Å, respectively, whereas the secondary nitrogen atom gives rise to a shorter M–N distance (2.190(4) for [Fe(DO3A)] and 2.314(8) Å for [In(DO3A)]). The metal–oxygen bonds are, as expected, shorter, and average 2.02(3) Å in [Fe(DO3A)] and 2.18(2) Å in [In(DO3A)]. The macrocycle has a (3,3,3,3)-B conformation with the acetate moieties located on the same side of the plane passing through the four nitrogen atoms [(R,S,R,S) or type-I configuration].

Although [Gd(DO3A)H_2O] is readily prepared from Gd_2O_3 in an unbuffered solution following the general procedure outlined above, X-ray quality single crystals are difficult to obtain: this requires the presence of methanol and sodium carbonate in a 1:3 ratio with the complex [148]. The asymmetric unit contains a nearly C_3-symmetric trimer of three crystallographically independent but highly similar [Gd(DO3A)] molecules, one Na_2CO_3, and 17 water molecules (Fig. 9). Each gadoli-

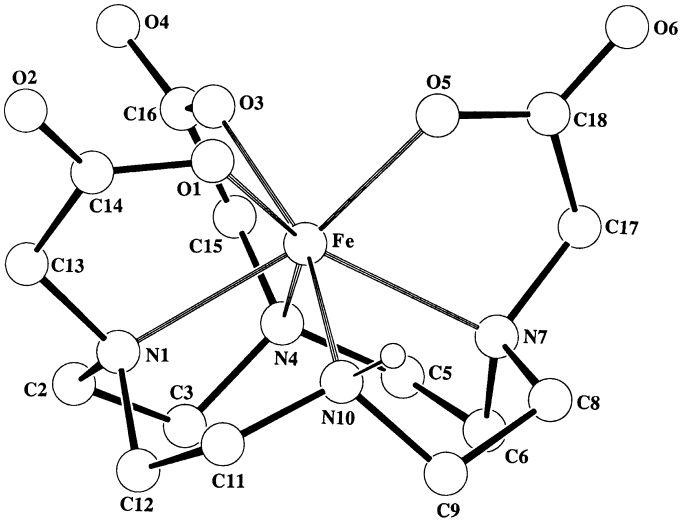

Fig. 8. Molecular view of [Fe(DO3A)] [148].

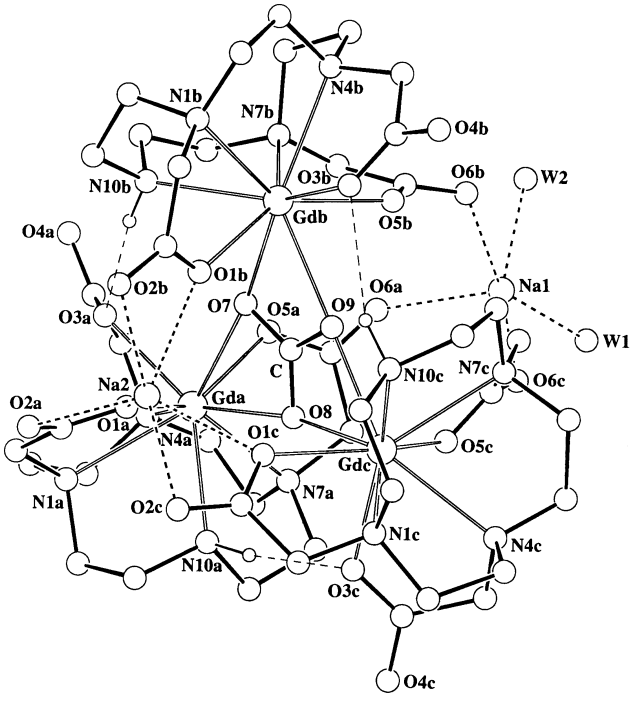

Fig. 9. Molecular view of $[Gd(DO3A)]_3.Na_2CO_3$ [148]. Intermolecular hydrogen bonds are indicated by thin dashed lines, and the sodium–oxygen bonds by thick dashed lines.

thium ion is bound to the four nitrogen atoms and to three carboxylic oxygen atoms with average Gd–N and Gd–O distances of 2.60(3) and 2.35(1) Å, respectively. The eighth and ninth coordination sites are occupied by two bidentate oxygen atoms of a bridging carbonate anion [Gd–O = 2.46(3) Å]. In addition, two sodium counterions cap the two opposite faces of the trimer through coordination to one carbonyl oxygen atom of each of the three [Gd(DO3A)] units [Na–O = 2.40(9) Å] and to two water molecules [Na–O = 2.31(3) Å] for the first Na^+ cation, and to six oxygen atoms from one bidentate carboxyl group of each [Gd(DO3A)] unit for the second Na^+ cation [Na–O = 2.45(6) Å]. The stability of the trimer is reinforced by hydrogen bonding between each secondary NH group with a carboxylate oxygen atom from another [Gd(DO3A)] unit.

Kang et al. [128] probed the effect of additional rigidity and steric encumbrance of the aminocarboxylate macrocycle by introducing a α-methyl group on each acetate side-chain. Although an alternative preparation method at pH 8 has been successfully devised, crystals suitable for X-ray analysis of the gadolinium complex of 1,4,7-tris[(*R*)-1-carboxy)ethyl]-1,4,7,10-tetraazacyclododecane (H_3**9**) were isolated from a reaction mixture maintained at pH 5.0 and recrystallized by slow evaporation of an aqueous DMF solution (1:1 v/v). A diffraction study of [Gd(**9**)H_2O]$_2$.4H_2O revealed the formation of a dimer in the solid state (Fig. 10): the asymmetric unit contains two crystallographically independent diastereoisomeric [Gd(**9**)(H_2O)$_2$] and [Gd(**9**)] complexes and four lattice water molecules. In the dimer, the carboxyl arms exhibit the same chirality and all α-methyl groups have (R) configurations, but the quadrangular (3,3,3,3)-B conformations of the tetraazacyclododecane rings are enantiomeric. The average values of the N–C–C–N, C–C–N–C and C–N–C–C torsion angles are 56(2), −160(3) and 81(7)° in one unit and −58(1), 162(2) and −74(5)°

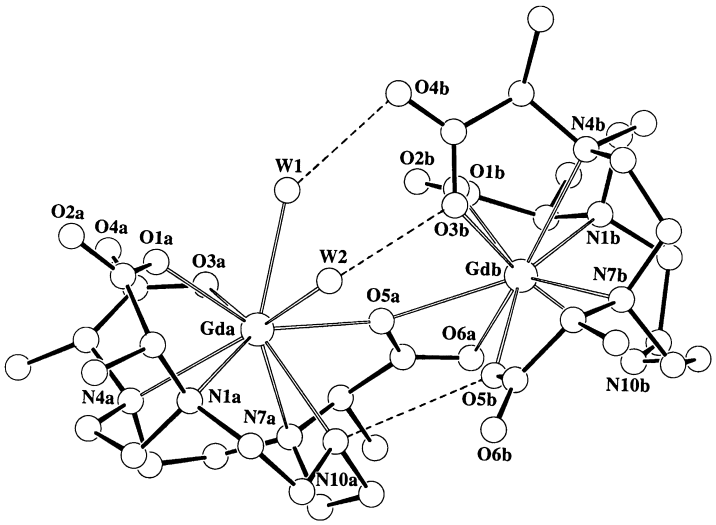

Fig. 10. Molecular view of the [Gd(**9**)H_2O]$_2$ dimer [128]. Intermolecular hydrogen bonds are indicated by dashed lines.

in the other. In order to distinguish the square-antiprismatic (SA) Λ-(δ,δ,δ,δ) or Δ-(λ,λ,λ,λ) geometry from the Δ-(δ,δ,δ,δ) or Λ-(λ,λ,λ,λ) arrangement, the coordination polyhedron of the latter diastereoisomer has been described as an inverted-square-antiprism (ISA). In both complexes, the gadolinium(III) ion is coordinated to the four essentially coplanar nitrogen atoms [Gd–N = 2.66(2) Å for the tertiary amines and Gd–N = 2.58(1) Å for the secondary N10 nitrogen atom] and to one oxygen atom from each of the three carboxyl groups [Gd–O = 2.35(2) Å]. The metal center lies 1.62(1) Å above the average four nitrogen-atom plane (RMS deviation = 0.02 Å) and 0.83(7) Å below the least-squares plane defined by the oxygen donors (RMS deviation = 0.09 Å): the dihedral angle between both planes is equal to 4°. The twist angle between both planes is 38.5° in the square-antiprismatic [Gd(**9**)(H_2O)$_2$] unit (a 45° angle is expected for a perfect square-antiprism), while it is only 30° in the inversed-square-antiprismatic [Gd(**9**)] complex. This appears to be a quite general trend among octa- and nonacoordinated complexes of tri- and tetracarboxylic cyclen derivatives: twist angles of inversed-square-antiprismatic structures are between 20 and 30° (vide infra). The coordination polyhedron is completed by two oxygen atoms, one in an apical position [Gd–O = 2.56(4) Å], and the other in the equatorial plane of the three coordinating carboxyl oxygen atoms [Gd–O = 2.451(5) Å]. In the [Gd(**9**)(H_2O)$_2$] subunit, both additional oxygen atoms are provided by two bound water molecules which are hydrogen-bonded to two carboxylate oxygen atoms from the second subunit [W1–O4 + 5b = 3.00(1) Å and W2–O3b = 2.75(1) Å]. In the latter, the eighth and ninth oxygen atoms are donated by the bridging tridentate carboxyl group attached to N7a which belongs to the [Gd(**9**)(H_2O)$_2$] complex. Thus, one of the two bridging carboxyl oxygen atoms (O5a) is in the apical position in the [Gd(**9**)] unit, whereas it is in an equatorial position in the other unit. Both subunits are further bridged by a single NH···O hydrogen bond involving the N10a secondary amine of the [Gd(**9**)(H_2O)$_2$] entity and the O5b coordinating carboxyl oxygen atom of [Gd(**9**)] [N10a–O5b = 3.02(1) Å].

Several octadentate derivatives of $DO3A^{3-}$ which form neutral complexes with trivalent metal ions have appeared in the literature. Two types of functional groups have been introduced, including amides [163,129,164] and alcohols [158,165], which compensate about half of the stability loss observed between $DO3A^{3-}$ and $DOTA^{4-}$ complexes [166–168,127]. The stability enhancement is due to the coordination of the additional oxygen atom, which occupies the eighth position of a square-antiprism capped by an axial water molecule. This nine-coordinate geometry has been found in the amide-substituted [Gd(**10**)H_2O].3H_2O structure [129] and in the hydroxyl-substituted [Y(DO3AHP)H_2O].1.97H_2O and [Gd(DO3AHP)H_2O].1.75H_2O complexes (Fig. 11) [125]. [Gd(**10**)H_2O] and the isostructural yttrium(III) and gadolinium(III) $DO3AHP^{3-}$ chelates possess the same (3,3,3,3)-B ring conformation as the free H_5DO3A^{2+} ligand, which suggests a high level of predisposition of the scaffold [125]. The crystal structure of [Y or Gd(DO3AHP)H_2O] reveals the presence of two independent diastereoisomeric molecules per asymmetric unit. As in [Gd(**9**)H_2O]$_2$.4H_2O, the two macrocycles feature opposite chiralities, whereas the helicity due to the side-chains is identical.

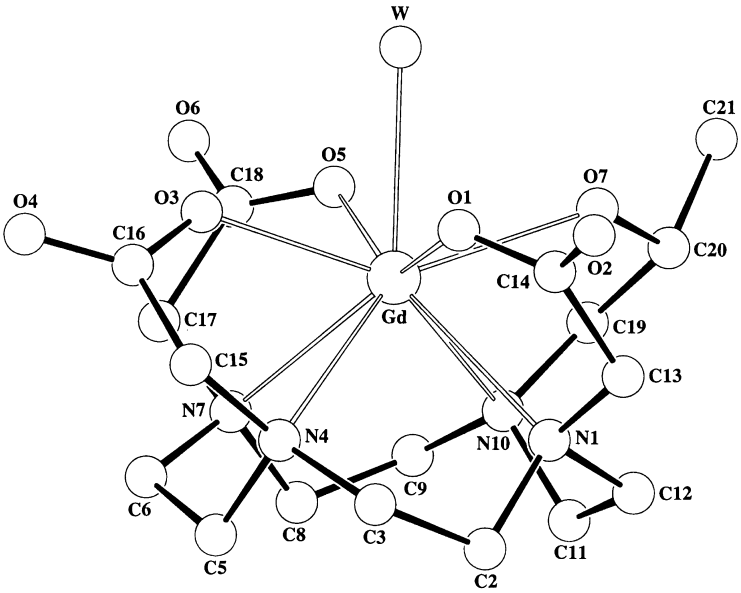

Fig. 11. Molecular view of the square-antiprismatic [Gd(DO3AHP)H_2O] diastereoisomer [125].

Interestingly, each single crystal contains only one stereoisomer of the chiral 2-hydroxypropyl group ($P2_12_12_1$ space group), indicating the spontaneous resolution of the racemate during crystallization. However, the coordination environment around the metal center in the three complexes shows many similarities, and the relevant structural parameters are summarized in Table 3. Furthermore, the structures of the $DO3AHP^{3-}$ and the corresponding $DOTA^{4-}$ lanthanide complexes

Table 3
Structural properties of [Gd(**10**)H_2O], [M(DO3AHP)H_2O] (M = Y, Gd), and [Gd(**11**)] complexes

	[Gd(**10**)(H_2O)]	[Y(DO3AHP)(H_2O)][a]	[Gd(DO3AHP)(H_2O)][a]	[Gd(**11**)]
Conformation	(3,3,3,3)-B	(3,3,3,3)-B	(3,3,3,3)-B	(3,3,3,3)-B
M–N (Å)	2.67(4)	2.62(3), 2.65(2)	2.65(1), 2.67(4)	2.68(4)
M–O carboxylate (Å)	2.36(2)	2.29(4), 2.30(4)	2.37(2), 2.38(6)	2.38(4)
M–O (Å)	2.392(6)	2.34(1), 2.38(1)	2.32(1), 2.34(1)	2.41(1)
M–W (Å)	2.429(5)	2.51(1), 2.46(1)	2.51 (1), 2.50(1)	2.43(1)[b]
M–N4[c] (Å)	+1.65	+1.58, +1.69	+1.61, +1.68	+1.69
M–O4[c] (Å)	−0.68	−0.75, −0.77	−0.75, −0.78	−0.75
N4–O4 twist angle (°)	39(1)	38, 28	39, 27	28
N4–O4 dihedral angle (°)	0.5	~0	~0	2.1
Ref.	[129]	[125]	[125]	[165]

[a] Values are given for both independent complexes of the asymmetric unit.
[b] Carboxylate oxygen atom form an adjacent centrosymmetrically related molecule.
[c] Distance of the metal center to the least-squares plane. The plus sign indicates that the metal ion lies above the plane, while a minus sign indicates that the metal ion lies below the plane.

(vide infra) are very similar. A least-squares fitting of the 28 non-hydrogen atoms common to [Gd(DO3AHP)] and [Gd(DOTA)]$^-$ gives an RMS deviation of 0.06 Å.

In the gadolinium(III) complex of *rac*-1,4,7-tris(carboxymethyl)-10-(1-hydroxymethyl-2,3-dihydroxypropyl)-1,4,7,10-tetraazacyclododecane, i.e. [Gd(**11**)].H_2O, the capping water molecule is replaced by a carboxylate oxygen atom of a centrosymmetrically related adjacent molecule [165]. Although the cocrystallized water molecule is not involved in the coordination, the geometry around the metal center is not significantly changed (Table 3). In solution, relaxivity and osmolality measurements suggest a monomeric structure with a bound water molecule rather than the presence of a dimer. Among the 24 possible[2] stereoisomers, only one diastereoisomer is formed upon complexation of gadolinium(III) by a racemic mixture of (R,S)- and (S,R)-**11**. The structural features of the biologically relevant calcium complexes with two tricarboxylate cyclen derivatives, DO3AHP^{3-} and **11**, have been documented previously [147,165]. The neutral [Ca(**11**)]H compound is used as an additive in the pharmaceutical formulation of the corresponding gadolinium chelate, which is currently undergoing clinical trials as an MRI contrast agent [165]. Crystals of [Ca(**11**)]H.1.5H_2O were obtained from water–ethanol mixtures by reacting the free triprotonated ligand with $CaCO_3$. Two almost identical molecules are present in the asymmetric unit which differ slightly in the arrangement of the 1-hydroxymethyl-2,3-dihydroxypropyl substituent. The eight-coordinate calcium cation is embedded in a N_4O_4 inversed-square-antiprism [$\alpha_{twist} = 21(2)^\circ$] formed by four nitrogen [Ca–N = 2.64(4) Å], three carboxylate [Ca–O = 2.40(3) Å] and one hydroxyl [Ca–O = 2.35(3) Å] oxygen atoms. The low quality of the crystal (R = 7.7%, R_w = 8.6%) did not allow us to localize the proton. The cyclen scaffold adopts the (3,3,3,3)-B square conformation. Except for the missing axially coordinated carboxyl oxygen atom, the calcium and gadolinium structures of **11** are similar.

Treatment of H_3DO3AHP with $CaCO_3$ in water (pH = 7.95) yields, after evaporation to dryness, at least four hydrated forms of Ca[Ca(DO3AHP)]$_2$, and three of them, i.e. the α, β and γ phases, have been structurally characterized by X-ray diffractometry [147]. The stoichiometry and stability of the phases which interconvert in the solid state are critically dependent on the vapor pressure. The hexanuclear α structure of formula {Ca(H_2O)$_3$[Ca(DO3AHP)]$_2$.3H_2O}$_2$ was crystallized from aqueous DMF solutions of the crude material and was not observed to interconvert into any of the other forms in the solid state. The trinuclear Ca(H_2O)$_4$ [Ca(DO3AHP)]$_2$.10H_2O species, designated as the β form, was obtained by crystallization from aqueous acetone. At a relative humidity lower than 52%, the topotactic partial dehydration of the β phase to the γ form was obtained after several hours under ambient conditions (22 °C, 35% relative humidity), and was followed by X-ray diffraction. γ-Ca(H_2O)$_4$[Ca(DO3AHP)]$_2$.2H_2O has only been obtained by solid-

[2] Since each hydroxyl group is able to interact with the metal, three constitutional isomers are possible. Furthermore, the chiral 1-hydroxymethyl-2,3-hydroxypropyl group contains two asymmetric carbon atoms of opposite configuration which give rise to a diastereomeric differentiation of the four stereoisomers generated upon complexation (vide infra). Thus, the racemic mixture of (R,S)- and (S,R)-**11** can in principle form a total number of 24 stereoisomers.

state transformation, and differs from the β form only by the number and spatial distribution of the uncoordinated lattice water molecules. Further dehydration leads to a fourth uncharacterized δ phase which predominates at a relative humidity of 6% or less. In the β and γ compounds, two $[Ca(DO3AHP)]^-$ anions and one bridging hydrated octa-coordinated Ca^{2+} cation form a C_2-symmetric trinuclear cluster, the C_2 crystallographic axis passing through the bridging Ca3 cation. In the α form where the two-fold symmetry is noncrystallographic, two trinuclear clusters are associated to form a hexanuclear centrosymmetric aggregate (Fig. 12). Each of the α, β or γ structure displays virtually identical $[Ca(DO3AHP)]^-$ anions which are strikingly similar to the corresponding $[Gd(DO3AHP)H_2O]$ complexes. The macrocycles show the same (3,3,3,3)-B conformation and, like gadolinium, the calcium ion lies between the nearly parallel least-squares planes of the four coordinating nitrogen [Ca–N4 = 1.63(4) Å] and oxygen atoms [Ca–O4 = 0.92(4) Å] at average Ca–N and Ca–O distances of 2.66(4) and 2.41(2) Å, respectively. One of the water molecules of each bridging hydrated Ca^{2+} cation is located in the axial position [Ca1–W1 = 2.698(3) Å and Ca2–W2 = 3.231(4) Å in form α, whereas Ca–W = 2.793(2) and 2.72(1) Å in form β and γ, respectively] above each inversed-square-antiprismatic $[Ca(DO3AHP)]^-$ anion [$\alpha_{twist} = 24(1)^\circ$].

3.5.3. Structural characteristics of DOTA complexes

3.5.3.1. Six- and seven-coordinated transition metals. For metal ions with coordination numbers smaller than 8, only a part of the donor groups is involved in the

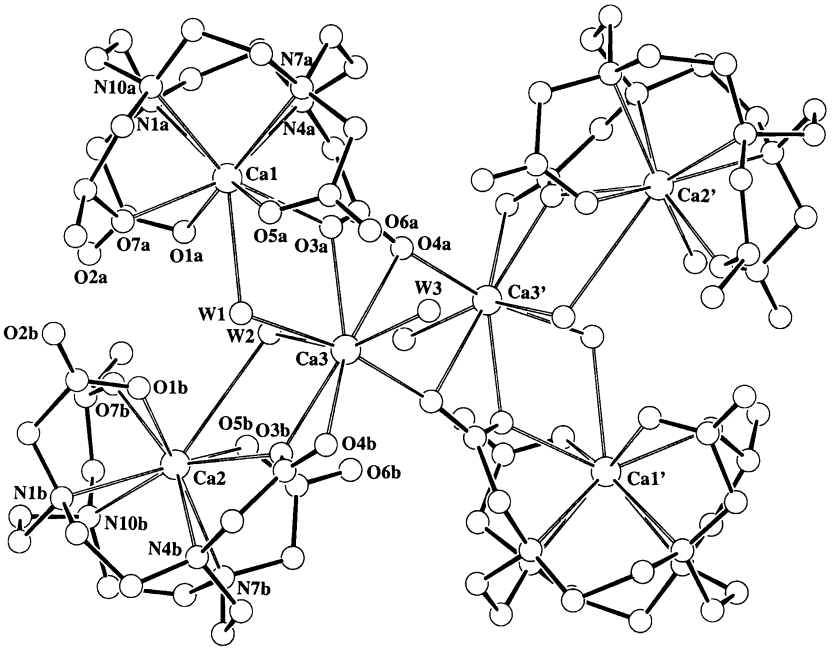

Fig. 12. Molecular view of the hexanuclear α-$\{Ca(H_2O)_3[Ca(DO3AHP)]_2\}_2$ complex [147].

coordination scheme. Riesen et al. [80,150] crystallized the high-spin violet [Ni(H_2DOTA)], and the isostructural [Cu(H_2DOTA)], and [Zn(H_2DOTA)] (Fig. 13) complexes from equimolar mixtures of the free H_4DOTA ligand and of the metal salt dissolved in water at pH 2.5. In these three complexes, the metal ion is located on a C_2 axis. The four nitrogen atoms and the carboxylate moieties attached to N1 and N1′ are coordinated to the central cation in a *cis*-I octahedral geometry. The protonated acetate groups, linked to the axial N4 and N4′ atoms, are not involved in the coordination. They point away from the metal ion in an extended conformation and give rise to hydrogen bonds with the O2 carboxyl oxygen atom of neighboring molecules. The coordination polyhedron is more distorted in the copper(II) complex due to a Jahn–Teller effect: the M–N1 distance is 0.06 Å longer than the M–N4 distance for the nickel and zinc complexes [Ni–N1 = 2.114(7) and Ni–N4 = 2.177(6) Å, Zn–N1 = 2.171(3) and Zn–N4 = 2.232(3) Å]. For the copper complex, the difference between the two M–N bond lengths (0.21 Å) is larger [Cu–N1 = 2.107(5) and Cu–N4 = 2.318(6) Å]. The Cu–O bond is also shorter than that found in the Ni^{2+} and Zn^{2+} complexes [1.965(5), 2.025(6) and 2.037(3) Å, respectively]. The coordination polyhedron angles are similar for the three complexes. The macrocycle is folded along the N4–N4′ axis, adopting a (2,4,2,4)-B conformation.

The deprotonated complexes M[Ni or Cu(DOTA)].6H_2O (M = Ca^{2+}, Sr^{2+}, Ba^{2+}) were prepared by neutralization at pH 10 of the isolated di-protonated [Ni or Cu(H_2DOTA)] complexes in the presence of an earth-alkaline salt, followed by precipitation with acetone. Visible absorption and IR spectroscopic data suggest that deprotonation of the acetic acid functions does not substantially modify the coordination scheme [80].

As well as mononuclear complexes, polymeric copper(II) species have also been reported by the same authors, although such complexes have not been identified in solution equilibrium studies [169,170]. Dark-green crystals of [Cu_2(DOTA)H_2O].4H_2O are obtained when two equivalents of $CuSO_4$.5H_2O and one

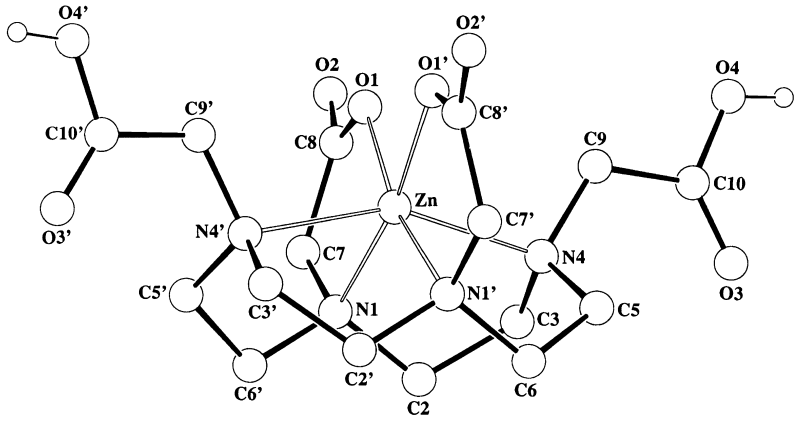

Fig. 13. Molecular view of [Zn(H_2DOTA)] [150].

equivalent of H_4DOTA dissolved in water are let stand at pH 4. The crystal structure (Fig. 14) reveals a two-dimensional network with two different coordination schemes for the Cu1 and Cu2 ions. The geometrical features of the Cu1 macrocyclic unit are close to those corresponding to the mononuclear copper(II) species, except that each oxygen atom of the two acetate arms attached to N4 and N10 is coordinated to a distinct Cu2 center [Cu2–O = 1.961(8) Å and Cu2–Cu2′ = 2.652(2) Å]. The resulting Cu2 coordination scheme is similar to that encountered in $[Cu_2(acetate)_4].(H_2O)_2$ [171], where two Cu2 ions are bridged by four extended carboxylate groups, each of them belonging to a different macrocycle. This type of coordination can also be compared with that found for a [Ce(TETP)] complex (see Section 4.6.2). The tetragonal–pyramidal coordination polyhedron of each Cu2 ion is completed by one axially bound water molecule [Cu2–W = 2.164(8) Å].

The anionic $[Fe(DOTA)]^-$ complex is heptacoordinated by the four nitrogen atoms and by one oxygen atom from three of the four carboxyl groups [Fe–O = 2.050(7) Å]: the macrocycle adopts a (3,3,3,3)-B conformation [148]. The face-capped trigonal–prismatic structure resembles that of [Fe(DO3A)], except for the additional and uncoordinated carboxylate arm which is turned away from the cavity,

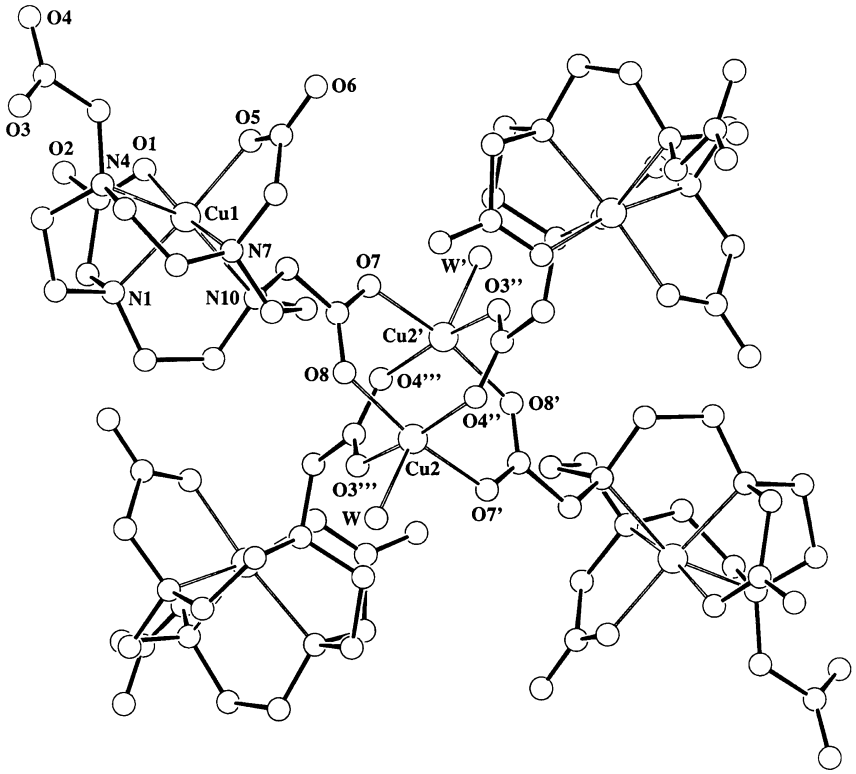

Fig. 14. Molecular view of the dinuclear $[Cu_2(DOTA)H_2O]$ complex [170].

and which is the acceptor of two hydrogen bonds from cocrystallized water molecules. The coordination scheme of the carboxylate groups has no effect on the Fe–N distances: the bond which involves the uncoordinated carboxyl group does not differ [2.269(7) Å] from the three other Fe–N interactions, which range between 2.207(7) and 2.353(7) Å.

3.5.3.2. Eight-coordinated metals. $\{Ca(OH_2)_3[Ca(DOTA)].7.7H_2O\}$ is the only eight-coordinated DOTA complex to be characterized by X-ray diffraction (Fig. 15) [151]. Single crystals were obtained by the addition of acetone to a mixture containing 2.5 equivalents of $Ca(OH)_2$ and the fully deprotonated $DOTA^{4-}$ ligand in presence of excess NaOH. The solid-state structure contains two independent eight-coordinated $[Ca(DOTA)]^{2-}$ units where both Ca^{2+} ions, located on a C_2 axis, are bonded to one oxygen atom of each of the four carboxyl groups [Ca–O = 2.42(2) Å] and to the four nitrogen atoms [Ca–N = 2.59(2) Å]. The resulting coordination polyhedron is a distorted inversed-square-antiprism ($\alpha_{twist} = 19$ and 24° for Ca1 and Ca2, respectively) in which the four oxygen atoms occupy the top vertices and the four nitrogen atoms occupy the bottom vertices. The metal ion is displaced towards

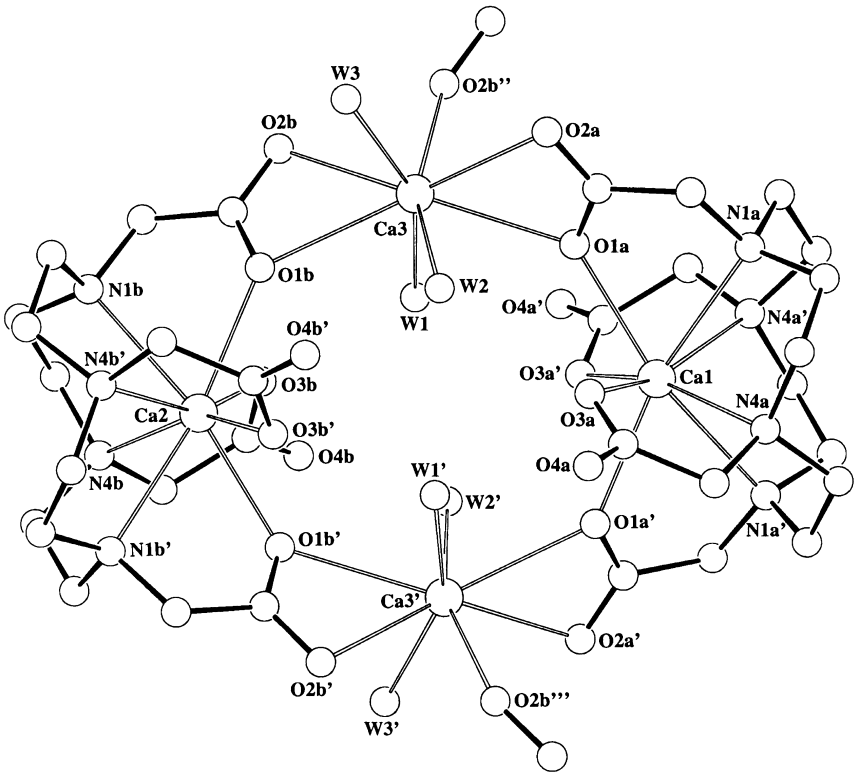

Fig. 15. Molecular view of the tetranuclear $\{Ca(OH_2)_3[Ca(DOTA)]\}_2$ cluster [151].

the four oxygen-atom plane [1.094(3) Å for Ca1 and 1.075(3) Å for Ca2] and is away from the four nitrogen-atom plane by 1.548(4) and 1.509(4) Å for Ca1 and Ca2, respectively. The two $[Ca(DOTA)]^{2-}$ units are bridged together by two Ca^{2+} counterions via all the oxygen atoms of two carboxyl groups of each $[Ca(DOTA)]^{2-}$ unit, leading to a neutral tetranuclear assembly. In addition to these four oxygen atoms, the Ca^{2+} counterions are coordinated to three water molecules and to another carboxylate oxygen atom bridging two surrounding tetranuclear clusters. This generates a one-dimensional chain of molecules running parallel to the diagonal of the *ac* plane. The tetraazamacrocycle exhibits a (3,3,3,3)-B square conformation. In solution, $DOTA^{4-}$ forms the most stable calcium complex known today [$\log \beta = 17.23(1)$ for $[Ca(DOTA)]^{2-}$ at 25 °C and $I = 0.1$ $N(CH_3)_4NO_3$ [73,172]]. The rigidity of the scaffold, up to 100 °C, induces the magnetic inequivalence of the four detected ethylenediamine protons of $[Ca(DOTA)]^{2-}$ [124]. In contrast, the less stable magnesium complex [$\log \beta = 11.92(1)$ [73,172]] undergoes fast interconversion on the NMR timescale at room temperature [124].

Brief accounts of the solution behavior of octadentate scandium, zirconium and thorium DOTA complexes appeared recently in the literature [173–175]. Although the highest coordination number for Sc^{3+} is eight and its ionic radius is somewhat smaller ($r_i = 0.870$ Å) than that of Lu^{3+} ($r_i = 0.977$ Å for CN = 8), the cation exhibits some analogies with the lanthanide(III) ions. In aqueous solution, two slow exchanging isomers of $[Sc(DOTA)]^-$ exist at the NMR timescale (up to 8 °C) in a 5:1 concentration ratio [173]. By analogy with $Lu(DOTA)^-$ (vide infra), Aime et al. [173] claimed that the minor and major square-antiprismatic $[Sc(DOTA)]^-$ isomers possess a Λ-(λ,λ,λ,λ)/Δ-(δ,δ,δ,δ) and a Δ-(λ,λ,λ,λ)/Λ-(δ,δ,δ,δ) conformation, respectively. Similarly, the aqueous solution ^1H NMR spectra of the sparingly soluble [Zr(DOTA)] complex suggest the presence of two isomers in a ~92:8 concentration ratio at room temperature, the major form possessing a time-averaged C_4 symmetry. At higher temperatures, both isomers are in fast exchange on the NMR timescale, and the resulting species exhibit a lower symmetry [174]. Jacques and Desreux [175] have also observed a C_4 square-antiprismatic coordination geometry and a rigidity similar to that of the lanthanide chelates for [Th(DOTA)], the only reported actinide complex of DOTA.

3.5.3.3. Nine-coordinated yttrium and lanthanide metals. The diamagnetic $[Y(DOTA)]^-$ complex is also described in this section, since the Y^{3+} ion exhibits some similarities with the lanthanides: both the size and coordination properties of Y^{3+} ($r_i = 1.019$ and 1.075 Å for coordination numbers 8 and 9, respectively) resemble those of Er^{3+} ($r_i = 1.004$ and 1.062 Å, respectively).

Recently, a dinuclear lanthanum complex of DOTA, $Na[La_2(DOTA)(HDOTA)].10H_2O$, has been characterized by X-ray crystallography [176]. The asymmetric unit contains two different $[La(DOTA)]^-$ complexes bridged by one carboxylate arm (Fig. 16) which give rise to a polymer extended along the crystallographic *b* axis. In each $[La(DOTA)]^-$ unit, the La^{3+} ion is coordinated to the four nitrogen atoms [2.77(2) and 2.795(8) Å for La1 and La2, respectively], and to an oxygen atom from each of the four carboxylate groups [La–O=

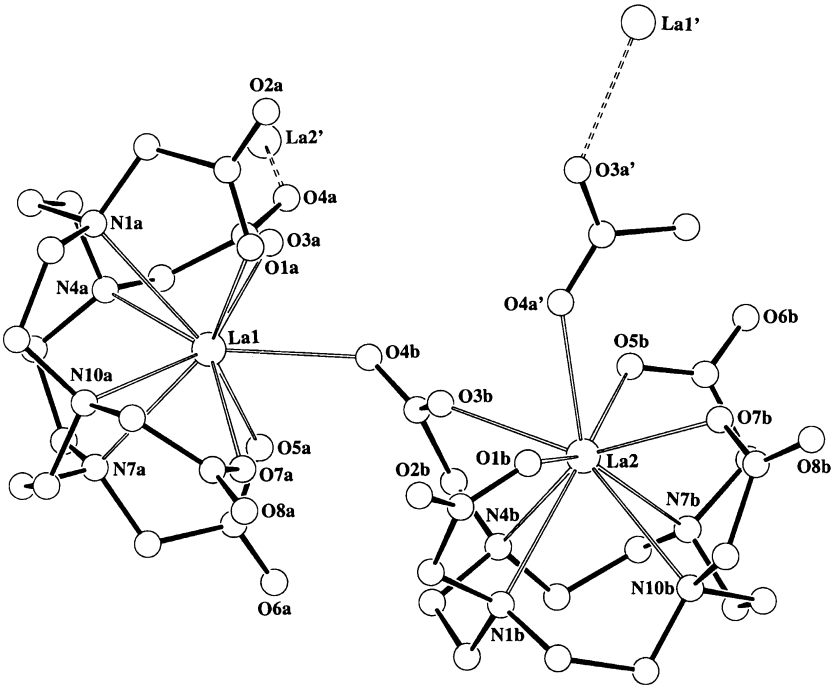

Fig. 16. Molecular view of the $[La_2(DOTA)(HDOTA)]^-$ dimer [176].

2.49(1) Å]. The two similar inversed-square-antiprismatic coordination polyhedra [$\alpha_{twist} = 22(1)^\circ$] are capped by an oxygen atom of the carboxylic group which bridges two adjacent units [La1–O4b = 2.537(5) and La2–O4a′ = 2.568(5) Å]. Despite the numerous water molecules in the asymmetric unit, none are directly coordinated to the lanthanum ions. Only one sodium ion of the asymmetric unit has been detected in the difference Fourier maps. Compared with the average C–O distance [1.26(1) Å for oxygen atoms coordinated to La^{3+} ions and 1.23(1) Å for uncoordinated oxygen atoms], the longer C–O1b bond [1.297(9) Å] suggests that O1b is protonated.

In contrast, Y^{3+} [148,174], Eu^{3+} [177,178], Gd^{3+} (Fig. 17) [148,179], Ho^{3+} [178] and Lu^{3+} [180] form $Na[M(DOTA)H_2O].4H_2O$ complexes containing nearly C_4-symmetric anions. The macrocycle adopts a strained and sterically crowded quadrangular (3,3,3,3)-B conformation[3]. In the five complexes, the central lanthanide cation is nine-coordinated to the four nitrogen atoms, to one oxygen atom from each of the four carboxylate groups of the octadentate, fully deprotonated ligand, and to one water molecule. The mean M–N distances [2.65(1), 2.68(14), 2.66(2), 2.64(1) and 2.61(2) Å for Y^{3+}, Eu^{3+}, Gd^{3+}, Ho^{3+} and Lu^{3+}, respectively] are longer than the mean M–O bond lengths [2.323(4), 2.39(10), 2.368(8), 2.330(7) and 2.279(6) Å for Y^{3+}, Eu^{3+}, Gd^{3+}, Ho^{3+} and Lu^{3+}, respectively]. The two

[3] A (3,3,3,3)-A conformation has inadvertently been reported for $[Lu(DOTA)]^-$ [180].

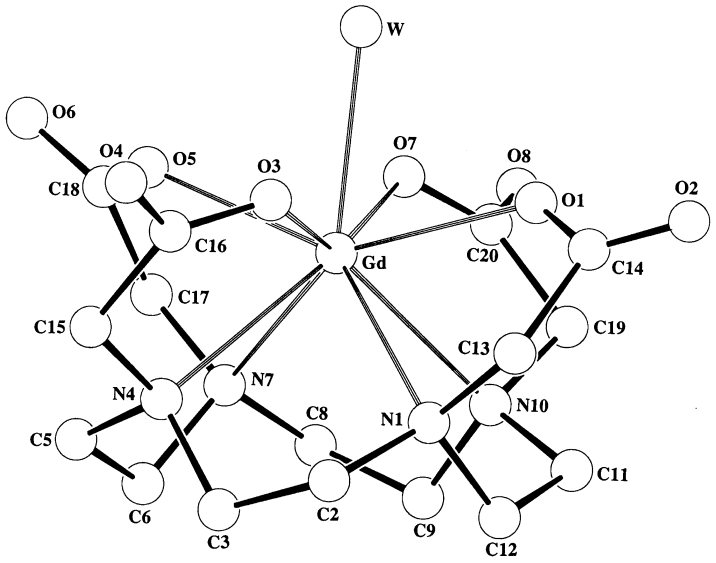

Fig. 17. Molecular view of $[Gd(DOTA)H_2O]^-$ [179].

parallel planes going through the four nitrogen and the four oxygen atoms are twisted by 39(1)° compared with the ideal value of 45°. The distorted Λ-(δ,δ,δ,δ) or Δ-(λ,λ,λ,λ) square-antiprismatic coordination sphere is capped by the apical water molecule [M–W = 2.435(3) (Y^{3+}), 2.480(3) (Eu^{3+}), 2.463(3) (Gd^{3+}), 2.444(2) (Ho^{3+}), and 2.416(4) Å (Lu^{3+})]. In solution, this water molecule exchanges rapidly with the bulk solvent [181], resulting in the case of $[Gd(DOTA)H_2O]^-$ in a significant increase in the water proton relaxation rate. This property, coupled with the long electronic relaxation time, has been used extensively for magnetic resonance imaging [65].

Insights into the aqueous solution geometry of the complexes along the lanthanide series were gained by ^1H and ^{13}C NMR studies of the diamagnetic La^{3+} and Lu^{3+} complexes. However, detailed analysis of the dipolar shifts induced by the paramagnetic lanthanide cations (LIS) has provided valuable structural information which, in several cases, was fully supported by the a posteriori X-ray structures [182]. The measured lanthanide-induced dipolar shifts ($\Delta\delta_i$) have two contributions: the Fermi contact (δ_i^c) and the dipolar shift (δ_i^d), which can be expressed as the product of a magnetic susceptibility factor (D_1 and D_2) and a mean geometric coefficient according to the following equation:

$$\delta_i^d = D_1\left(\frac{3\cos^2\theta_i - 1}{r_i^3}\right) + D_2\left(\frac{\sin^2\theta_i \cos 2\phi_i}{r_i^3}\right), \quad (1)$$

where r, θ, and ϕ stand for the spherical coordinates of the ith nucleus with respect to the origin of the principal magnetic axis coordinate system chosen at the lanthanide ion site [183,184]. Eq. (1) reduces to Eq. (2) for a complex possessing an axial

symmetry due to motional averaging:

$$\delta_i^d = D_1 \left(\frac{3\cos^2 \theta_i - 1}{r_i^3} \right). \quad (2)$$

Eq. (1) or Eq. (2) allows us to extract geometric information by varying the internal coordinates of a given structural model until the lowest agreement factor R between the calculated ($\delta_i^{d,cal}$) and observed ($\delta_i^{d,obs}$) shifts is reached:

$$R = \frac{\sum (\delta_i^{d,obs} - \delta_i^{d,cal})^2}{\sum (\delta_i^{d,obs})^2}. \quad (3)$$

The r distances can be evaluated independently from the magnetic-field strength dependence of the longitudinal ($1/T_1$) [185] or transverse ($1/T_2$) [186] relaxation rates, a prerequisite if Eq. (1) is used.

As well as NMR, luminescence spectroscopy is a powerful and complementary tool to study the solution structure of europium(III) and terbium(III) complexes [187]. The ground manifolds of Eu^{3+} and Tb^{3+} are split by spin–orbit coupling into seven ^7F_J ($0 \leq J \leq 6$) states, each of them being split by the crystal field into a maximum of $2J+1$ states. When the europium ion is promoted to the first excited state, it undergoes radiationless decay to the $^5D_0$ state, from which virtually all luminescence to the ^7F_J manifold arises in solution at room temperature. In the case of terbium, radiative emission originates from a $^5D_4$ state. The $^5D_0 \rightarrow {}^7F_0$ transition is of particular interest, since neither the $^5D_0$ nor the $^7F_0$ state can be split by the crystal field. Thus, the number of emission lines corresponds to the number of emitting lanthanide complexes present in solution. The $^5D_0 \rightarrow {}^7F_1$ transition provides the symmetry information required for the dipolar shift analysis: axially symmetric complexes give rise to two emission lines, whereas the occurrence of a third peak is an indication of lower symmetry. In addition, the empirical correlation proposed by Horrocks et al. [188] enables the accurate evaluation of the number of water molecules (± 0.5) bound in the first coordination sphere of Eu^{3+} and Tb^{3+} [189]. As pointed out by Kropp and Windsor [190–192] and later by Haas and Stein [193,194], who pioneered the luminescence deactivation effect of water molecules, this number is directly proportional to the difference in luminescence decay rate constants measured in H_2O and D_2O.

In contrast to the solid state, the complexes are present upon dissolution as a mixture of two isomers in equilibrium [152,173,195–198]. Along the lanthanide series, three distinct species have been identified. Their relative proportions are related to the ionic radius of the coordinated cation, and vary upon addition of inorganic salts (Fig. 18) [173,199]. Aime et al. [198] inferred that the main $La(DOTA)^-$ species in solution has an inverted-square-antiprismatic geometry similar to that found in the crystalline state [176]. The minor species differs by the inverted spatial arrangement of the appended acetate groups, while the (3,3,3,3) ring conformation is maintained, defining a square-antiprismatic isomer (Fig. 19). While the distribution of both $[Nd(DOTA)]^-$ isomers is equimolar, the fraction of the ISA diastereoisomer decreases with increasing atomic number until total disap-

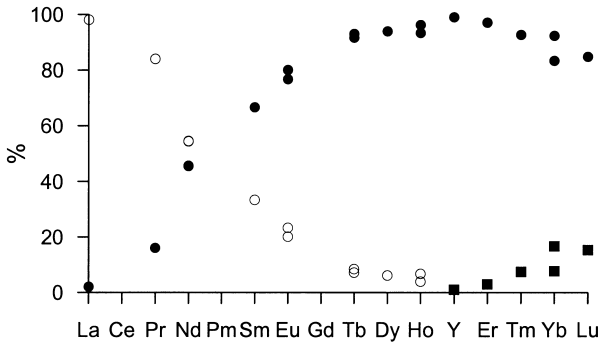

Fig. 18. Relative concentrations in neutral D_2O of nine-coordinated square-antiprismatic (●), nine-coordinated inversed-square-antiprismatic (○), and eight-coordinated inversed-square-antiprismatic (■) $[Ln(DOTA)]^-$ isomers. (Data taken from Refs. [173,199]).

pearance is reached for $[Er(DOTA)]^-$ and $[Y(DOTA)]^-$. Analysis of the luminescence spectrum of Eu[(DOTA)]$^-$ [195], of the diamagnetic ^1H and ^{13}C NMR spectra of $[Lu(DOTA)]^-$ [180], and of the ^1H NMR dipolar shifts induced by paramagnetic lanthanide cations [152,198–200] suggests that the conformation of the second isomer in solution exhibits an axial symmetry which closely resembles the square-antiprismatic structure found by X-ray diffraction studies of the Y^{3+}, Eu^{3+}, Gd^{3+} and Lu^{3+} complexes. Luminescence [195,196] and ^{17}O dipolar shift [183] data indicate that a single water molecule is coordinated to the metal cation. For lanthanides heavier than Ho^{3+}, the main square-antiprismatic diastereoisomer is in equilibrium with an eight-coordinated minor species, showing identical conformational features to the nine-coordinated inverted-square-antiprismatic Λ-(λ,λ,λ,λ) or Δ-(δ,δ,δ,δ) isomer, except for the inner coordination sphere depleted by one water molecule [173]. The relevance of a third, desolvated species is supported by recently published ^1H NMR data for $Sc(DOTA)^-$ [173]. Originally, a square-antiprismatic structure with one uncoordinated acetate arm in fast exchange at room temperature has been proposed for this isomer [152,197].

Variable-pressure experiments clearly indicated that the isomerization equilibria (depicted schematically in Fig. 19) for the La^{3+} to Ho^{3+} complexes do not involve a change in the lanthanide coordination number ($\Delta V^0 = -1.7(5)$ and $-0.5(6)\,cm^3\,mol^{-1}$ for $[Nd(DOTA)]^-$ and $[Eu(DOTA)]^-$, respectively), whereas the ligand rearrangement in $[Yb(DOTA)]^-$ and $[Lu(DOTA)]^-$ proceeds with a decrease of the coordination number from 9 to 8 as a result of the loss of the inner-sphere water molecule ($\Delta V^0 = 9.0(4)$ and $15(2)\,cm^3\,mol^{-1}$ for $[Yb(DOTA)]^-$ and $[Lu(DOTA)]^-$, respectively) [173]. The equilibrium constants calculated for the desolvation reaction of the ISA diastereoisomers ($K \approx 10^{-3}$ M) is quite constant over the lanthanide series, including scandium and yttrium.

Extensive variable-temperature ^1H and ^{13}C NMR studies combined with lineshape analysis and two-dimensional exchange spectroscopy (EXSY) enabled us to unravel the dynamic processes (Fig. 19) interconverting the diastereoisomers and their mirror images. Isomerization may take place by a twist along the C_4 axis of the four

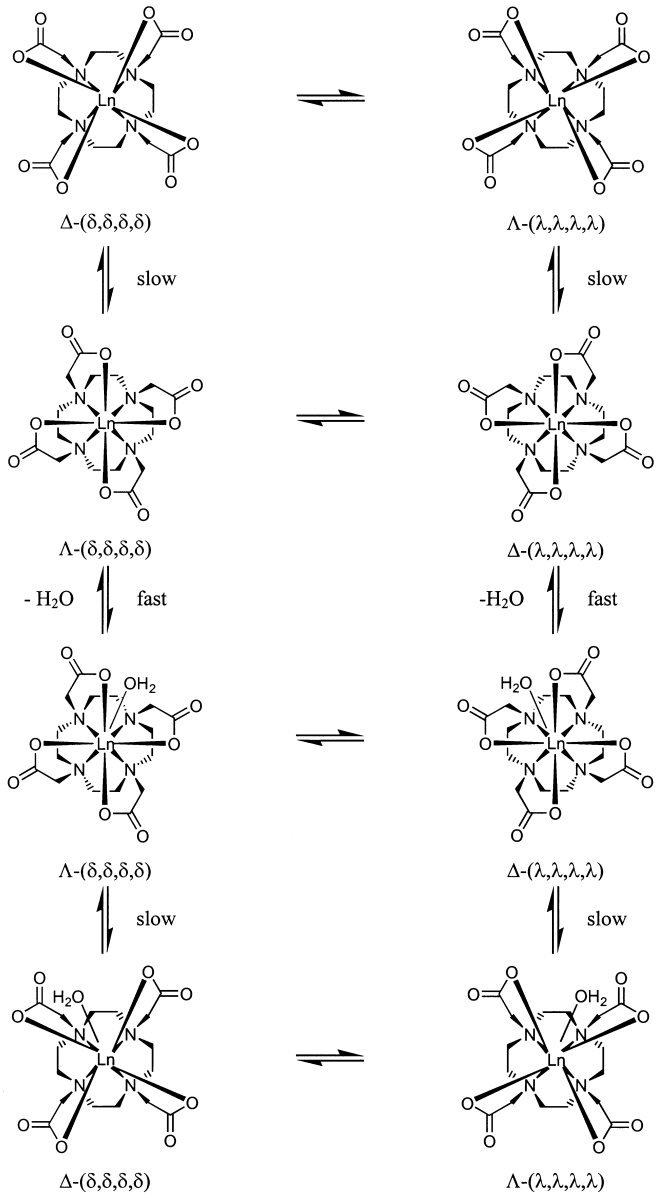

Fig. 19. Rearrangement scheme of $[Ln(DOTA)]^-$ complexes in aqueous solution.

oxygen-atom plane relative to the four nitrogen-atom plane, passing through a C_{4v} transition state (square-prismatic) while maintaining the same conformation of the macrocyclic ring [Λ-(δ,δ,δ,δ)↔Δ-(δ,δ,δ,δ) and Δ-(λ,λ,λ,λ)↔Λ-(λ,λ,λ,λ)] [199]. Since inversion of the acetate arms occurs on the NMR timescale by rotation rather than

by bond-breaking exchange of the coordinated oxygen atoms, the lanthanide–DOTA complexes are rare examples of nonlabile lanthanide-oxygen bonds. The second isomerization pathway involves a sequential inversion of the staggered ethylenediamine protons without changing the layout of the acetate arms [Λ-(δ,δ,δ,δ)↔Λ-(λ,λ,λ,λ) and Δ-(λ,λ,λ,λ)↔Δ-(δ,δ,δ,δ)]. Depending on the size of the coordinated cation, rearrangement may or may not be accompanied by the fast dissociation of the bound water molecule during the transition state ($\Delta G^{\neq} \approx 35$ kJ mol^{-1} from ^{17}O NMR data [181]). For larger ions (La^{3+} to Ho^{3+}), isomerization occurs without desolvation, as evidenced by near-zero activation vol -umes (Table 4). The relative rigidity of the yttrium and lanthanide–DOTA complexes on the NMR timescale is reflected by an activation free energy of 64(5) kJ mol^{-1} at room temperature [180,200–202]. The activation parameters collected in Table 4 indicate, however, that for $[Lu(DOTA)]^-$ and $[Yb(DOTA)]^-$ the kinetics are faster in the inverted-square-antiprismatic→square-antiprismatic exchange than in the reverse reaction. The more crowded situation in the minor inverted-square-antiprismatic isomer might be the cause of this effect [201]. Whether the energy barrier for the rotation around the acetate nitrogen is lower than the barrier related to conformational exchange in the tetraaza ring is still a question of controversy. Aime et al. [176,198] and Hoeft and Roth [199] found that the acetate inversion corresponds to the fastest process along the entire lanthanide series, whereas Desreux et al. [200,201] established that both motions considered are synchronous, and argued that the dynamic behavior of the acetate groups is controlled by the stereochemical features of the macrocycle. On the other hand, enantiomerization [Λ-(δ,δ,δ,δ)↔Λ-(λ,λ,λ,λ) and Δ-(λ,λ,λ,λ)↔Δ-(δ,δ,δ,δ)] requires a concerted or stepwise interconversion of both the acetate and ethylenediamine chelate rings. In 1980, Desreux proposed that the dynamic behavior of the acetate substituents coordinated to La^{3+}, Pr^{3+} and Eu^{3+} is controlled by the sequential inversion of the staggered ethylenediamine protons, but the presence of a second isomer in equilibrium was not taken into account [200]. Later, a two-consecutive-step mechanism involving a fast inversion of configuration of the acetate groups followed by the scaffold inversion was proposed [180,199]. However, this model does not agree with EXSY results [201], suggesting that both motions take place simultaneously. The activation parameters derived from Eyring plots or from coalescence temperatures for La, Pr, Yb and $[Lu(DOTA)]^-$ are summarized in Table 4. As the 4f shell fills up, the increasing activation enthalpy is balanced by more and more positive $\Delta S^{\neq}$ values, resulting in an almost unchanged activation free energy. In spite of large errors, the significant increase in the activation entropy correlates with the loss of the coordinated water molecule in the transition state for the heavy lanthanides [201].

3.5.4. Structural characteristics of other tetracarboxylate complexes

The search of more efficient MRI contrast agents which conserve the chelating ability of DOTA has been directed towards the synthesis of gadolinium complexes of functionalized DOTA derivatives. Aime et al. described the synthesis of ligands H_4**12**–H_4**16** bearing either one *p*-nitrophenyl [185] or β-benzyloxy-α-propionic [203]

Table 4
Activation parameters for the isomerization and enantiomerization reactions of lanthanide DOTA complexes

	Ref.	$\Delta G^{\neq}_{298}$ (kJ mol^{-1})	$\Delta H^{\neq}$ (kJ mol^{-1})	$\Delta S^{\neq}$ (J mol^{-1} K^{-1})	$\Delta V^{\neq}$ (cm^3 mol^{-1})
Isomerization					
Square-antiprismatic→inverted-square-antiprismatic					
Yb^{3+}	[201]	65(1)[a]	79(8)[a]	46(26)[a]	
		65(1)[b]	80(15)[b]	49(51)[b]	
Lu^{3+}	[176]	63(2)	69(1)	22(3)	
Eu^{3+}	[173]				0.6(4)
Inverted-square-antiprismatic→square-antiprismatic					
Yb^{3+}	[201]	61(1)[a]	64(8)[a]	9(27)[a]	
		62(1)[b]	66(13)[b]	14(45)[b]	
Lu^{3+}	[176]	59(2)	54(1)	−14(4)	
Enantiomerization					
Λ-(δ,δ,δ,δ)↔Δ-(λ,λ,λ,λ)					
La^{3+}	[200]	61(1)	59.4(8)	−4.6(3.3)	
Pr^{3+}	[200]	60.7[c]			
Eu^{3+}	[200]	61.9[d]			
Yb^{3+}	[201]	67(22)	82(12)	52(39)	
Lu^{3+}	[176]	66(2)	101(1)	116(2)	

[a] Acetate group inversion.
[b] Ethylenediamine group inversion.
[c] Measured at 61 °C.
[d] Measured at 57 °C.

residues. The influence of tetrasubstituted carboxylate groups on the coordination properties of DOTA has been explored by Brittain and Desreux with the ligand H_4**17** (1,4,7,10-tetrakis[((R)-1-carboxy)ethyl]-1,4,7,10-tetraazacyclododecane) [197]. The corresponding Gd^{3+} complexes were prepared in a similar way to $[Gd(DOTA)H_2O]^-$ by reacting equimolar quantities of ligand and lanthanide trichloride at a constant pH of 6.5. Another possibility is to solubilize the DOTA derivatives H_4**13**–H_4**16** by adding one equivalent of the chiral D(-)-*N*-methylglucamine base before carrying out the complexation reaction with half an equivalent of Gd_2O_3 at 70 °C until a clear solution is obtained.

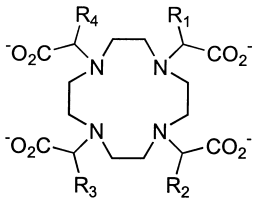

	R_1	R_2	R_3	R_4	Ref.
12	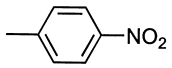	-H	-H	-H	[185]
13	$-CH_2OBz$	-H	-H	-H	[203]
14	$-CH_2OBz$	$-CH_2OBz$	-H	-H	[203]
15	$-CH_2OBz$	-H	$-CH_2OBz$	-H	[203]
16	$-CH_2OBz$	$-CH_2OBz$	$-CH_2OBz$	-H	[203]
17	$-CH_3$	$-CH_3$	$-CH_3$	$-CH_3$	[197]

As a general guideline, the essential coordination features found in lanthanide DOTA complexes are not altered by the introduction of α-substituents on the acetate pendant arms. Luminescence and relaxivity data are consistent with the presence of one water molecule in the inner octadentate coordination sphere. Thus, the sequestering ability of the parent DOTA ligand toward gadolinium(III) ($\log K = 27.0$) is reduced by less than one order of magnitude by the presence of one or two benzyloxymethyl residues under identical experimental conditions [$I = 0.1N(CH_3)_4NO_3$]: $\log K = 25.93$ and 25.95 for [Gd(**13**)]$^-$ and [Gd(**14**)]$^-$, respectively [203]. Chemical modification of the DOTA ligand primarily affects the stereochemical and related properties of the corresponding complexes. The α-monofunctionalization of the acetate groups introduces for each substituent a chiral center which doubles the total number of possible species in solution. Accordingly, monosubstituted DOTA derivatives may form a total of four pairs of (R) and (S) enantiomers. For the main isomer of [Ho(**12**)]$^-$ and [Yb(**12**)]$^-$, which represents 88 and 67% of the total complex concentration at 25 °C, respectively, the acetate proton resonance pattern is in agreement with a (R)-Δ-(λ,λ,λ,λ)/(S)-Λ-(δ,δ,δ,δ) stereochemistry [185]. In the

case of [Yb(**12**)]$^-$, the (R)-Δ-(δ,δ,δ,δ)/(S)-Λ-(λ,λ,λ,λ) chirality could be assigned to the minor species, which is in dynamic equilibrium with the major square-antiprismatic form. Unlike DOTA complexes, the interconversion process between both isomers at room temperature involves only the rearrangement of the cyclododecane scaffold. In spite of an outward orientation with respect to the coordination cage of the freely rotating *p*-nitrophenyl substituent, steric effects prohibit the interconversion of the acetate arms. Chiral ligand H_4**17** containing four (R) asymmetric carbons has been used to probe the influence of the four methyl-substituted carboxylate groups in α position on the coordination geometry and dynamics [197]. High-resolution fluorescence spectra of [Eu(**17**)]$^-$ as a microcrystalline powder revealed an effective C_2 symmetry. In neutral aqueous solutions, ^{1}H NMR, together with circular-polarized luminescence spectra, indicated that the C_2-symmetric species characterized in the solid state is in slow exchange with a second complex which does not possess an axial symmetry. Similar to [Yb(DOTA)]$^-$, an ISA coordination geometry was also assigned to the minor [Yb(**17**)]$^-$ species. However, the twist angle (70°) is much larger than that of [La(DOTA)]$^-$ as a consequence of steric crowding induced by the staggered orientation of the α-methyl substituents relative to the macrocyclic ring. Compared with [La(DOTA)]$^-$, the rigidity of the ligand is increased in the tightly packed [La(**17**)]$^-$ complex for which only a lower limit of the activation free energy (77.5 kJ mol^{-1}) related to ethylenediamine scaffold inversion has been measured.

Brunner et al. [132] described the synthesis of the tetrasubstituted carboxyphenyl ligand H_4**18**.2HCl [**18** = 1,4,7,10-tetrakis(2-carboxybenzyl)-1,4,7,10-tetraazacyclododecane] together with the crystal structure of the corresponding [Cu(H_3**18**)]ClO_4.4H_2O complex obtained at pH 3–4 where the ligand is triprotonated (Table 1).

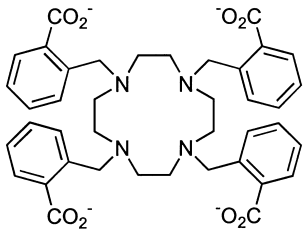

18

Like [Cu(H_2DOTA)], the macrocycle is folded and adopts a type-I conformation in spite of a different square-pyramidal pentacoordinated geometry. This difference might be due to sterical effects of the appended side-chains and to their mutual interactions. The Cu^{2+} ion is located 0.49 Å out of the nearly perfect four nitrogen-atom plane towards the axially bound carboxylate oxygen atom [Cu–O = 2.079(2) Å, Cu–N = 2.0l3(3)–2.063(3) Å]. The aromatic ring of the coordinated carboxybenzyl substituent is bent over the macrocycle towards the neighboring amino site. The three other carboxylate substituents are protonated and oriented above the nitrogen

atom plane. The maximum of the d–d absorption band shifts in aqueous methanol (1:1 v/v) from 607 ($\epsilon_{max} = 380\ M^{-1}\ cm^{-1}$) to 654 nm $\epsilon_{max} = 525\ M^{-1}\ cm^{-1}$) upon the addition of a base, as expected when a carboxylate oxygen atom axially binds a Cu^{2+} ion [204]. Interestingly, spectrophotometry coupled to potentiometric measurements indicated the formation of MHL [$\log K_1^H = 3.95(2)$, $I = 0.5$] and MH_2L [$\log K_2^H = 3.12(2)$, $I = 0.5$] species in addition to the ML complex [$\log K_{ML} = 19.78(1)$, $I = 0.5$], but the triprotonated form characterized by X-ray crystallography has not been reported in solution.

3.6. Tetrasubstituted carbamoylmethyl derivatives

Studies in the gas phase have shown that ligands containing neutral amide oxygen atoms are stronger donors than alcoholic or ethereal oxygen donors [205,206]. Consequently, a neutral amide group would efficiently replace a negatively charged carboxyl group. The steric hindrance induced by an amide or carboxylate oxygen atom is equivalent, since both are bonded to an sp^2 carbon center [76]. Due to the limited aqueous solubility of neutral amide chelates, crystals of earth-alkaline and heavy metal complexes have been obtained by treating the corresponding perchlorate salts with an equimolar quantity of ligand in a refluxing methanol–water mixture followed by precipitation with ethanol and recrystallization from water [207]. In the case of the lanthanide complexes, trifluoromethanesulfonate salts were employed in refluxing anhydrous ethanol and the complexes were precipitated by the addition of hexane instead of ethanol. Recrystallization of the solid material was carried out in a polar solvent like methanol or acetonitrile. Contrary to the corresponding carboxylate analogs, pH has a very limited effect (if any) on the resulting structure. Furthermore, the electron-withdrawing properties of the neutral amide groups significantly reduce the proton affinity of the amine sites, as evidenced by the protonation constants measured for 1,4,7,10-tetrakis(carbamoylmethyl)-1,4,7,10-tetraazacyclododecane (**19**) in 0.1 M $NaNO_3$ at 25 °C: $\log K_1^H = 7.70(1)$ and $\log K_2^H = 6.21(1)$ (actually, these apparent $\log K^H$ values are underestimated by ~ 2 orders of magnitude as a result of competitive sodium complexation) [207].

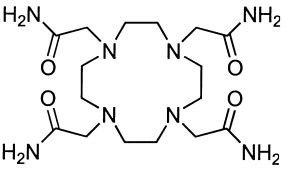

19

3.6.1. Primary amides

The difficulty of obtaining X-ray quality crystals of DOTA complexes contrasts with the ease of crystallizing complexes of ligand **19**. To date, structural data are

available for a large number of divalent metal complexes, including zinc ($r_i = 0.74$ Å), cadmium ($r_i = 0.95$ Å), calcium ($r_i = 1.00$ Å) and lead ($r_i = 1.19$ Å) [207], as well as for a few lanthanides [208,209]. These cations cover a wide range in radius and coordination number, and thus enable investigation of the process by which they adapt to the cavity size offered by the ligand.

In [Zn(**19**)]$(ClO_4)_2.H_2O$ (Fig. 20), [Cd(**19**)]$(ClO_4)_2.1.5H_2O$ and [Ca(**19**)]$(ClO_4)_2$ $.2.5H_2O$, the cation is encapsulated by the four nitrogen atoms of the macrocyclic ring and by the oxygen atoms of the amide groups [207]. Zinc(II) is too small to be coordinated in an octadentate fashion [Zn–N = 2.25(4) Å], and thus only two of the four carbamoyl oxygen atoms which define a square are ligated, as evidenced by the two short M–O bonds [2.10(6) Å] in *trans* position. The two remaining oxygen atoms (O2 and O4) are located 3.062(5) and 3.304(4) Å away from the zinc cation. The coordination polyhedron of the cadmium complex is better described as a distorted square-antiprism [Cd–N = 2.44(2) Å] with two sets of Cd–O bond lengths [2.34(2) and 2.64(1) Å]. The slightly larger calcium ion has the optimal size to accommodate the four oxygen atoms at almost equal Ca–O bond distances [2.395(8) and 2.418(7) Å], giving rise to a square-antiprismatic coordination polyhedron [Ca–N = 2.59(2) Å].

Variable-temperature ^{13}C NMR investigations in D_2O and DMF-d_7 support a nondissociative Bailar-twist mechanism for the tetraaza ring inversion process in the Zn^{2+}, Cd^{2+}, Hg^{2+}, Ca^{2+} and Pb^{2+} complexes [207,210], which proceeds through a concerted twist along the pseudo-C_4 axis via a cubic transition state [211]. On the NMR timescale, all four acetamide groups are equivalent at temperatures above

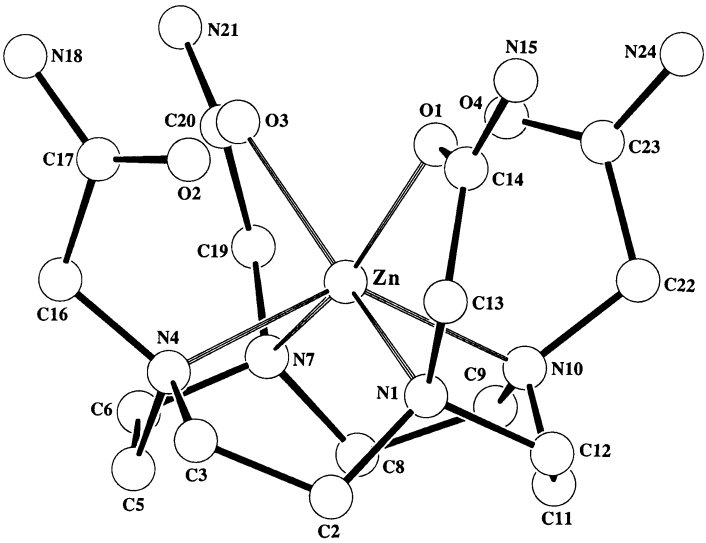

Fig. 20. Molecular view of $[Zn(\mathbf{19})]^{2+}$ [207].

−55 °C. Contrary to the solid state, the interchange between the different environments in which the M–O bond lengths are unequal is fast in solution. Thus, $[Zn(\mathbf{19})]^{2+}$ adopts in solution an eight-coordinate square-antiprismatic geometry, in spite of its hexacoordinated crystal structure. The correlation between the inversion of configuration activation free energy [$\Delta G^{\neq} = 46.8$ (−33 °C), 56.4 (14 °C), 57.3 (22 °C), 60.6 (35 °C) and 64.0 (32 °C) kJ mol^{-1}] and the length difference between the longer and the shorter pairs of M–O bonds (1.04, 0.37, 0.30, 0.02 and 0.00 Å for M = Zn^{2+}, Hg^{2+}, Ca^{2+}, Ca^{2+} and Pb^{2+}, respectively) suggests severe bond elongation in the course of helicity interchange, and further supports the proposed nondissociative twist mechanism.

Amin et al. have reported on the coordinating properties of ligand **19** towards lanthanide ions [208,209]. The lanthanum complex was found to efficiently promote RNA cleavage by phosphate ester transesterification, while the corresponding europium complex is inactive. This difference in catalytic activity has been attributed to the different coordination number of the lanthanide metal in $[La(\mathbf{19})(C_2H_5OH)(CF_3SO_3)](CF_3SO_3)_2$ [208] and $[Eu(\mathbf{19})H_2O](CF_3SO_3)_3.2CH_3OH$ [209]. The X-ray crystal structure of $[La(\mathbf{19})(C_2H_5OH)(CF_3SO_3)]^{2+}$ defines an encapsulated ten-coordinated La^{3+} cation bound to four amine nitrogen atoms [La–N = 2.85(7) Å] and four carbamoyl oxygen atoms, to an oxygen atom of a coordinated ethanol molecule and to an oxygen atom of a coordinated trifluoromethanesulfonate anion. The six oxygen atoms form a regular pentagonal pyramid [La–O = 2.54(4) Å, O-center of the pentagonal plane–O = 72(2)°], the ethanol molecule providing the cap. The La^{3+} ion is located 0.69 Å below the pentagonal plane and 1.87 Å above the almost parallel mean plane defined by the four nitrogen atoms.

The smaller Eu^{3+} ion ($r_i = 1.120$ Å for CN = 9 versus 1.27 Å for La^{3+} and CN = 10) is nine-coordinated in $[Eu(\mathbf{19})H_2O](CF_3SO_3)_3.2CH_3OH$ (recrystallized from methanol–methylene chloride; Fig. 21) with one axial water molecule capping the N_4O_4 square-antiprism [209]. The four upper coordination sites are occupied by the oxygen atoms, coplanar within 0.020 Å, while the four coplanar nitrogen atoms (within 0.015 Å) define the lower base of the antiprism, which is parallel and twisted by 30.3(1)° with respect to the four oxygen atom plane. The Eu^{3+} ion lies 0.79 Å below the four oxygen atoms [Eu–O = 2.39(1) Å] and 1.64 Å above the four nitrogen atoms [Eu–N = 2.64(1) Å]. The apical Eu–W bond length of 2.442(6) Å, is similar to that reported for $[Eu(DOTA)H_2O]^{+}$ (2.48 Å) [177]. Structure refinement evidenced that the 12-membered macrocycle is disordered: the asymmetric unit contains two overlapping diastereoisomers which occupy each site. Thus, the four stereoisomers are present in the crystal. Similarly to the gadolinium complex of ligand **9** [128], both diastereoisomers differ by the (λ,λ,λ,λ) or (δ,δ,δ,δ) configuration of the tetraazacyclododecane ring, although the ordered pendant amide groups are rotated in the same sense.

In a single crystal, each of the two diastereoisomers gives rise to a separate $^7F_0 \rightarrow {}^5D_0$ luminescence excitation band occurring at 580.24 and 580.52 nm. In neutral to weakly basic aqueous solution, the emission spectrum of $[Eu(\mathbf{19})]^{+}$ features one excited-state lifetime, while the $^7F_0 \rightarrow {}^5D_0$ transition leads to two peaks

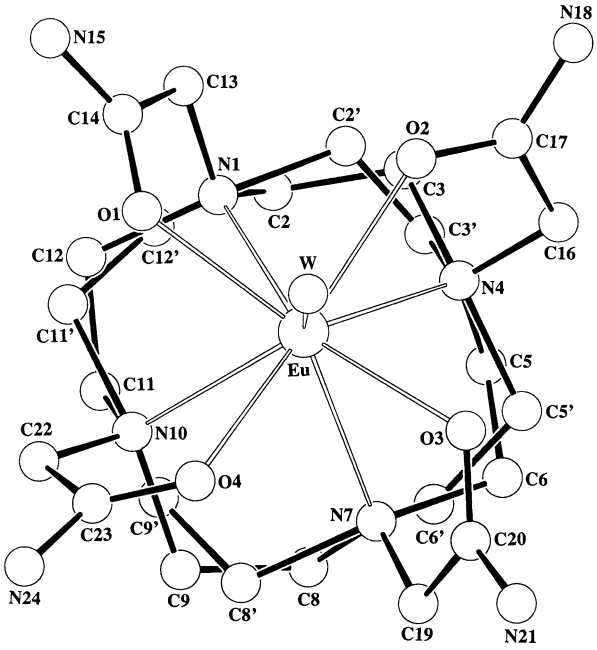

Fig. 21. Molecular view of the disordered $[Eu(\mathbf{19})H_2O]^{3+}$ cation showing the overlay of both diastereoisomers [209]. The macrocyclic carbon atoms corresponding to the second diastereoisomer have primed labels.

(579.96 and 580.14 nm) which are assigned to two species in rapid exchange on the luminescence timescale. Both species may differ in the arrangement of the amide substituents, the luminescence data suggesting that one solution species might be structurally similar to one of the cations in the solid state. Initially, it was also suggested that the species could differ in the number of water molecules bound to europium [1.5(5) on average]. However, this estimated value of 1.5 does not take into account the contribution of the amide N–H oscillators in the luminescence deactivation process. When a correction for this effect is applied, only one bound water molecule is found, which rules out the latter hypothesis [189].

3.6.2. Secondary amides

Chiral complexes of luminescent lanthanide ions have recently attracted some interest since they may be used as chiroptical sensors in biological media [212]. Hence, the optically active europium and the isostructural dysprosium complexes $[Eu((S)\text{-}\mathbf{20})H_2O]$ $(CF_3SO_3)_3.3CH_3CN$, $[Eu((R)\text{-}\mathbf{20})H_2O]$ $(CF_3CO_2)_3.CF_3CO_2H.2CH_3CN$, and $[Dy((S)\text{-}\mathbf{20})H_2O](CF_3SO_3)_3.3CH_3CN$ have been prepared and structurally characterized [213], together with the sodium complex of the sterically crowded ligand **21**, $[Na(\mathbf{21})]CF_3CO_2.CH_3CN$ [214].

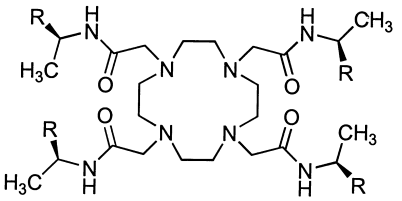

20 R = [213]

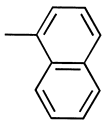

21 [214]

Diffraction studies have revealed an eight-coordinated, twisted square-antiprismatic N_4O_4 geometry around the encapsulated ion which is coordinated to an additional water molecule [M–W = 2.425(4) Å] for the Eu^{3+} and Dy^{3+} complexes. Characteristic parameters for $M = Na^+$, Eu^{3+} and Dy^{3+} are M–O = 2.46(3), 2.37(2), and 2.34(3) Å, M–N = 2.72(4), 2.69(2) and 2.65(2) Å, respectively. The shorter bonds for dysprosium reflect its smaller ionic radius. In the sodium complex, the twist angle equals 28° and the four 1-naphtyl rings are inclined by 81–103° with respect to the four oxygen-atom plane and are nearly orthogonal to each other. This particular arrangement gives rise to an exciton coupling effect in the solid state.

Solution NMR and luminescence studies in CH_3OH-d_4 of [Eu(**20**)]$^{3+}$ and [Eu(**21**)]$^{3+}$ indicated the presence of a single C_4 symmetric and rigid complex in the temperature range −70–+40 °C. Strong exciton coupling in methanol and the absence of an excimer band in the emission spectrum support a similar orientation of the naphtyl groups in solution and in solid state. Emission lifetime measurements for the ytterbium(III) complex of **21** carried out in H_2O and D_2O suggest the presence of one bound water molecule [215]. Similar luminescence studies concerning potential optical sensors related to **21** [216–218] and a phenanthridiniumcarbamoyl triphosphinate derivative of cyclen have been reported by Parker et al. [219,220].

3.6.3. Tertiary amides

The crystal structure of the sodium complex of ligand **22** (1,4,7,10-tetrakis(diethylacetamido)-1,4,7,10-tetraazacyclododecane), [Na(**22**)]Cl.CH_2Cl_2, shows an octadentate twisted-square-antiprismatic coordination geometry [221]. The sodium cation is encapsulated into the cavity formed by the four amido oxygen atoms (Na–O = 2.57 Å) and the four macrocyclic nitrogen atoms (Na–N = 2.56 Å). The macrocycle's conformation is (3,3,3,3)-B.

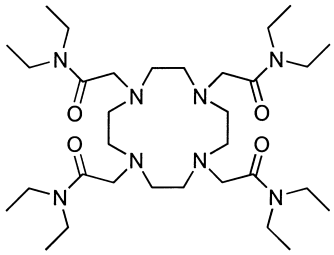

22

Forsberg et al. [222] established the structure in deuterated acetonitrile solution of the lanthanide complexes formed with **22** from LIS analysis based on Kemple's approach [184], combined with MM calculations using an extended Allinger's MM2 force field [223]. The lanthanide ion is encapsulated by the octadentate tetraamide ligand as described for DOTA, with the four amine nitrogen atoms and the four amide oxygen atoms located at the vertices of a distorted square-antiprism having approximate C_4 symmetry. The optimal calculated Ln–N and Ln–O bond lengths are reported in Table 5, together with the distances between the metal center and the centroid of the mean planes defined by the four nitrogen and by the oxygen atoms. Although nonmonotonic, the Ln–N and Ln–O bond distances decrease across the series with the ionic radius of the eight-coordinated Ln^{3+} cations. As shown in Table 5, the smaller the ionic radius, the stronger are the interactions of the pendant arms with the metal, which goes further inside the cyclododecane cavity. The twist angle of 47° between the opposite faces of the square-antiprism in the optimized structures is close to the theoretical value of 45° and is significantly higher than the corresponding angle observed in $[Ln(DOTA)H_2O]^-$ (39°) or $[Eu(\mathbf{19})H_2O]^{3+}$ (30.1°). This may arise from the probable absence in $[Ln(\mathbf{22})]^{3+}$ of an axially coordinated water molecule capping the antiprism in the ninth position. Contrary to the carboxymethyl and carbamoylmethyl cyclen derivative complexes,

Table 5
Optimal structural parameters calculated from the LIS values of $[Ln(\mathbf{22})]^{3+}$ complexes. (Data taken from Ref. [222])

Ln	Ln–N (Å)	Ln–O (Å)	Ln–N4 plane (Å)	Ln–O4 plane (Å)
Pr	2.82	2.47	1.74	0.63
Nd	2.82	2.47	1.74	0.63
Sm	2.78	2.41	1.73	0.64
Eu	2.74	2.30	1.69	0.68
Tb	2.64	2.30	1.54	0.70
Dy	2.60	2.28	1.49	0.75
Ho	2.62	2.30	1.46	0.78
Er	2.64	2.33	1.46	0.79
Tm	2.54	2.26	1.41	0.83
Yb	2.56	2.21	1.45	0.79

the LIS data also established that only one pair of enantiomers is present in solution across the entire lanthanide series. The steric requirements favor a Δ or clockwise rotation of the acetamide side-chains, which is associated to a ring (λ,λ,λ,λ) conformation, or the mirror image Λ-(δ,δ,δ,δ) configuration. Compared with [La(DOTA)]$^-$, the increased steric bulk of the amide groups has only a moderate effect on the dynamics of interconversion between the ring ethylenediamine λ and δ configurations ($\Delta G^{\neq} = 58.8$ kJ mol^{-1}, $\Delta H^{\neq} = 52.1$ kJ mol^{-1} and $\Delta S^{\neq} = -22.5$ J mol^{-1}K^{-1} versus $\Delta G^{\neq} = 61$ kJ mol^{-1}, $\Delta H^{\neq} = 59.4$ kJ mol^{-1} and $\Delta S^{\neq} = -4.6$ J mol^{-1} K^{-1} for [La(DOTA)]$^-$; cf. Table 4 [200]).

3.7. Tetrasubstituted 2-carbamoylethyl derivatives

The *N*-propionamide analog of ligand **19**, 1,4,7,10-tetrakis(2-carbamoylethyl) 1,4,7,10-tetraazacyclododecane (**23**), has been synthesized by Morrow et al. [224] in their continuing effort to develop abiotic lanthanide(III)-based ribonucleases.

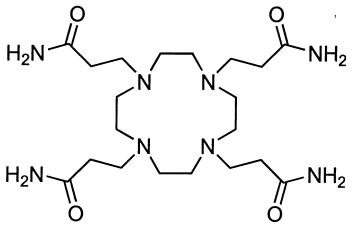

23

In the course of these studies, they have crystallized the lanthanum complex [La(**23**)](CF$_3$SO$_3$)$_3$.CH$_3$CN from an acetonitrile–methylene chloride solution (Fig. 22). The complex was prepared under anhydrous conditions by treatment of **23** with La(CF$_3$SO$_3$)$_3$ in refluxing acetonitrile containing trimethylorthoformate as a drying agent. In contrast to the ten-coordinated [La(**19**)(C$_2$H$_5$OH)(CF$_3$SO$_3$)](CF$_3$SO$_3$)$_2$ structure, the [La(**23**)]$^{3+}$ cation coordination polyhedron has a four-fold symmetry and is chiral. The lanthanum(III) ion is eight-coordinated and is encapsulated by the four nitrogen atoms of the macrocyclic ring [La–N = 2.718(8) Å] and the four oxygen atoms of the amide groups [La–O = 2.42 (2) Å]. As found in the lanthanide complexes of DOTA, the La–O bonds are shorter than the La–N bonds. The resulting coordination polyhedron is a distorted-square-antiprism. The dihedral angle between the four nitrogen and the four oxygen atom planes is 1.3°, while the twist angle equals 26.5°. The four nitrogen atoms of the amide groups define a third plane which is parallel to the nitrogen and oxygen atom planes. The La^{3+} ion, which is too large to lie inside the macrocyclic cavity [*trans*-N–N = 4.356(3) Å], is located above the 12-membered tetraazamacrocycle, which is folded in a type-I (3,3,3,3)-B conformation.

In water and dimethyl sulfoxide, lanthanide complexes of ligand **23** are labile, and thus hydrolyze rapidly. Both solvents bind strongly to lanthanide ions, displacing

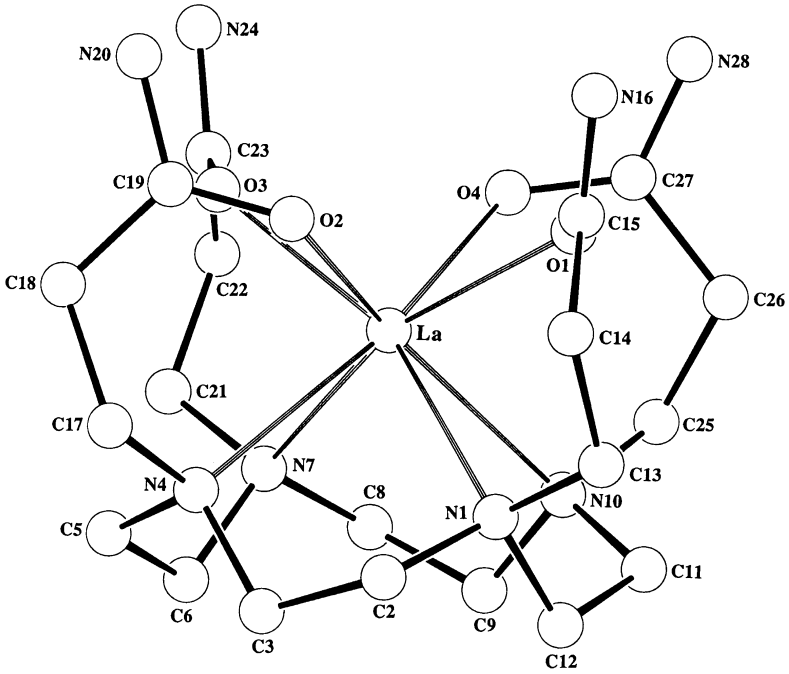

Fig. 22. Molecular view of $[La(\mathbf{23})]^{3+}$ [224].

the six-membered amide chelate rings, which are known to be less stable than five-membered rings [76]. The structural properties of $[La(\mathbf{23})]^{3+}$ in solution were studied by ^{1}H and ^{13}C NMR spectroscopy in CH_3CN-d_3, which does not dissociate the complex. Upon dissolution, the C_4 symmetry of the cation is preserved, which is characteristic of a (3,3,3,3) ring conformation. Below 0 °C, all macrocyclic ethylenic groups are locked into a staggered conformation, while the pattern of four resonances corresponding to the ethylenic amide protons is consistent with an asymmetric environment around each nitrogen atom. The dynamic behavior of $[La(\mathbf{23})]^{3+}$ is reminiscent of that described in Section 3.5.3.3 for the lanthanide(III) DOTA complexes. An activation barrier of 58.9(3) kJ mol^{-1} at the coalescence temperature (29 °C) has been calculated for the cyclen ring interconversion, which indicates a rigidity similar to that found in $[La(DOTA)]^{-}$ [61(1) kJ mol^{-1} [200]].

4. 1,4,8,11-tetraazacyclotetradecane (cyclam) derivatives

4.1. Protonation scheme of cyclam

The X-ray structures of cyclam, $H_2cyclam^{2+}$ and $H_4cyclam^{4+}$ are shown in Fig. 23. The deprotonated macrocycle adopts an endodentate, centrosymmetric, anangular conformation and a type-III configuration [225] which, according to MM calculations, is the most stable among the five possible configurations (Table 6 [230]). The torsion

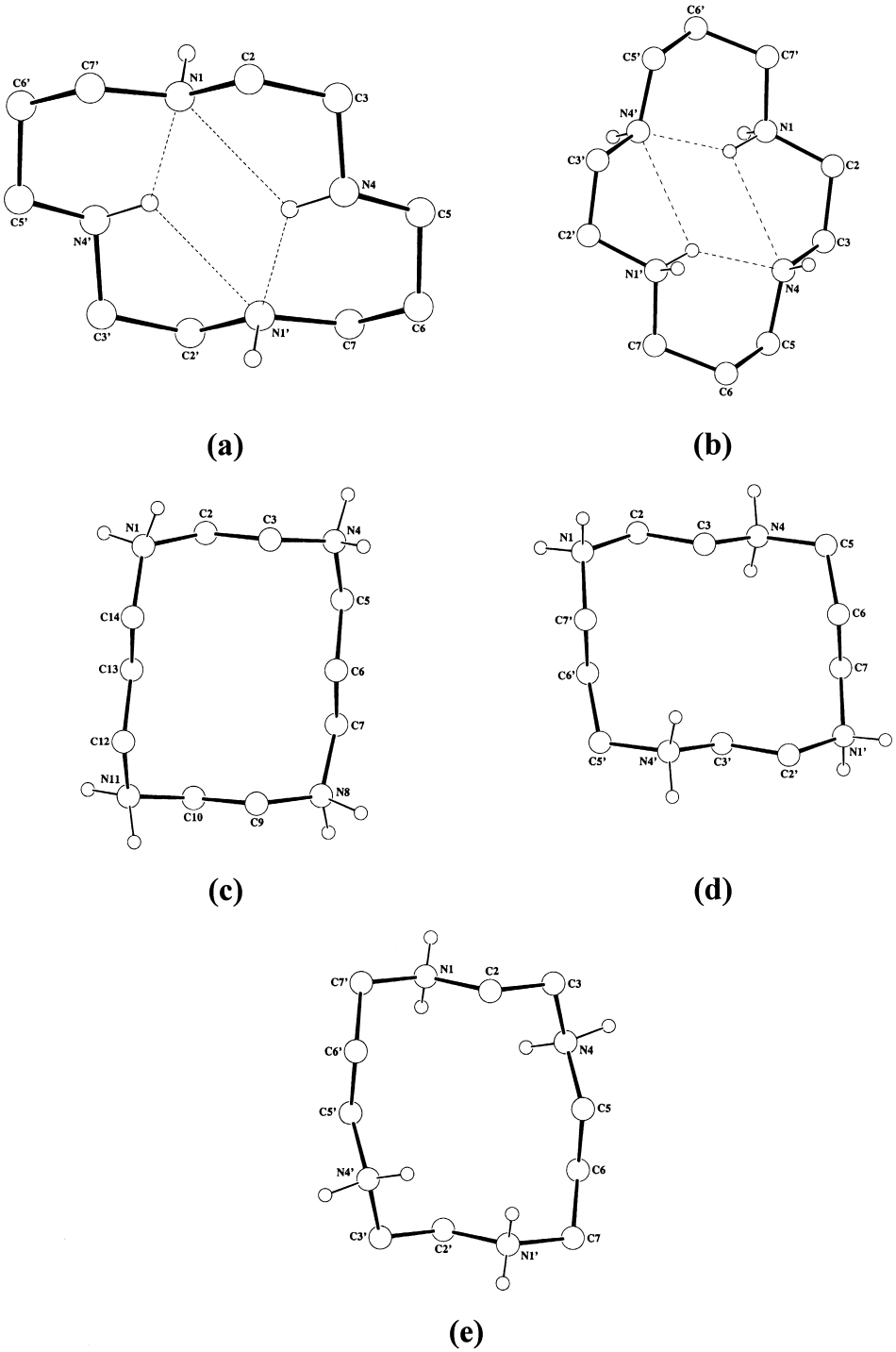

Fig. 23. Molecular views of (a) cyclam [225], (b) H_2cyclam^{2+} [226], (c) H_4cyclam^{4+} in the (3,4,3,4)-A conformation [227], (d) H_4cyclam^{4+} in the (3,4,3,4)-D conformation [228], and (e) H_4cyclam^{4+} in the (3,4,3,4)-B conformation [229]. Intramolecular hydrogen bonds are indicated by dashed lines.

Table 6
Relative energies calculated for the five isomers of cyclam and H_2cyclam^{2+} (Data taken from Ref. [230])

Configuration	Cyclam (kJ mol^{-1})	H_2cyclam^{2+} (kJ mol^{-1})
I (R,S,R,S)	2.13	1.13
II (R,S,R,R)	1.00	0.00
III (R,R,S,S)	0.00	0.00
IV (R,S,S,R)	1.96	2.17
V (R,R,R,R)	2.13	1.13

angles for cyclam are 63, −175, −179, −66, 72, −172 and 169° for τ_1–τ_7, respectively. The average C–N bond length is 1.461(6) Å. Both facing protons connected to N4 and N4′ are almost coplanar with the plane defined by the four nitrogen atoms, and they form two three-center hydrogen bonds involving N1 and N1′ as acceptor atoms [N1···N4′ = 2.882(5) Å and N1···N4 = 2.953(6) Å]. This intramolecular hydrogen bond pattern gives rise to two IR bands at 3270 and 3190 cm^{-1} [4]. It should be pointed out that Hancock et al. [133] mistakenly reported a two-center hydrogen-bonding pattern for the minimum energy conformers of cyclam.

The stable anangular conformation of the di-protonated cyclam characterized by single-crystal diffraction studies of [H_2cyclam]$(CF_3SO_3)_2$ [230], [H_2cyclam]$(ClO_4)_2$ [226] and [H_2cyclam]$_2(Sb_4F_{16}).2H_2O$ [231] corresponds exactly to that described for the deprotonated form [Fig. 23(b)]. The torsion angles for [H_2cyclam]$(ClO_4)_2$ are 64, −174, −180, −67, 67, −171 and 170° for τ_1–τ_7, respectively [226]. The two additional protons on N1 and N1′ [C–N1 = 1.497(7) Å] are *trans* to each other and interact through three-center hydrogen bonds with the nonprotonated N4 and N4′ nitrogen atoms [N1···N4′ = 2.870(4) Å, N1···N4 = 2.924(5) Å, C–N4 = 1.467(6) Å].

According to MM calculations, the addition of a third proton induces an approximately four-fold increase in the strain energy, whatever the value of the dielectric constant. This result is indicative of a significant contribution to the overall strain energy of van der Waals repulsion between the protons, since the electrostatic component is minimized at high permitivities [133]. The macrocycle is therefore more folded in its lowest-energy conformation with a concomitant loss of one of the two hydrogen bonds. In addition, the computer-minimized structure of H_3cyclam^{3+} differs significantly from that of H_4cyclam^{4+}.

MM calculations carried out using the TAFF force-field in vacuum for the four possible (3,4,3,4) quadrangular conformations of H_4cyclam^{4+} predict an increase in relative strain energy in the order (3,4,3,4)-A (ΔU = 0 kJ mol^{-1}), (3,4,3,4)-D (ΔU = 20.9 kJ mol^{-1}), (3,4,3,4)-C (ΔU = 54 kJ mol^{-1}) and (3,4,3,4)-B (ΔU = 67 kJ mol^{-1}) [133]. With a dielectric constant of 80.4, arrangement (3,4,3,4)-D is slightly favored over the (3,4,3,4)-A conformation. These predictions are supported by the X-ray structures obtained for the trifluoroacetate [227], aquapentachloroferrate(III) [227], perchlorate [133,232], bromide [232] and nitrate [233] salts, in which the H_4cyclam^{4+} cation has a (3,4,3,4)-A conformation [Fig. 23(c)]. The exo orientation of the four nitrogen atoms gives rise to the maximal charge separation. Several X-ray structures of the (3,4,3,4)-D conformer [Fig. 23(d)] are also known, including

the chloride [225,228,232], thiocyanate [232] and tosylate [232] salts. In spite of unfavorable electrostatic interactions, the endo (3,4,3,4)-B conformation [Fig. 23(e)] is observed for the sulfate [232], hexachlorocuprate(II) [229], hexachlororhenate(IV) [234] and decafluorodiantimonate(III) [231] tetraprotonated cyclam. Extensive hydrogen bonding with the counter anions might stabilize this conformation. Currently, there is no example of a (3,4,3,4)-C conformer.

Recently, Hancock et al. [133] revisited the protonation behavior in solution and confirmed the unusual sequence of protonation constants previously observed by Micheloni et al. [235] and Thom et al. [236], the fourth log K^H values being larger than the third. This reversal in protonation constants has been attributed to the important increase in both the electrostatic and the van der Waals repulsion energy and to the break down of the hydrogen bond network on the addition of a third proton to H_2cyclam^{2+}, which results in a high-energy conformation of the macrocycle. Structural and molecular mechanics data suggest a possible structural rearrangement accompanying the fourth protonation which balances the increase of electrostatic repulsion energy.

4.2. Monosubstituted carboxylate derivatives

Various carboxylic groups differing in their length and structure have been introduced as a single substituent on the cyclam scaffold, allowing a systematic investigation of the coordination mode as a function of pH. For a flexible side-chain of suitable length, it might be expected that the equilibrium between a tetra- and a pentacoordinated complex is displaced in favor of the apically chelated form at pH values above the protonation constant of the carboxylate substituent.

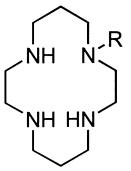

	R	log K_1^H	log K_2^H	log K_3^H	Ref.
24	-$CH_2CO_2^-$	12.18(2)	10.87(3)	3.01(3)	[237]
25	-$CH_2CH_2CO_2^-$	11.45(3)	10.11(2)	3.66(3)	[237]
26	-$CH_2CH_2CH_2CO_2^-$	11.58(3)	9.93(9)	4.30(5)	[237]
27	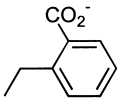	11.44(2)	9.94(4)	3.85(6)	[237,239]
28	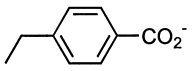	11.69(3) 10.63	9.91(3) 8.87	3.84(3) 3.71	[237] [238]

As already described for cyclen and cyclam, the first two protonation constants of compounds **24**–**28**, determined at 25 °C and $I=0.5(KNO_3)$ [237], are assigned to the protonation of both unsubstituted nitrogen atoms *trans* to each other. The third constant corresponds to the neutralization of the pendant carboxylate function, the value of which increases with the length of the chain due to weaker interactions with the ammonium sites. As observed for the parent cyclam, the protonation of the last two amines occurs below pH 2. The values of $\log K_4^H = 1.88$ and $\log K_5^H = 1.51$ [25 °C, $I=0.1(KCl)$] reported for ligand **28** by Motekaitis et al. [238], are in favor of similar conformational changes upon the addition of a third and fourth proton to the amine sites as reported for cyclam itself [133]. Based on the large discrepancy in the first two protonation constants for ligand **28**, these authors argued that the corresponding values for ligands **24**–**27** might also be overestimated.

A deprotonated copper(II) complex of **27**, $[Cu(\mathbf{27})]ClO_4.2.5H_2O$, has been isolated from an equimolar solution of H**27**.4HCl and $CuCl_2$ adjusted at pH 8–9, where the $H_2\mathbf{27}^+$ species with its deprotonated arylcarboxylate substituent predominates [239]. Acidifying the mixture at pH 1 yields the protonated $[Cu(H\mathbf{27})](ClO_4)_2.H_2O$ compound. In both the protonated and unprotonated complexes, the Cu^{2+} ion, coordinated to the four nearly coplanar nitrogen atoms, is also axially bonded to the carboxylic or carboxylate oxygen atom [Cu–N = 2.025(7) Å, Cu–O = 2.23(3) Å], giving rise to a square-pyramidal coordination polyhedron. The macrocycle is in the anangular *trans*-III configuration and wraps around the Cu^{2+} ion, which lies 0.18 and 0.11 Å above the four nitrogen atom mean plane for $Cu(\mathbf{27})^+$ and $Cu(H\mathbf{27})^{2+}$, respectively. Both structures exhibit identical bond lengths and angles, within experimental errors. They differ only significantly for the C–O bond lengths: as expected, these bonds are similar in $Cu(\mathbf{27})^+$ [1.24(1) Å], and clearly different in $Cu(H\mathbf{27})^{2+}$, with 1.216(9) Å compared with 1.31(1) Å for the protonated uncoordinated oxygen atom.

In solution, the copper(II) complexes of ligands **24**–**30** were shown to be involved in a pH-dependent equilibrium between two species which differ in their protonation state and in the coordination of the appended side-chain [237,240,241].

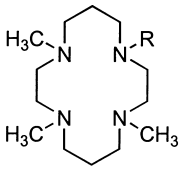

29 R= -$CH_2CO_2^-$

30 -$CH_2CH_2CO_2^-$

Below pH 1, the UV–visible absorption features in water due to the d–d transitions of the $[Cu(HL)]^{2+}$ species are similar to those of copper(II) cyclam ($\lambda_{max}=510$ nm, $\epsilon_{max}=125\ M^{-1}\ cm^{-1}$ [237]) or 1,4,8-trimethyl-1,4,8,11-tetrazacyclotetradecane ($\lambda_{max}=567$ nm, $\epsilon_{max}=235\ M^{-1}\ cm^{-1}$ [240]), showing that the carboxylic group is not coordinated in solution, contrary to the solid-state structure of

$[Cu(H\mathbf{27})]^{2+}$. In a neutral or alkaline medium, a bathochromic shift suggests an axial binding of the acetate, propionate or *o*-benzoate oxygen atom, leading to a stable five-, six- or seven-membered chelate ring, respectively. Molecular models suggest that the five-membered chelate ring is almost planar and does not influence the macrocyclic conformation. However, the axial coordination of an oxygen atom belonging to a six-membered chelate ring induces a displacement of at least one nitrogen atom from the equatorial plane, weakening the ligand field and shifting the absorption maxima to longer wavelengths. The more flexible butyrate and rigid *p*-benzoate substituents remain free and dangling in $[Cu(\mathbf{26})]^{+}$ and $[Cu(\mathbf{28})]^{+}$. Extended MM force-field calculations on $[Cu(H\mathbf{28})]^{2+}$ and H**28** confirmed the folded structure of the *p*-toluic acid substituent [238]. Geometrical minimization around the planar four-coordinated copper cation affords *trans*-N–Cu–N angles of 178(1)° and *cis*-N–Cu–N angles of 85(1)°.

As well as cyclam, the more rigid *meso*-5,5,(S)-7,12,12,(R)-14-hexamethyl-1,4,8,11-cyclotetradecane (*tet a*) scaffold has also been functionalized, yielding the 1-carboxymethyl-5,5,7,12,12,14-hexamethyl-1,4,8,11-cyclotetradecane (**32**) ligand [242].

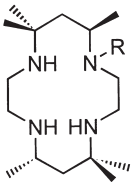

31 *tet a* R = -H
32 $-CH_2CO^{2-}$

A brief description of the X-ray structure of the free triprotonated compound H**32**.2HBr. H_2O (Fig. 24) has been reported [242,243]. The macrocycle adopts an anangular *trans*-III conformation with four coplanar nitrogen atoms [mean deviation = 0.028(7) Å]. The existence of a short C=O1 [1.18(1) Å] and a long C–O2 [1.33(1) Å] bond clearly indicates the protonation of the carboxylate side-chain. The proton distribution on the tetraazamacrocycle has not been quoted by the authors, but considering the N–C distances [(1.50(3), 1.506(8), 1.467(7) and 1.50(2) Å, for N1, N4, N8 and N11, respectively], it seems that the N8 nitrogen atom is not protonated. The two remaining protons are more certainly located on the N4 and N11 secondary amines, in *trans* position from each other, in agreement with the protonation scheme described above for the monocarboxylic cyclam derivatives. Typical IR absorption bands appear at 3400 and 3360 (ν_{OH}), 3200 (ν_{NH}), 2900–2650 (δ_{NH} for NH_2^+), and 1730 cm^{-1} ($\nu_{C=O}$ for COOH).

The five-coordinated copper(II) complex, $[Cu(\mathbf{32})]Br.H_2O$, exhibits a distorted square-pyramidal environment around the Cu^{2+} center which lies 0.148(2) Å out of the equatorial plane defined by the four nitrogen atoms [mean deviation =

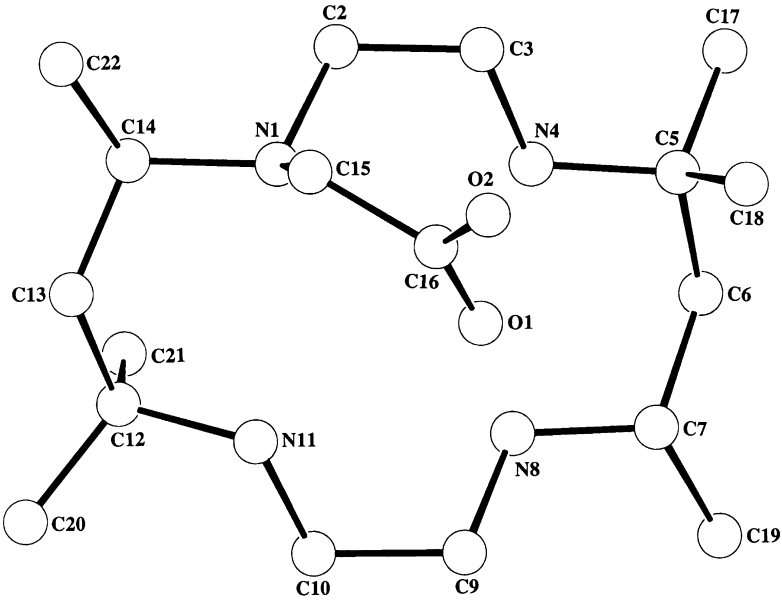

Fig. 24. Molecular view of the free triprotonated H_3**32**$^{2+}$ ligand [242,243]. The hydrogen atoms are not shown, as their coordinates have not been deposited with the Cambridge Crystallographic Data Centre.

0.072(2) Å] towards the axial oxygen atom [Cu–O = 2.157(3) Å] [244]. The Cu–N1 bond distance [2.088(4) Å] is 0.05 Å longer than the corresponding distance with the secondary nitrogen atoms [2.038(7) Å]. Like the red isomer of copper(II) complexes of *meso*-5,5,7,12,12,14-hexamethyl-1,4,8,11-cyclotetradecane (*tet a*) [245], the macrocycle of [Cu(**32**)]Br possesses an anangular *trans*-III conformation.

Two nickel(II) complexes, [Ni(**32**)H_2O]Br and [Ni(**32**)NCS].H_2O, have been isolated and their X-ray structure determined [242,246,247]. Violet crystals of [Ni(**32**)H_2O]Br have been obtained from H**32**.2HBr.H_2O and $NiBr_2.6H_2O$ in aqueous solution. The pH was adjusted during the reaction to 5 in order to ensure the deprotonation of the acetate substituent, yielding the H_2**32**$^{+}$ species. Exchange of Br^- by OH^- followed by the addition of sodium thiocyanate leads to another violet [Ni(**32**)NCS].H_2O complex. The molecular structure of [Ni(**32**)H_2O]Br consists of a discrete hexacoordinated [Ni(**32**)H_2O]$^+$ cation and of a bromide counter anion. The coordination polyhedron of the Ni^{2+} ion is an axially elongated octahedron formed by the four equatorial nitrogen atoms [Ni–N = 2.09(1) Å] and by two axial oxygen atoms, one belonging to the carboxylate arm [Ni–O = 2.065(2) Å] and the other to a bound water molecule [Ni–O = 2.223(3) Å]. The structure and distances relative to [Ni(**32**)NCS].H_2O are very similar to those of [Ni(**32**)H_2O]Br, excepted that the thiocyanate anion is bound to the metal ion through the nitrogen atom [Ni–NCS = 2.092(3) Å]. In each case, the macrocycle adopts, as in the free ligand, an anangular *trans*-III conformation and the nitrogen atoms are essentially coplanar

[mean deviation = 0.041(3) Å]. In [Ni(**32**)H_2O]Br, the nickel ion is almost situated in the nitrogen mean plane [deviation = 0.002(1) Å] [242], whereas it deviates from this plane by 0.044(1) Å towards the thiocyanate ligand for [Ni(**32**)NCS].H_2O [247]. In solution, pH-dependent structural rearrangements take place as described above for the copper(II) complexes. In 10 M $HClO_4$, the visible absorption spectrum is in agreement with a square-planar geometry and with an uncoordinated carboxylic side arm. In 5 M $HClO_4$, spectral shifts indicate a pseudooctahedral coordination environment which is maintained in basic solutions after replacement of the coordinated water molecule by a hydroxide ion.

4.3. Disubstituted carboxylate derivatives

Pertinent experimental conditions relative to the synthesis of transition metal complexes involving biscarboxymethyl substituted cyclam derivatives are gathered in Table 7. Dissolution of the metal salt and of the ligand in medium (H_2L, H_3L^+) to strong acid (H_4L^{2+}) solutions affords the desired complexes. The pH conditions have no significant influence since no protonated species have yet been characterized in the solid state: reactions carried out in 0.1 M acid lead only to the cocrystallization of a molecule of mineral acid [250]. The conformation of the cyclotetradecane framework and the coordination geometry encountered in the complexes of this class of ligands are difficult to predict. Even so, steric hindrance, rigidity and electronic properties play a key role in determining the stereochemistry.

The synthesis of 1,4-bis(carboxymethyl)-1,4,8,11-tetraazacyclotetradecane (**33**) has recently been achieved by intramolecular alkylation using cobalt(III) as a template ion [253].

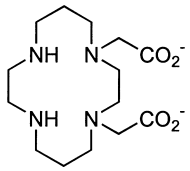

33

[Co(**33**)]ClO_4 is obtained by reaction of the tertiary cobalt(III) complex of *N*,*N*′-elethylenediaminediacetic acid (EDDA) and *N*,*N*′-bis(3-chloropropyl) ethylenediamine at pH 12 after ion-exchange chromatography. The macrocycle has an anangular *trans*-III conformation and the coordination geometry around the cobalt ion defines a pseudo-octahedron with two carboxylate oxygen atoms in axial positions [Co–O = 1.890(3) Å]. The Co–N bond lengths for the secondary nitrogen atoms [1.961(4) Å] are slightly shorter compared with those related to the tertiary nitrogen atoms [1.977(4) Å].

Structural data of copper(II) complexes of 1,8-biscarboxymethyl derivatives of cyclam have been reported by Parker et al. [248,249].

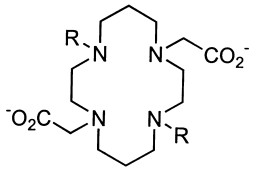

34 R = -H

36 R = -CH_3

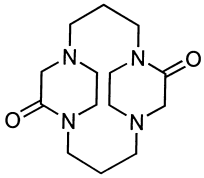

35

Complexation of H_2**34** [1,8-bis(carboxymethyl)-1,4,8,11-tetraazacyclotetradecane] with $Cu(ClO_4)_2$ in acidic aqueous solution affords, after slow evaporation, pale-blue crystals of the general formula [Cu(**34**)](H_2**35**)(ClO_4)$_2$. Due to the competitive lactamization at room temperature of H_2**34** during the synthesis, a molecule of the diprotonated tricyclic lactam **35** cocrystallizes. The Cu^{2+} ion is centrosymmetrically bound by the four nitrogen atoms [Cu–N = 2.095(3) and 2.014(4) Å for the tertiary and secondary amines, respectively] and by both carboxymethyl oxygen atoms [Cu–O = 2.263(3) Å] in a slightly distorted *trans*-III octahedral geometry.

Methylation of ligand **34** affords macrocycle **36** (1,8-bis(carboxymethyl)-4,11-dimethyl-1,4,8,11-tetraazacyclotetradecane), which does not lactamize. Blue crystals of [Cu(H_2**36**)](ClO_4)$_2$.2H_2O were obtained by reacting stoichiometric amounts of H_2**36**.2HCl and $CuClO_4$ at pH 3 [249]. The centrosymmetrical and anangular *trans*-III structure of [Cu(H_2**36**)]$^{2+}$ resembles that of [Cu(**34**)] with four short Cu–N bonds [2.070(3) Å (NCH_2CO_2) and 2.096(3) Å (NCH_3)] and two longer Cu–O bonds [2.369(3) Å]. In the crystal lattice, both uncoordinated carboxylic oxygen atoms are protonated [C–OH = 1.315(5) Å compared with 1.198(5) Å for the C=O bonds], and each of them is hydrogen-bonded to a water molecule, which accounts for the Cu–O bond elongation in [Cu(H_2**36**)]$^{2+}$ compared with

Table 7
Relevant experimental conditions relative to the synthesis of metal complexes of biscarboxymethyl cyclam derivatives

Compound	Metal salt	pH	Solvent of crystallization	Ref.
[Cu(**34**)](H_2**35**)(ClO_4)$_2$	$Cu(ClO_4)_2.6H_2O$	<7		[248,249]
[Cu(H_2**36**)](ClO_4)$_2$	$Cu(ClO_4)_2.6H_2O$	3	H_2O	[249]
[Co(**38**)]	$CoBr_2.6H_2O$	5	H_2O	[250]
[Ni(**38**)].HBr	$NiBr_2.6H_2O$	5	H_2O–HBr, pH 1	[250]
[Cu(**38**)].HBr	$CuBr_2.6H_2O$	1	H_2O–HBr	[250]
[Cu(**38**)].HNO_3	$Cu(NO_3)_2.6H_2O$	5	H_2O	[250]
[Cu(**38**)]	$Cu(CH_3CO_2)_2.2H_2O$	3	CH_3CN–C_2H_5OH	[251]
[Cu_2(**38**)]Br_2	$CuBr_2.6H_2O$	5	H_2O	[250]
[Ni(**39**)]	$NiCl_2.6H_2O$	5	C_2H_5OH–H_2O (1:1)	[252]
[Co(**39**)]	$CoCl_2.6H_2O$	5	C_2H_5OH–H_2O (1:1)	[252]
[Cu(**39**)]	$CuSO_4.5H_2O$	2	Ethyl ether–C_2H_5OH	[252]
[Cu_2(**39**)]Cl_2	$CoCl_2.2H_2O$	5	H_2O	[252]

[Cu(**34**)]. The *N*-alkylation in ligand **36** gives rise to longer Cu–N bonds due to van der Waals repulsions.

C-substituted analogs of ligand **33** and **34**, 1,4-bis(carboxymethyl)-*meso*-5,5,7,12,12,14-hexamethyl-1,4,8,11-cyclotetradecane (**37**) [254], 1,8-bis(carboxymethyl)-*meso*-5,5,7,12,12,14-hexamethyl-1,4,8,11-cyclotetradecane (**38**) [250] and 1,8-bis(carboxymethyl)-*meso*-5,12-diphenyl-7,14-dimethyl-1,4,8,11-cyclotetradecane (**39**) [252] have been described.

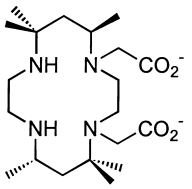

37

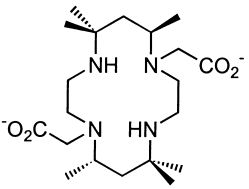

38

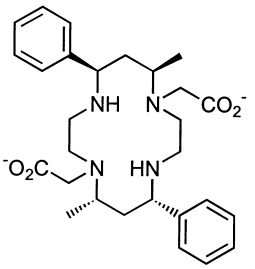

39

The sterically encumbered 1,4-biscarboxymethyl isomer **37** was isolated as a side product during the synthesis of **38** [254]. The coordination polyhedron of the copper(II) complex, [Cu(**37**)].1.5$HClO_4$.1.5H_2O, is a square-pyramid defined by the four coplanar nitrogen donor atoms [mean deviation: 0.002(7) Å] and one oxygen atom from the carboxyl group attached to N4 (Fig. 25). The Cu^{2+} cation lies 0.079(1) Å above the four nitrogen-atom plane and 2.226(6) Å away from the bonded oxygen atom. The Cu–N bond lengths vary significantly as a consequence of the peculiar conformation of the macrocycle: 2.105(6) and 2.053(7) Å for the tertiary N1 and N4 atoms, and 2.038(6) and 1.980(7) Å for the secondary N8 and N11 atoms, respectively. Both protons and both carboxylate groups project in the same direction, giving rise to a type-I structure according to the rules of Bosnich et al. [5], whereas the six methyl substituents are oriented in the opposite direction. One of the six-membered chelate rings (Cu, N4, C5, C6, C7, N8) adopts a chair conformation and the other a boat form (Cu, N11, C12, C13, C14, N1). The five-membered rings are both in a *gauche* conformation. Thus, the macrocycle adopts an unusual distorted biangular (7,7)-F conformation with two "genuine corners" (C3 and C10), but with only one "pseudocorner" (C6) and a sequence of three consecutive *gauche* ($g^+g^-g^-$) bonds in place of the second "pseudocorner" (C13). The torsion angles follow the order −50(1), −100.1(9), 175.4(8), −66(1), 63(1), 178.3(7), 152.2(8)^0, −44(1), −90(1), 162.7(7), 43(1), −78(1), −84.8(9) and 166.0(8)^0 for τ_1–τ_{14}, respectively.

The 1,8-biscarboxymethyl substituted ligands **38** and **39** constitute an interesting example where the ring conformation is controlled by the coordinated metal. The MM results for cyclam predict *trans*-I or *trans*-III geometries for six-coordinate nickel(II) (r_i=0.69 Å) and copper(II) (r_i=0.73 Å) cyclam derivatives, the *trans*-I form being favored for M–N bond lengths shorter than 1.9 Å [236,255–257]. The

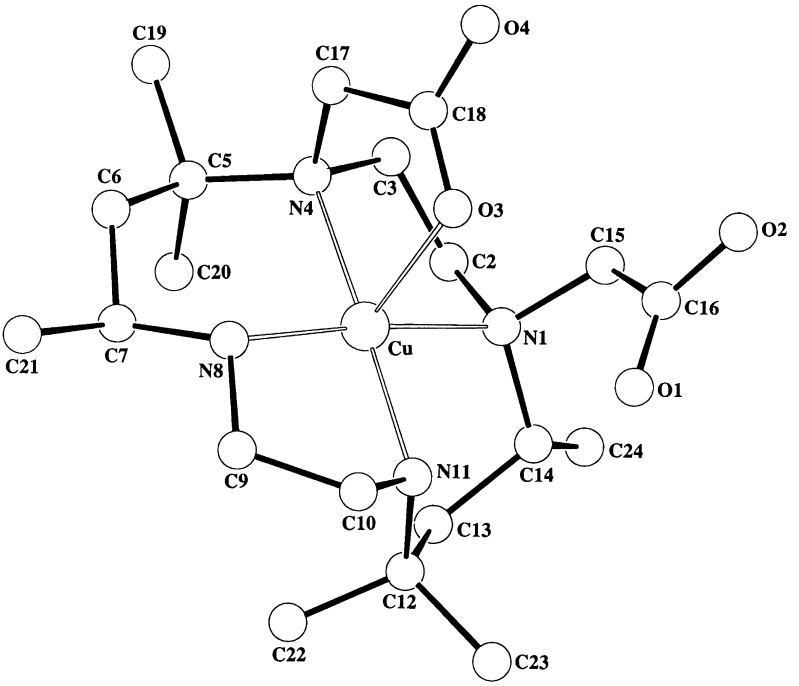

Fig. 25. Molecular view of the [Cu(**37**)] complex [254].

copper(II) complex [Cu(**38**)].$4H_2O$ was crystallized from acetonitrile–ethanol mixtures [251], while [Cu(**39**)].$2C_2H_5OH$ (Fig. 26) was obtained by diffusion of ethyl ether into an ethanolic solution of [Cu(**39**)] prepared in acidic water (pH = 2) by reacting the tetraprotonated form of the ligand with Cu^{2+} [252]. The metal ion is located at the inversion center of the molecule and shows a distorted octahedral *trans*-III coordination environment. Typical Cu–N distances were measured for both the secondary N4 [2.070(3) Å] and tertiary N1 [2.094(3) Å] amines in [Cu(**38**)]. For [Cu(**39**)], similar lengths were found according to the data deposited with the Cambridge Crystallographic Data Centre [2.056(2) and 2.109(2) Å for the secondary and tertiary nitrogen atoms, respectively]. These distances are in agreement with those quoted in Table 3 and Fig. 2 of Ref. [252], but contradict those reported in the body of the text. Due to Jahn–Teller effects, the apical Cu–O bonds are elongated [2.309(3) Å for [Cu(**38**)] and 2.248(1) Å for [Cu(**39**)], as compared with 2.263(3) Å for [Cu(**34**)]].

Binuclear copper(II) complexes have been briefly reported for ligands **38** and **39**. The experimental conditions employed to obtain [Cu_2(**38**)]Br_2 are similar to those used for the mononuclear species [250]. IR data ($\nu_{NH} = 3180\ cm^{-1}$ and $\nu_{C=O} = 1580\ cm^{-1}$ for COO^-) suggest a polymeric material. The ESR spectrum of [Cu_2(**39**)]Cl_2 shows a single, broad resonance in the solid state at room temperature at $g = 2.10$ which is split at 77 K into a perpendicular ($g_\perp = 2.10$) and a parallel

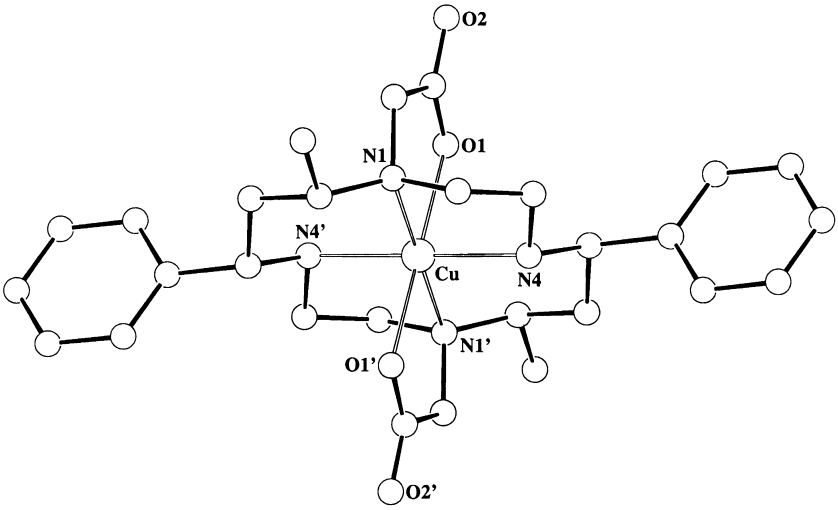

Fig. 26. Molecular view of the [Cu(**39**)] complex [252].

($g_{\parallel} = 2.20$) component [252]. The magnetic moment (1.72 BM per copper center) is close to the spin-only value for copper(II).

More interestingly, the octahedral N_4O_2 coordination of nickel(II) in [Ni(**38**)].HBr.H_2O [250] and [Ni(**39**)].2H_2O (Fig. 27) [258] is achieved by folding

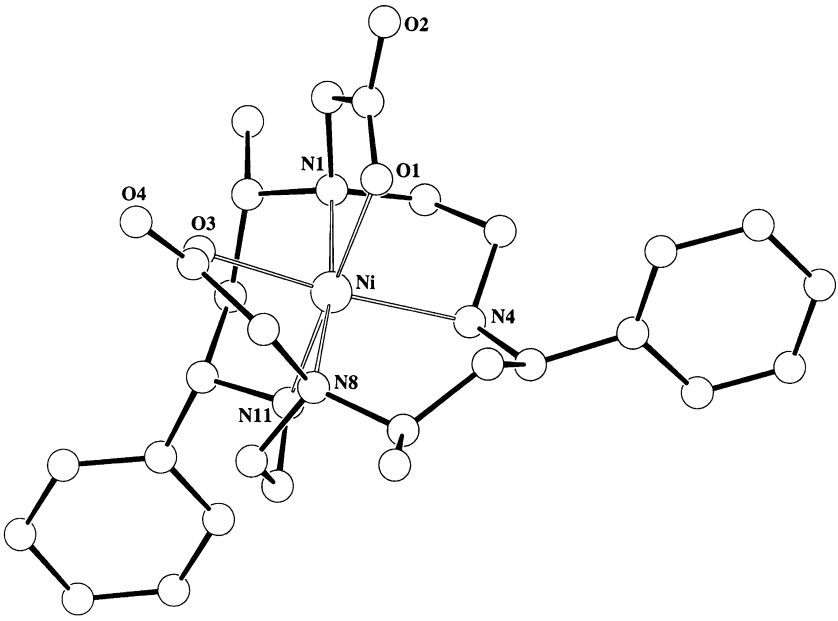

Fig. 27. Molecular view of the [Ni(**39**)] complex [258].

the macrocycle along the N1–Ni–N8 axis into a *cis*-V conformation. Xu et al. [250] assigned the switch from a *trans*-III to a *cis*-V conformation to the peculiar stereochemical features of ligand **38**. This is obviously not the only factor, since the geometry depends also on the nature of the metal ion. The nickel–tertiary nitrogen atom bonds are surprisingly shorter [2.073(3) Å for [Ni(**38**)] and 2.06(1) Å for [Ni(**39**)]] than those involving the secondary nitrogen atoms [2.099(8) Å for [Ni(**38**)] and 2.10(1) Å for [Ni(**39**)]]. Xu et al. [250] tentatively explained this unusual inversion by inductive effects of the electron-withdrawing acetate groups. Since this elongation is only observed in nickel(II) complexes of ligands **38** and **39**, this argument does not hold. More likely, the unusual bond-length pattern is a consequence of the *cis*-V conformation. The Ni–O distances are shorter when compared with the corresponding Cu–O bonds due to the absence of Jahn–Teller elongation [2.199(5) and 2.065(3) Å for [Ni(**38**)], and 2.104(7) and 2.051(5) Å for [Ni(**39**)]].

4.4. Trisubstituted acetate derivatives

Riesen et al. [149] reported the preparation of [In(**40**)].$4H_2O$. The heptacoordinated complex was obtained in water maintained at 40 °C and pH 4 by reacting equimolar amounts of In^{3+} and H_4**40**, although potentiometric titrations showed that [Im(**40**)] is formed in 10^{-2} M acidic medium. Despite its high stability ($\log \beta > 25$), the complex is dissociated in vivo as indium is picked up by transferrin.

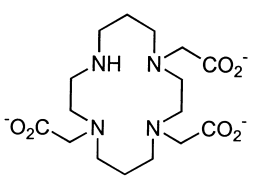

40

The X-ray structure resembles that described for the 12-membered [In(DO3A)] analog, despite a larger dispersion of the In–N bond lengths [2.43(3) and 2.266(5) Å for the tertiary and secondary nitrogen atoms compared with 2.37(3) and 2.314(8) Å for [In(DO3A)], respectively]. Moreover, a nonplanar arrangement of the four nitrogen atoms [mean deviation = 0.29 Å compared with 0.016 Å for [In(DO3A)]] is also responsible for a less compact and less symmetrical situation around the metal center. The In^{3+} cation is located at 0.98 and 1.46 Å from the four nitrogen atom and the three oxygen atom planes, respectively, while the cation lies almost half way between both planes in [In(DO3A)] (1.18 and 1.39 Å, respectively).

4.5. Tetrasubstituted acetate derivatives

4.5.1. Protonation scheme

The structure of H_4TETA.$6H_2O$ (Fig. 28) has been described independently by Maurya et al. [259] and by Spirlet et al. [260].

The macrocyclic ring, centered on a crystallographic inversion site, adopts a rectan-

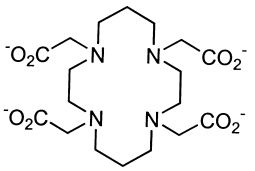

$TETA^{4-}$ **41**

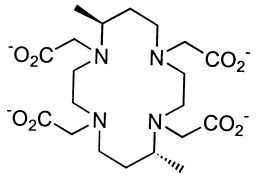

42

gular (3,4,3,4)-B conformation, where C3 and C7 lie at corner positions. The H_4TETA ligand is a double zwitterion made of two $NH^+CH_2CO_2^-$ and two NCH_2CO_2H groups, respectively. The protonated carboxylic arms attached to the unprotonated N1 atoms are hydrogen-bonded to the O3 atom of an adjacent molecule. The protonated N4 atoms are in the *trans* position, reducing the electrostatic repulsion. The carboxylate O3 and O4 atoms remain unprotonated. The proton linked to N4 defines a four-center hydrogen bond network, involving O3 [N4···O3 = 2.704(4) Å, N4–H···O3 = 101(3)°], N1 [N4···N1 = 2.974(3) Å, N4–H···N1 = 105(3)°], and two water molecules above and below the ring as acceptor atoms [N4–H···N1 = 2.978(3) Å, N4–H···W = 159(3)°]. The latter oxygen atoms are also

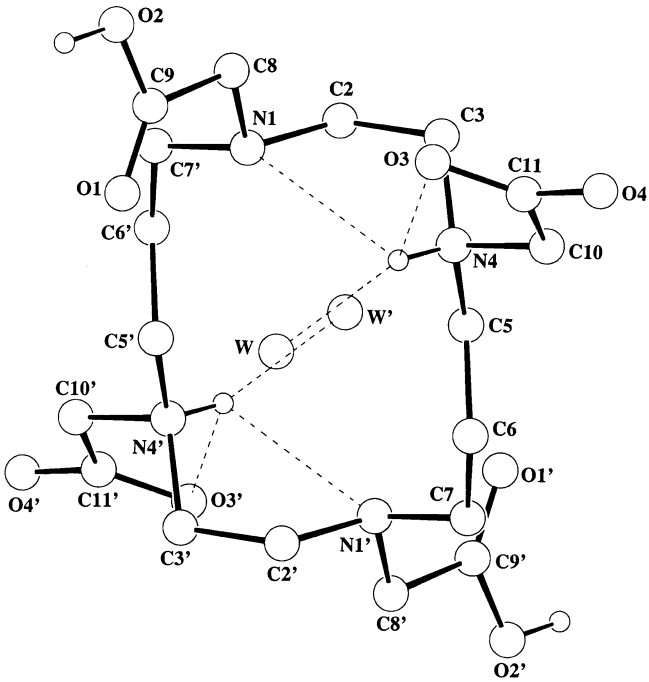

Fig. 28. Molecular view of the free H_4TETA ligand [259,260]. The four-center hydrogen bonds are indicated by dashed lines.

involved as donors in two other hydrogen bonds with O1 and another cocrystallized water molecule.

Consistently, the IR spectra of H_4TETA and H_4**42** (*meso*-5,12-dimethyl-1,4,8,11-tetrakis(carboxymethyl)-1,4,8,11-tetraazcyclotetradecane) exhibit two strong carbonyl bands at 1600–1630 and 1695–1730 cm^{-1} typical for COO^- and COOH groups, respectively, and one characteristic NH^+/OH intercombination band (2500–2600 cm^{-1}) [80,259,261]. In the fully protonated H_4**42**.4HCl ligand, only one asymmetric carboxyl stretching mode is observed at 1725 cm^{-1} [261].

^{1}H NMR studies in D_2O demonstrate that the protonation sequence of $TETA^{4-}$ (Table 1) is similar to that reported for $DOTA^{4-}$ [134,138]. The two first protonation sites are two nitrogen atoms located in a *trans* position, followed by two pairs of *trans* acetate moieties. Based on the structural data of H_4TETA, the strongly acidic character of two of the tertiary amines can be attributed to electrostatic repulsion and hydrogen bonding effects. Fig. 29 shows the distribution curves of the various protonated species of TETA using the protonation constants reported in Table 1.

4.5.2. Structural characteristics of earth-alkaline–metal complexes

Earth-alkaline–metal complexes of TETA provide an interesting type of coordination [259]. The preparation in strongly basic conditions of a binuclear $[Ca_2(TETA)].3H_2O$ complex in which all acidic functionalities are deprotonated has been reported [259]. However, the reaction of stoichiometric amounts of ligand with magnesium, calcium or strontium chloride in water at pH values where the predominant ligand species is H_2TETA^{2-} (pH 6.0–8.7) yields a white solid of formula $[M(H_2TETA)].2H_2O$. Infrared data are consistent with the presence of protonated amine sites and deprotonated carboxylate functions. The solid-state structure of $[Mg(H_2TETA)(H_2O)_4].4H_2O$ (Fig. 30) is centrosymmetric with the magnesium cation lying on one inversion center. The coordination of the Mg^{2+} cation does not involve macrocyclic nitrogen atoms, but occurs exclusively through two laterally

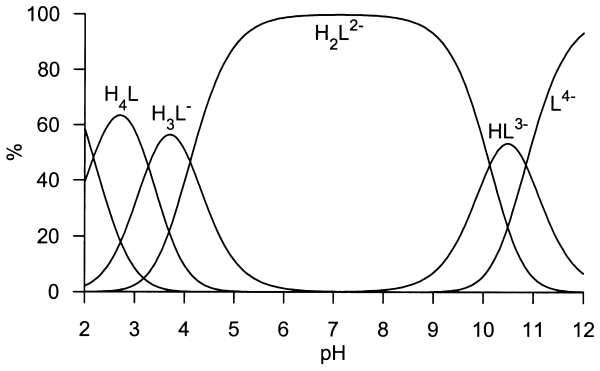

Fig. 29. Distribution diagram of the protonated species of TETA in water according to the protonation constants listed in Table 1. I=0.1 [$N(CH_3)_4Cl$] and 25 °C.

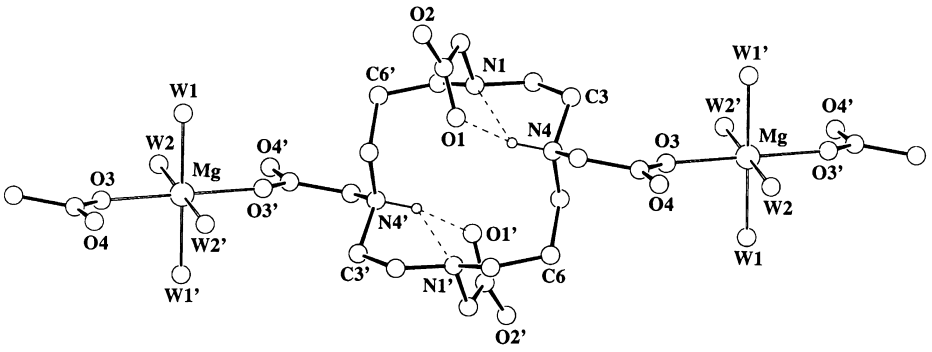

Fig. 30. Molecular view of the $[Mg(H_2TETA)(H_2O)_4]$ complex [259]. Intramolecular hydrogen bonds are indicated by dashed lines.

extended carboxylate groups [Mg–O3 = 2.028(2) Å], resulting in chains of alternating H_2TETA^{2-} and Mg^{2+} units. The compressed pseudo-octahedral coordination polyhedron of Mg^{2+} is completed by four water molecules [Mg–W = 2.072(4) Å]. Compared with H_4TETA, the quadrangular ring conformation is maintained, but the atoms are located at different positions [(3,4,3,4)-C conformer] since C3 and C6 define "genuine corners". Due to a three-center hydrogen bond between the protonated N4 atom and the N1 and O1 acceptor atoms, the pendant uncoordinated acetate groups are oriented above and below the macrocyclic framework. Additional hydrogen bonds between a W2 water molecule and an O2 acetate oxygen atom from an adjacent molecule further increase the steric hindrance around the macrocyclic cavity.

Interestingly, the $[M(H_2TETA)]$ stoichiometry found in the solid state has not been observed in solution [262], except for beryllium [172]. The only protonated species detected is $[M(HTETA)]^-$ [172]. Since labile complexes undergo rapid exchange on the NMR timescale and since the ligand is involved in rapid protonation equilibria and ring conformation interconversions, the concentration of $[M(H_2TETA)]$ is lower than the detection limits of ^1H NMR spectroscopy [259] and of glass electrode potentiometry [172].

4.5.3. Structural characteristics of transition-metal complexes

The barium salt of the fully deprotonated copper(II) TETA complex has been isolated in a similar way as the corresponding DOTA analog and has been structurally characterized [263]. The asymmetric unit of $Ba[Cu(TETA)].6H_2O$ contains two very similar half molecules where the Cu^{2+} ions lie on inversion centers. The octahedral-distorted coordination polyhedron is made up of the four macrocyclic nitrogen atoms in the equatorial plane and of two oxygen atoms belonging to two carboxyl groups in axial positions. The equatorial Cu–N bond lengths range between 2.023(6) and 2.184(6) Å, the longest bond lengths concerning the nitrogen atoms of the uncoordinated pendant acetate arms. Jahn–Teller distortion leads to an average axial Cu–O bond length of 2.29(1) Å. In the absence of a Jahn–Teller effect

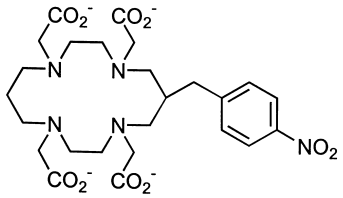

43

(i.e. in [Zn(H_2TETA)]; vide infra), elongation occurs along the N–M–N axis without changing the *trans*-III anangular conformation of the macrocycle.

The structure of [Zn(H_2TETA)].4H_2O is totally different from that of the corresponding DOTA complex in spite of their identical [Zn(H_2L)] stoichiometries [150]. The larger size of the anangular cyclam scaffold allows a *trans*-III octahedral arrangement of the four planar amino nitrogen atoms and of the two axial carboxylate oxygen atoms around the Zn^{2+} ion which is located on an inversion center (Fig. 31). As in [Zn(H_2DOTA)], the octahedron is elongated along the N4–Zn–N4′ axis [Zn–N4 = 2.253(2) Å compared with Zn–N1 = 2.110(2) and Zn–O = 2.127(1) Å]. Both uncoordinated pendant arms bound to N4 and N4′ are protonated and are involved in a hydrogen bond with a water molecule.

The X-ray structure of a C-substituted analog of [Cu(H_2TETA)], [Cu(H_2**43**)].$C_2H_5OH.H_2O$ (**43** = 6-(*p*-nitrobenzyl)-1,4,8,11-tetrakis(carboxymethyl)-1,4,8,11-tetraazacyclotetradecane), shows a coordination polyhedron similar to that of [Zn(H_2TETA)], built up of four tertiary nitrogen and two carboxylate oxygen atoms (Fig. 32) [264].

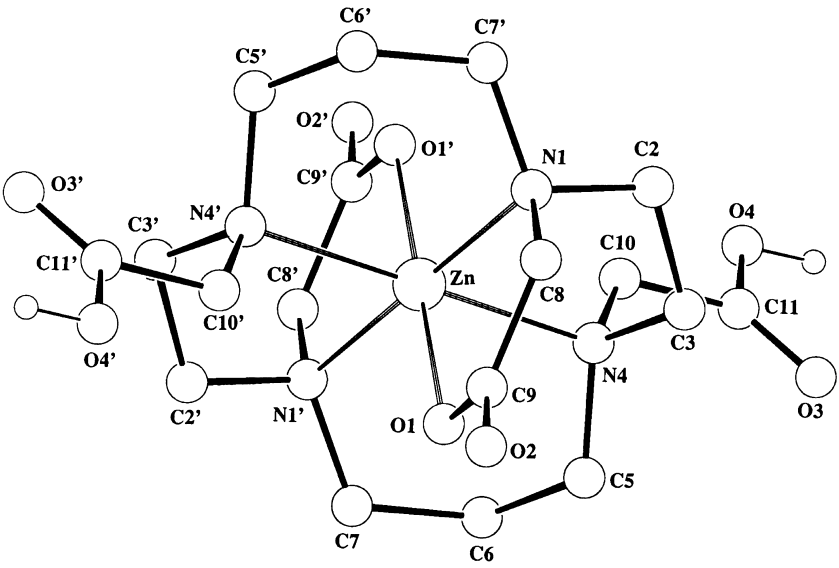

Fig. 31. Molecular view of [Zn(H_2TETA)] [150].

Crystals were obtained at neutral pH in a mixed water–ethanol (3:5 v/v) solvent. Two carboxylate groups attached to N4 and N11 are protonated and extend away from the macrocycle in an anangular *trans*-III conformation. The geometry around the copper atom shows a tetragonal distortion: the Cu–N4 [2.367(6) Å] and Cu–N11 [2.428(6) Å] bonds are elongated relative to the Cu–N1 [1.994(6) Å] and Cu–N8 [2.016(6) Å] bonds. The four donor atoms N1, N8, O1 and O5 lie in a distorted square plane (mean deviation = 0.013 Å) which is almost perpendicular to the N4–N11 axis. The Cu^{2+} cation lies in this plane within 0.016 Å. The stronger Cu–O [2.005(6) Å] interactions compared with those involving two of the four tertiary nitrogen atoms (N4 and N11) is unusual. The 77 K EPR spectrum of frozen [Cu(H_2**43**)] at pH 7 in water exhibits four peaks ($g_{\parallel} = 2.237$, $A_{\parallel} = 160$ G) supporting an approximate D_{2h} symmetry with rhombic distortion. In aqueous solution, deprotonation of both uncoordinated carboxylic side-chains does not alter the N_4O_2 chromophore ($\lambda_{max} = 650$ nm, $\epsilon_{max} = 270\ M^{-1}\ cm^{-1}$ at pH 7 and 12).

Prior to the diffraction studies of [Zn(H_2TETA)] [150], Riesen et al. [80] proposed the same solid-state coordination scheme for [Cu(H_2TETA)], [Ni(H_2TETA)] and [Zn(H_2TETA)] isolated at pH 3.5–4. Typical IR bands at 1600 ($\nu_{C=O}$ for COO^- or $COO^-\cdots M^{2+}$), 1730–1740 ($\nu_{C=O}$ for COOH) and 2500–2800 cm^{-1} (NH^+/OH intercombination bands) suggest the presence of at least one, most probably two, protonated amino groups in the three complexes, indicating that the metal does not actually enter the cavity. Unfortunately, no details concerning the preparation of the [Zn(H_2TETA)] crystals studied by X-ray diffraction is given. An octahedral $N_2O_2(H_2O)_2$ coordination mode has also been inferred in [M(H_2**42**)].xH_2O complexes (M = Co^{2+}, $x = 2.5$; Ni^{2+}, $x = 3$; Cu^{2+}, $x = 2.5$; Zn^{2+}, $x = 4$) [261]. They display IR features similar to those of the related TETA counterparts and solid-state visible absorption spectra resembling those of the corresponding EDDA chelates. Furthermore, the $MN_2O_2(H_2O)_2$ chromophore is not modified on going from MH_2L to ML^{2-} species in solution. The NMR spectrum of the [Zn(**42**)]$^{2-}$ anion

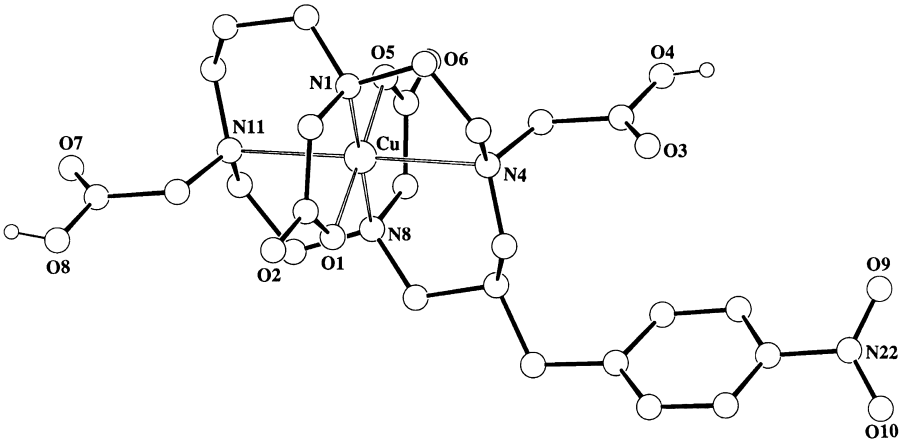

Fig. 32. Molecular view of [Cu(H_2**43**)] [264].

shows that the symmetry of the free ligand is not altered upon complexation, and reveals two distinct carboxylate resonances assigned to free and to coordinated COO^- groups. In the solid state, the IR NH^+/OH intercombination band disappears upon deprotonation.

In aqueous solution, the late transition-metal complexes of TETA undergo protonation, forming MLH and MLH_2 species [172]. Furthermore, the divalent cations have to overcome a high energy barrier in order to insert into the tetraazamacrocyclic plane (thermodynamically stable in-isomer). For kinetic reasons, the metal remains outside the cavity giving rise to an out-isomer, the exact structure of which is unknown. The cation is probably bound to two of the ring nitrogens and to two carboxylate oxygen atoms, as suggested by Kaden et al. [80,261] on the basis of spectral studies. Madeyski et al. [265] assigned the higher stability of the TETA complexes relative to those of tetramethyl or tetrahydroxyethyl cyclam derivatives to a N_2O_2 versus N_4 coordination mode. In–out isomerism has been investigated extensively in the case of nickel. Kimura et al. [266] claimed that the violet out-$[Ni(TETA)]^{2-}$ species formed at pH 7 ($\lambda_{max}=355$ nm, $\epsilon_{max}=25\ M^{-1}\ cm^{-1}$; $\lambda_{max}=575$ nm, $\epsilon_{max}=17\ M^{-1}\ cm^{-1}$) rearranges into the thermodynamically stable *trans*-III in-$[Ni(TETA)]^{2-}$ isomer via electrochemical oxidation to out-$[Ni(TETA)]^-$ at 1.2 V/NHE. Incorporation of the smaller Ni^{3+} cation into the cyclam cavity is followed by reversible reduction at 0.59 V/NHE of the nickel(III) in-species. The latter process was found to be pH-independent between pH 3.5 and 10.5. Repeating the experiment under identical conditions, Ali et al. [267] showed that the one-electron oxidation process consumes ~ 5 Faraday per mole of complex, additionally producing two moles of formaldehyde. They concluded that the formation of nickel(III) species is accompanied by the oxidative decarboxylation of two acetate groups of the TETA ligand, affording dimethylcarboxylate-1,4,8,11-tetraazacyclotetradecane nickel(III) out-isomers which undergo intramolecular rearrangement to in-isomers prior to the electrochemical reduction to nickel(II) complexes. Oxidation of out-$Ni(TETA)^{2-}$ by $^{\cdot}OH$ radicals generated by pulse radiolysis also leads to a decarboxylation reaction and to the formation of a nickel(II) tricarboxylate complex, because $^{\cdot}OH$ radicals act as a single-electron oxidizing agent [267].

Similarly to DOTA, TETA forms a binuclear copper(II) complex when two equivalents of $CuCl_2$ and one equivalent of H_4TETA are refluxed in water at pH 5 before increasing the pH to 7–8 [169,170]. The dark blue $[Cu_2(TETA)H_2O].5H_2O$ crystals have an infinite chain structure (Fig. 33) which is totally different to that of $[Cu_2(DOTA)H_2O].4H_2O$. Two nitrogen and two carboxylate oxygen atoms define the basis of a square-pyramidal coordination polyhedron around each Cu^{2+} center, which is displaced from the N_2O_2 plane by 0.17 (Cua) and 0.22 Å (Cub), respectively. For Cua, the apical position is occupied by a bridging carboxylate group from an adjacent TETA molecule [Cua–O2b = 2.243(7) Å], whereas a water molecule provides the fifth bond to Cub [Cub–W = 2.236(6) Å]. The internuclear Cua–Cua′ and Cub–Cub′ distances are equal to 4.78 and 4.88 Å, respectively. The peculiar coordination geometry gives rise to a type-III configuration of the nitrogen atoms, while the macrocycle exhibits a rectangular (2,5,2,5) conformation with the four nitrogen

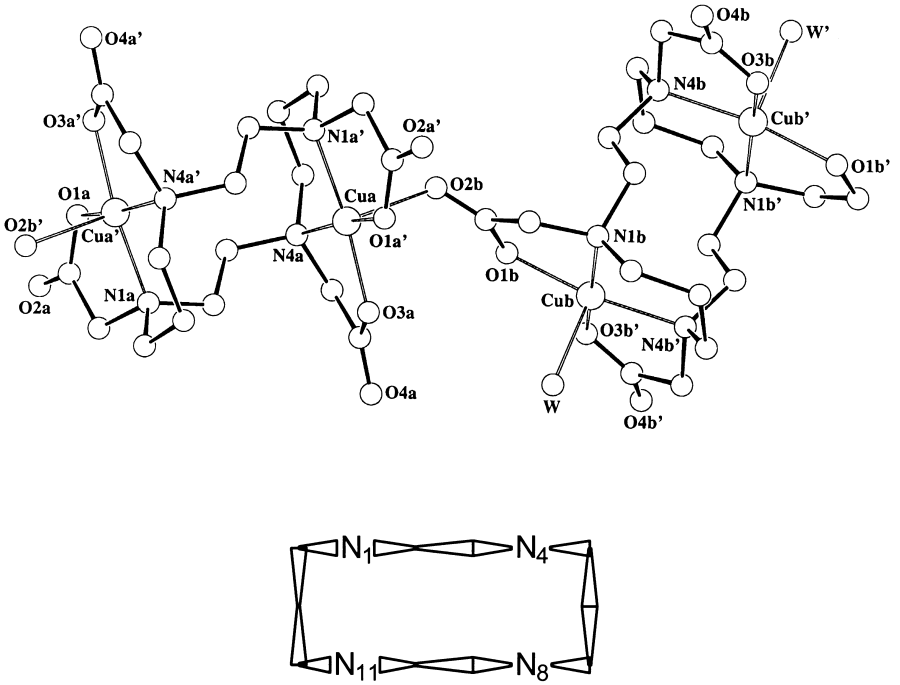

Fig. 33. Molecular view of the binuclear $[Cu_2(TETA)H_2O]$ complex and wedge-type representation of the (2,5,2,5) macrocyclic conformation [170]. Only one unit of the polymer is represented.

atoms in the α-position to the "genuine corners" (Fig. 33). The average values of the τ_1–τ_7 torsion angles are in the order 158.6, −170.1, 69.8, 65.0, −66.2, −68.8 and 169.7^0. This highly strained conformation [88] has only been observed in the dinuclear $[Cu_2(TETA)H_2O]$ and in the related $[Cu_2(\mathbf{43})H_2O]$ complexes (see below). The presence of two distinct types of acetate carbonyl functions gives rise to two IR stretches at 1610 and 1640 cm^{-1}. The different set of donor atoms in $[Cu_2(DOTA)H_2O]$ (2 N_{eq}, 2 O_{eq} and 2 N_{ax}) and $[Cu_2(TETA)H_2O]$ (2 N_{eq}, 2 O_{eq} and 1 O_{ax}) is responsible for a 100 nm blue shift of the absorption maximum corresponding to the d–d transition of $[Cu_2(TETA)H_2O]$ in water.

The polymeric binuclear copper(II) complex of ligand **43** differs from $[Cu_2(TETA)H_2O]$ by a different linkage pattern between each unit [264]. Mixing $H_2\mathbf{43}^{2-}$ with 2.8 equivalents of copper(II) acetate at pH 7 in water yields a precipitate which filtered out, dissolved in dilute NaOH (pH 12) and neutralized with formic acid affords $[Cu_2(\mathbf{43})H_2O].7H_2O$ crystals. In contrast to $[Cu_2(TETA)H_2O]$, each unit in the polymer is identical to the others. Both copper cations, situated above and below the plane of the four nitrogen atoms (Fig. 34), are coordinated in a distorted square-pyramidal fashion by two nitrogen and two carboxylate atoms. The fifth apical donor is either a water molecule [Cu1–W = 2.274(8) Å] located farthest away from the nitrobenzyl group or a carboxylate oxygen atom [Cu2–O8′ =

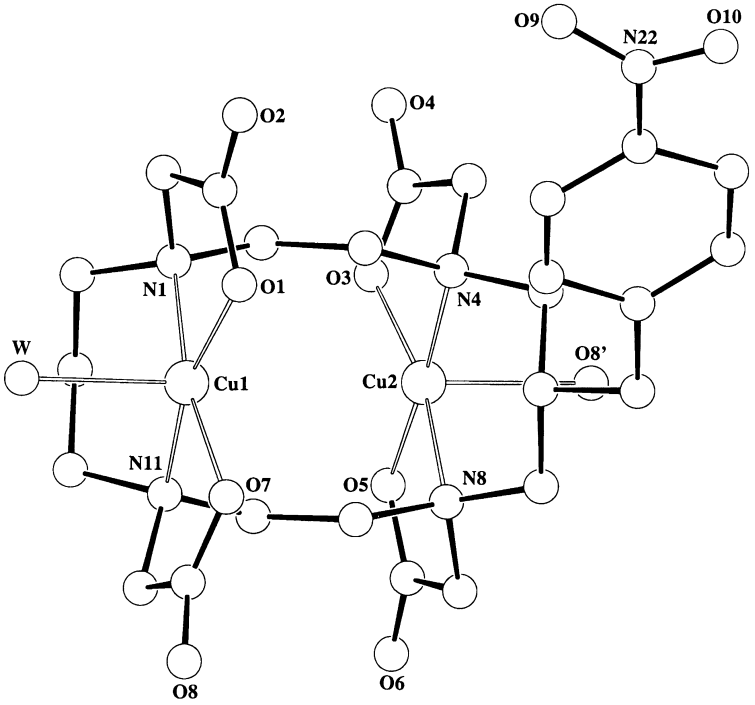

Fig. 34. Molecular view of the binuclear $[Cu_2(\mathbf{43})H_2O]$ complex [264]. Only one unit of the polymer is represented.

2.312(7) Å] from an adjacent unit. The steric hindrance introduced by the *p*-nitrobenzyl substituent induces a stronger distortion of the base of the square pyramid around Cu2 compared with Cu1: the mean deviation of the four nitrogen atoms from their least-squares plane equals 0.08 Å for Cu2 as compared with 0.02 Å for Cu1. The internuclear Cu1–Cu2 distance (4.83 Å) is similar to that measured for $[Cu_2(TETA)H_2O]$. Binuclear copper(II) and nickel(II) complexes of ligand **42** have also been formed in acidic (pH 2.5) aqueous solutions [261]. The polymeric nature of these nonelectrolytes is supported by conductivity measurements. The proximity of two Cu^{2+} centers leads to antiferromagnetic coupling.

4.5.4. Structural characteristics of lanthanide metal complexes

Increasing the ring size from 12 to 14 atoms induces important changes in the coordination properties of the corresponding tetraacetate sequestrants. In the $Na[Tb(TETA)].6H_2O.0.5NaCl$ complex, obtained by slow diffusion of ethanol into an aqueous solution of the complex at pH 6.8 [268], the ligand wraps around the terbium, forming a tight shell. Compared with the DOTA–lanthanide structures, both the coordination polyhedron and the tetraaza ring conformation are markedly altered (Fig. 35). The Tb^{3+} cation, owing to a complete deprotonation of the TETA ligand, is eight-coordinated to the four nitrogen atoms, and to one oxygen atom of

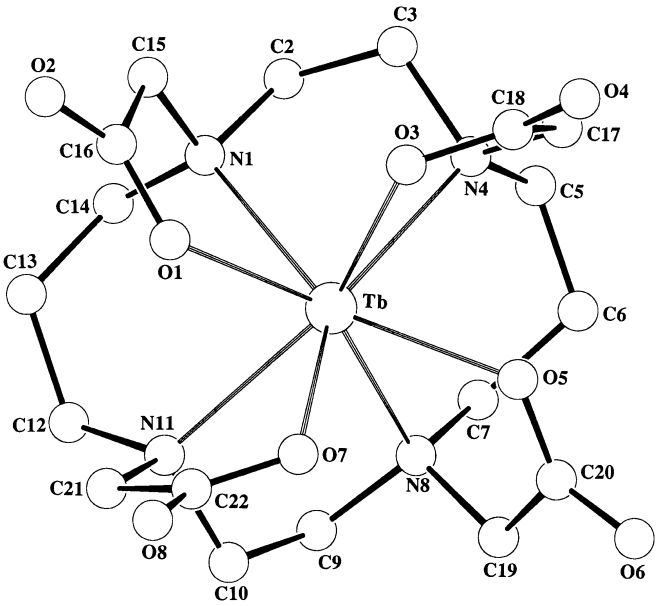

Fig. 35. Molecular view of $[Tb(TETA)]^-$ down the approximate C_2 axis [268].

each of the four carboxyl groups. Two *trans* located nitrogen atoms (N1 and N8) lie below the four nitrogen-atom mean plane, while the other pair (N4 and N11) are located above. Similarly, the oxygen atoms split into two groups with O1 and O5 below, and O3 and O7 above the oxygen atom mean plane, but all of them occupy the top vertices of the pseudo-dodecahedron. The metal center is located about half way between the four oxygen and the four nitrogen-atom mean planes [1.212(1) and 1.239(1) Å, respectively]. Since the distances between the coordinated oxygen atoms [2.786(4) and 2.842(4) Å] are close to twice the van der Waals radius of oxygen (1.40 Å [269]), there is no space left in the first coordination shell for a ninth ligand. The resulting coordination polyhedron is no longer a square antiprism, but is best described in terms of a severely distorted dodecahedron of C_2 symmetry. Compared with $[Eu(DOTA)H_2O]^-$, the shorter Tb–O and Tb–N bond lengths, ranging between 2.302–2.330 and 2.575–2.620 Å, respectively, reflect the difference in coordination number. The higher flexibility of TETA gives rise to less important deformation of the cycle which adopts the (7,7)-F biangular conformation. The folding of the acetate chains with regard to their position in the free ligand structure induces a rearrangement of the cyclic amine. Indeed, in the case of a (3,4,3,4) conformation, it is not possible to obtain a configuration where all nitrogen atoms are located on the same side of the cycle mean-plane (i.e. the *trans*-I configuration). Consequently, the macrocycle in the $[Tb(TETA)]^-$ complex adopts a (7,7) conformation.

In the absence of crystallographic data for other lanthanide–TETA complexes, information on structure and dynamics was gained by fluorescence and NMR

measurements in neutral aqueous solutions [195,270]. Observing two $^5D_0 \rightarrow {}^7F_0$ and three $^5D_0 \rightarrow {}^7F_1$ transitions in the luminescence spectrum of $[Eu(TETA)]^-$, Bryden and Reilley [195] suggested that two low-symmetric forms of this complex exist in solution. However, the minor species could not be detected by ^1H NMR spectroscopy along the entire lanthanide series, precluding further characterization [270]. In turn, the structure and the dynamic behavior of the major species is critically dependent on the size of the encapsulated metal ion. Lanthanides of large ionic radii, like Pr^{3+} ($r_i = 1.126$ Å for CN = 8), give rise to highly asymmetric conformations in which all protons become chemically and magnetically inequivalent at low temperatures (−55 °C for $[Pr(TETA)]^-$) [270]. At room temperature, the $[Pr(TETA)]^-$ complex exchanges rapidly according to a rearrangement process which is different from that observed for $[Eu(TETA)]^-$ or $[Lu(TETA)]^-$, but the exact mechanism is not yet understood. From Eu^{3+} to Lu^{3+}, the strong distortion of the dodecahedral coordination geometry, found in the solid state for $[Tb(TETA)]^-$, also accounts for an effective C_2 symmetry in solution. In spite of some stereochemical rigidity at low temperature, dynamic processes arise from an exchange between two equivalent dodecahedral geometries. While limited motions of the ligating atoms change the dodecane ring configuration of the DOTA complexes, a complete molecular rearrangement occurs for the heavy lanthanide complexes of TETA. It proceeds through a simultaneous up and down translation of the chelate rings which exchanges the ligated atoms lying below with those located above the four nitrogen-atom and the four oxygen-atom mean planes, respectively. The dynamic process is equivalent to a rotation of 90° along the C_2 axis and is characterized by an activation free energy of 64(8) kJ mol^{-1} at 25 °C for $[Lu(TETA)]^-$ [270]. Although Kepert's theoretical calculations predict a significantly higher repulsion energy for a dodecahedral geometry than for a square-antiprismatic one [271], the late lanthanide cations form complexes of similar rigidity with both the 12-membered DOTA and the 14-membered TETA ligands.

4.6. Tetrasubstituted propionate derivatives

4.6.1. Protonation scheme

Like $TETA^{4-}$, $TETP^{4-}$ (1,4,8,11-tetrakis(2-carboxyethyl)-1,4,8,11-tetraazacyclotetradecane) has eight different protonation states. Four of them (Fig. 36), the di-, tetra-, penta- and octaprotonated forms have been studied by X-ray diffraction [272,273].

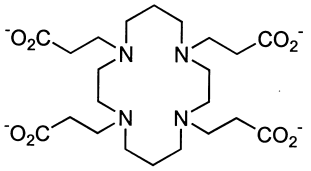

44 $TETP^{4-}$

The crystal structure of $Na_2[H_2TETP].16H_2O$ reveals that two nitrogen atoms in the *trans* position (N4 and N4′) are protonated [273], as already mentioned for other macrocyclic aminocarboxylates. The NH–C bond distances are on average longer than those involving the nonprotonated N1 and N1′ nitrogen atoms [1.503(4) and 1.470(4) Å, respectively]. The four propionate groups are deprotonated, the

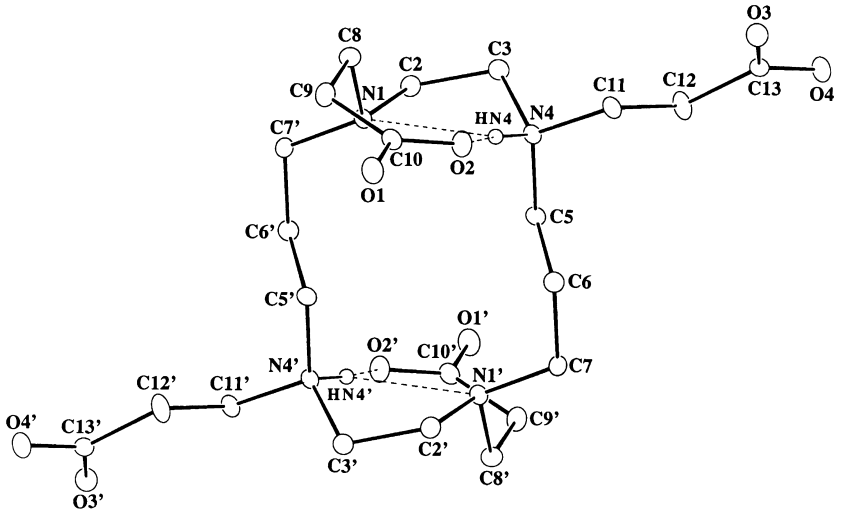

(a)

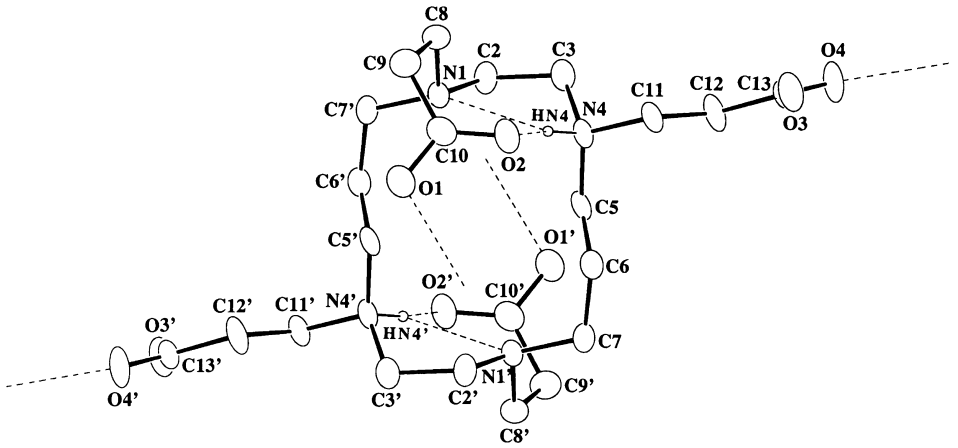

(b)

Fig. 36. ORTEP diagrams of (a) H_2TETP^{2-}, (b) H_4TETP, (c) H_5TETP^{+} and (d) H_8TETP^{4+} [272,273]. The thermal ellipsoids for non-hydrogen atoms are represented at 50% [(a) and (d)], or 40% [(b) and (c)] probability. Intramolecular hydrogen bonds are indicated by dashed lines.

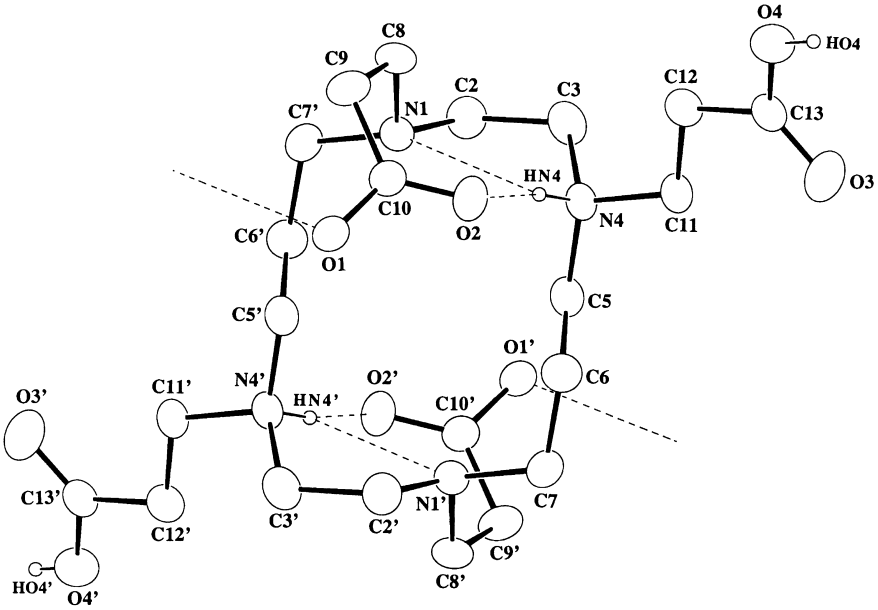

(c)

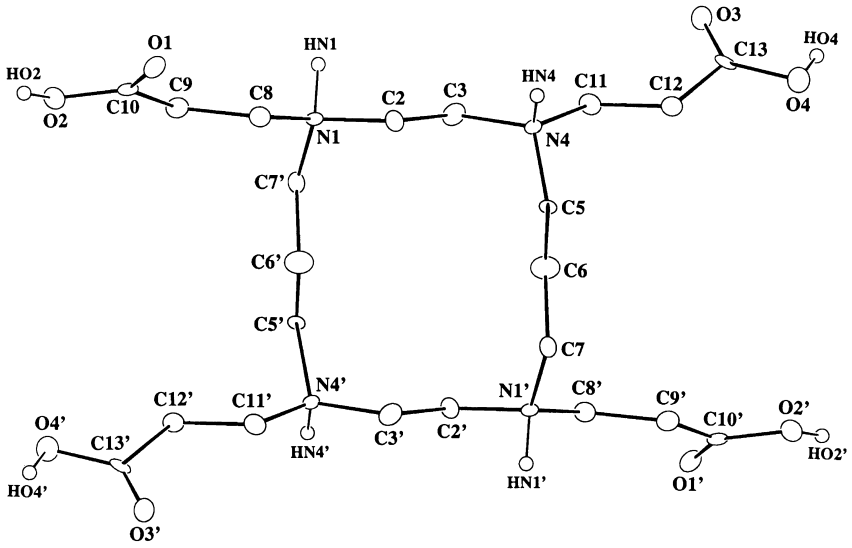

(d)

Fig. 36. (*continued*).

C–O bond lengths being almost equal [1.262(6) Å]. A very similar structure has also been reported for the iodide salt of the diprotonated form of the tetramethyl ester derivative of TETP [274].

The proton distribution in the neutral $H_4TETP.7H_2O$ species is more surprising [272]. In the crystal state, the protonation of both N4 and N4′ nitrogen atoms in the *trans* position is clearly established. However, it was not possible to draw a conclusion about the protonation state of the propionate groups by inspection of the differences between the C–O bond lengths [C10–O1 = 1.276(7), C10–O2 = 1.244(8); C13–O3 = 1.211(9), C13–O4 = 1.290(7) Å]. Furthermore, no hydrogen atom was found in difference electron density maps in the immediate vicinity of the carboxyl oxygen atoms. Examination of the intermolecular O···O distances in the crystal packing revealed two very short intermolecular contacts involving the O1 and O4 oxygen atoms: $O1(x,y,z)\cdots O1(-x,1-y,1-z) = 2.460(8)$ Å and $O4(x,y,z)\cdots O4(2-x,-y,-z) = 2.45(1)$ Å. These very short intermolecular distances are in keeping with the location of a single hydrogen atom along the O1(O4)···O1(O4) axes, equidistant or not from both oxygen atoms, forming a hydrogen bond. A "tandem" hydrogen bond, as defined by Jeffrey and Saenger [137], cannot occur as a result of the short O···O distances (2.45 Å). Indeed, "tandem" hydrogen bonds are characterized by nonbonded H···H interactions, which are much shorter than van der Waals contacts (2.40 Å [269]) and thus require O···O distances greater than 3 Å. More probably, the O···H···O system may be described by a half negative charge per carboxyl group. Thus, the two positive charges due to the protonation of N4 and N4′ and the four half negative charges brought by the four carboxylate units give rise to a neutral H_4TETP species.

In the crystal structure of the centrosymmetric $[H_5TETP]ClO_4$ compound [Fig. 36(c)], the N4 nitrogen atoms are protonated with N–C bond distances averaging 1.503(6) Å for N4 and 1.476(8) Å for N1 [272]. The propionate groups borne by these nitrogen atoms are also protonated, as shown by the short C13–O3 [1.202(5) Å] and the long C13–O4 [1.304(4) Å] bonds. For the two other carboxyl groups, the difference between the short and the long C–O bonds is slightly smaller [C10–O1 = 1.288(3) Å and C10–O2 = 1.220(4) Å], and no hydrogen atom was found in Fourier difference synthesis. The O1 atom is also involved in an intermolecular hydrogen bond which is identical to those described in H_4TETP [O1···O1 = 2.456(4) Å].

The cyclam skeletons of H_2TETP^{2-}, H_4TETP and H_5TETP^{+} possess a quadrangular (3,4,3,4)-B conformation with a methylene group located at each corner of the macrocycle, giving rise to an endodentate geometry. In these three forms of TETP, two of the propionate groups are extended outside of the ring, whereas the others two are folded above and below the cavity and are involved in intramolecular three-center hydrogen bonds between the N4–HN4 donor group and the O2 and N1 acceptors [275]: the sum of the three angles N4–HN4···O2, N4–HN4···N1 and O2···HN4···N1 is equal to 360, 360, and 359° for H_2TETP^{2-}, H_4TETP and H_5TETP^{+}, respectively.

In the centrosymmetrical crystal structure of $[H_8TETP]Cl_4.2H_2O$ [272], the protonation of all nitrogen and carboxylate oxygen atoms leads to identical N–C bond

lengths [1.514(9) Å] and to typical C–O [1.32(1) Å] and C=O [1.20(1) Å] distances. All protons bonded to nitrogen and oxygen atoms were clearly located in difference Fourier maps. The macrocycle also adopts a (3,4,3,4) conformation, as in H_2TETP^{2-}, H_4TETP and H_5TETP^{+}, but in this case each corner is occupied by a nitrogen atom, affording an exo or (3,4,3,4)-A geometry. This conformational change avoids steric repulsion between the HN1 and HN4 hydrogen atoms: simple geometric calculations for an endo orientation with N–H = 1.0 Å and H–N–C = 110° shows that the HN1···HN4 distance (1.9 Å) would be considerably shorter than the sum of the van der Waals radii. In addition, the N1···N4 distance [2.83(2) Å on average for H_2TETP^{2-}, H_4TETP and H_5TETP^{+}] would also be too short for two positively charged nitrogen atoms. Consequently, the exodentate conformation reduces both the steric and electrostatic repulsions, the shortest distance between two protonated nitrogen atoms being 3.82 Å. Moreover, the folding of any propionate group towards the inside of the ring becomes sterically impossible because of this arrangement. This uncommon quadrangular exo (3,4,3,4,)-A conformation confirms the great flexibility of the 14-membered tetraazamacrocycle, and is found in tetra-protonated cyclam.

The protonation scheme of the TETP ligand in the solid state is illustrated in Fig. 37. The two first protonation sites are two nitrogen atoms in *trans* position, giving rise to the H_2TETP^{2-} diprotonated form of the ligand. The intramolecular hydrogen bonds play an important role in stabilizing the flexible scaffold. In contrast to TETA, the propionate arm borne by the N4 protonated nitrogen atom does not fold up towards the cavity to form a N4–HN4···O intramolecular hydrogen bond. In turn, the propionate groups attached to the unprotonated N1 and N1′ nitrogen atoms are folded towards the inside of the ring and are hydrogen bonded, maintaining a (3,4,3,4)-B scaffold conformation. Based on the protonation scheme established for DOTA and TETA, it is likely that the third protonation occurs on a carboxylate oxygen atom appended to an unprotonated amine site. However, the crystal structures of H_2TETP^{2-} and H_4TETP suggest that the protonation is in competition with the two intramolecular hydrogen bonds HN4···O2 and HN4′···O2′ which gives rise to a half protonation of each of these two propionate chains in H_3TETP^{-}. At this stage, the protonation of the propionate arms attached to both protonated nitrogen atoms N4 and N4′ becomes more favorable than that involving the two remaining groups and all propionate chains are half-protonated in H_4TETP. The structure of H_5TETP^{+} indicates that the fifth protonation step corresponds to the full protonation of the propionate arms linked to the quaternary N4 and N4′ atoms. Thus, the four carboxylate groups are protonated in the hexaprotonated species. Finally, the octaprotonated form is associated to the protonation of the two remaining nitrogen atoms.

In solution, the protonation scheme of $TETP^{4-}$ is different since the neutral H_4TETP form observed by X-ray crystallography cannot exist in solution: either the carboxylate arms bound to the protonated nitrogen atoms or those bound to the unprotonated nitrogen atoms must be protonated. The latter possibility is likely due to a lower electrostatic repulsion between the negative charges. The protonation

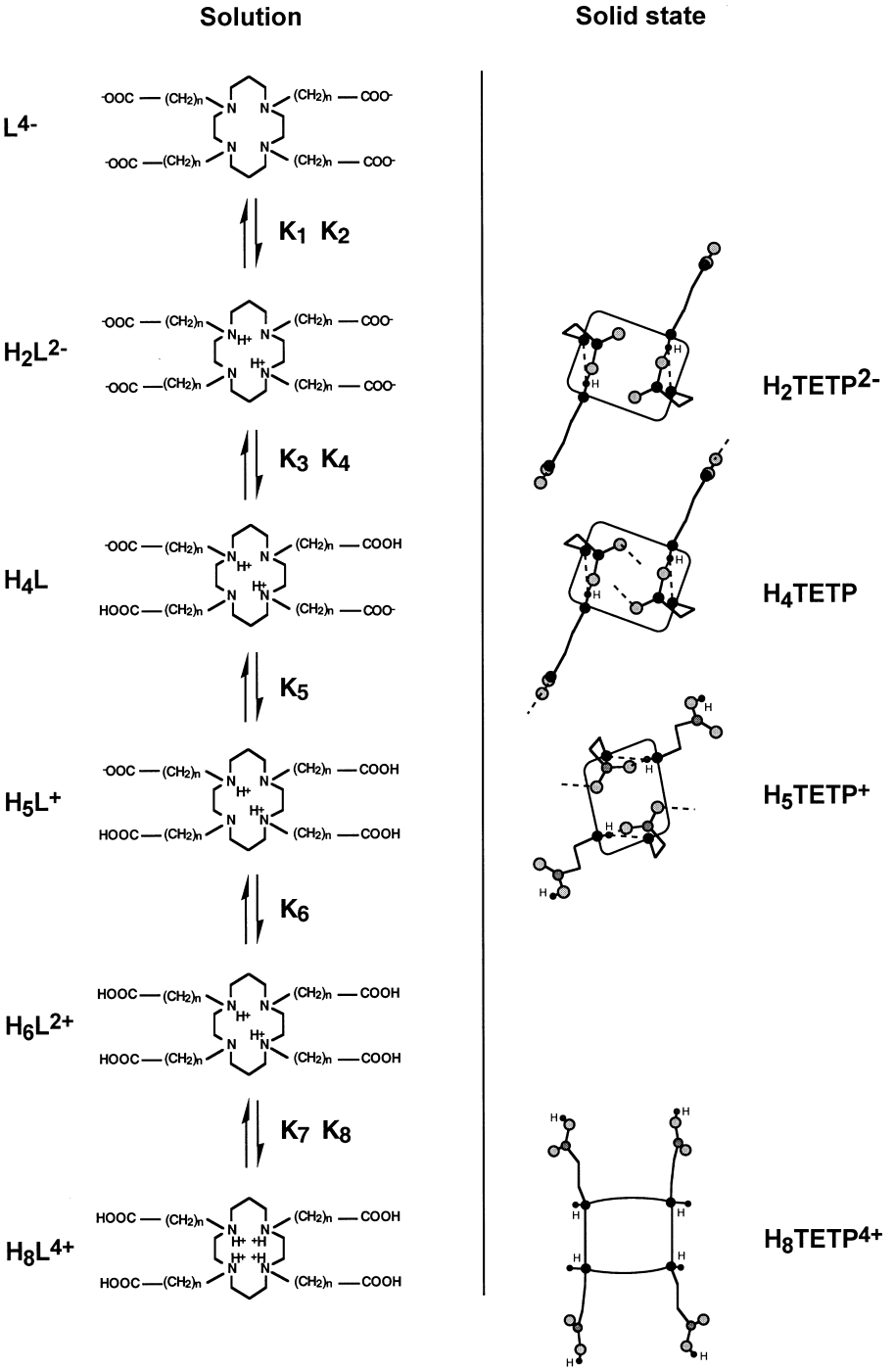

Fig. 37. Schematic representation of the protonation pattern of $TETP^{4-}$ in solution and in the solid state.

constants of $TETP^{4-}$ are listed in Table 1 and the corresponding distribution diagram of the various protonated species is represented in Fig. 38.

4.6.2. Structural characteristics of lanthanide metal complexes

The pH influence on the coordination mode of the TETP ligand with respect to three lanthanide(III) cations (cerium, europium and gadolinium) has been investigated by means of pH-controlled crystallization and X-ray diffraction studies (Ref. [81] and V. Dahaoui-Gindrey, C. Lecomte, F. Barbette, P. Pullumbi, C. Gros, R. Guilard, unpublished results). Contrary to the coordination schemes of DOTA and TETA, TETP does not encapsulate the lanthanide cation via its four nitrogen atoms and its four carboxylate groups. The formation of six six-membered chelate rings is not favored (see Section 5.4) and the metallic ions are coordinated only by oxygen atoms belonging to four different macrocyclic ligands as shown in Fig. 39. Furthermore, two different coordination modes of the TETP ligand have been identified, depending on the predominant protonated ligand species present during crystallization.

Following the standard procedure outlined in Section 3.5.1, crystals of $[Ce(H_2TETP)(H_2O)(OH)].10H_2O$ were prepared by reacting equimolar aqueous solutions of H_4TETP and $Ce(NO_3)_3.6H_2O$ [81]. A pH increase from 3.2 to 4.4 at the end of the reaction was observed as Ce^{3+} was coordinating the ligand. According to Fig. 38, the major ligand species in equilibrium at the beginning of the reaction was H_4TETP. As shown in Fig. 39(a), four TETP molecules are linked to the cerium ion via their extended bidentate propionate groups situated in the four nitrogen atom mean plane. Two of them participate in the coordination polyhedron by both carboxylate oxygen atoms [Ce–O3 = 2.624(6) Å, Ce–O4 = 2.613(6) Å], whereas the two others are coordinated to the metallic ion by only one oxygen atom [Ce–O4 = 2.437(5) Å]. The O4 oxygen atom acts as a bidentate coordinate, bridging two cerium ions related by an inversion center. The coordination polyhedron of the eight-coordinated Ce^{3+} is completed by one hydroxyl ion and one water molecule

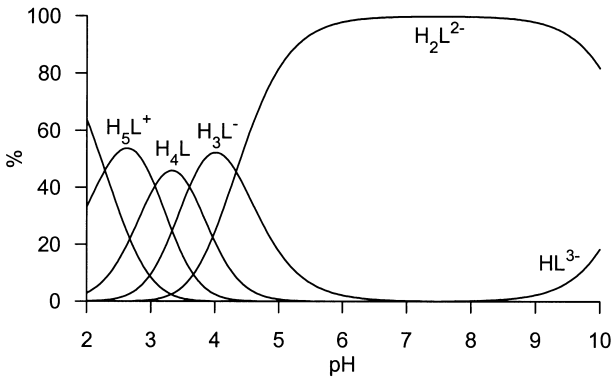

Fig. 38. Distribution diagram of the protonated species of TETP in water according to the protonation constants listed in Table 1. $I = 0.1$ (KCl) and 25 °C.

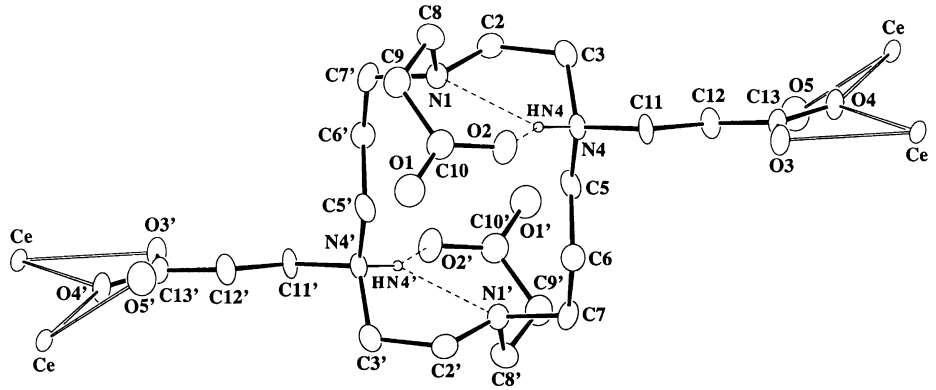

(a)

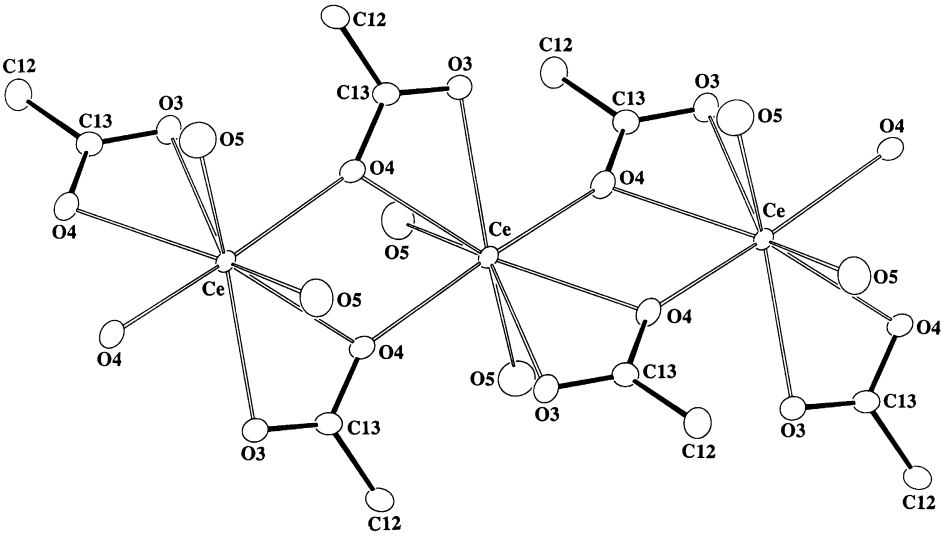

(b)

Fig. 39. ORTEP representations of the crystal structures of (a) $[Ce(H_2TETP)(H_2O)(OH)]$ [81] and (c) $[Ce(H_2TETP)]^+$ in $[Ce(H_2TETP)(H_2O)_3(NO_3)].3H_2O$ (V. Dahaoui-Gindrey, C. Lecomte, F. Barbette, P. Pullumbi, C. Gros and R. Guilard, unpublished results). Views (b) and (d) show the coordination polyhedron of the cerium ion in the $[Ce(H_2TETP)(H_2O)(OH)]$ and in the $[Ce(H_2TETP)(H_2O)_3(NO_3)]$ complexes, respectively. Thermal ellipsoids for non-hydrogen atoms are represented at 40% probability. Intramolecular hydrogen bonds are indicated by dashed lines.

or by two water molecules [Fig. 39(b)]: unfortunately, the resolution cannot distinguish both models. The structure of this complex, where the metallic ion is only coordinated via carboxylic oxygen atoms of only two of the four functionalized chains, is similar to that described for the $[Mg(H_2TETA)]$ complex [259].

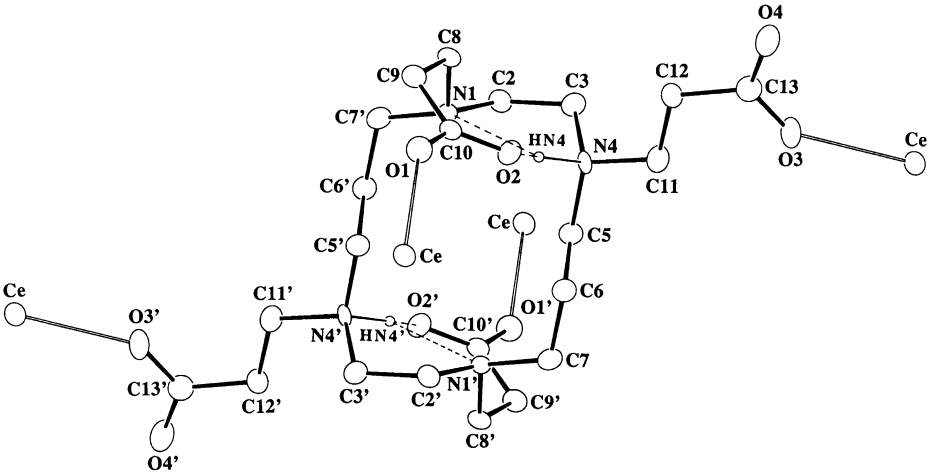

(c)

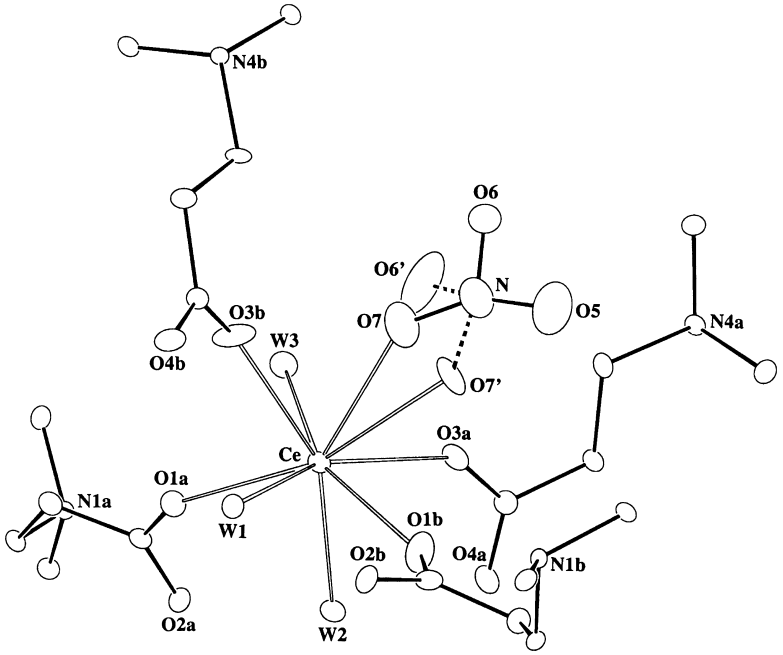

(d)

Fig. 39. (*continued*).

The crystal structures of $[M(H_3TETP)(H_2O)_4](OH)_2.H_2O$ (M = Eu, Gd) [81] and $[Ce(H_2TETP)(H_2O)_3(NO_3)_1.3H_2O$ (V. Dahaoui-Gindrey, C. Lecomte, F. Barbette, P. Pullumbi, C. Gros, R. Guilard, unpublished results) [Fig. 39(c) and (d)] clearly indicate that the coordination scheme of TETP is critically dependent on the pH of the complexation reaction. In the case of the gadolinium(III) and europium(III) complexes, the reaction was performed in solutions buffered at pH 3.5–3.8 where H_4TETP and H_3TETP^- represent each about 40% of the total ligand concentration (Fig. 38). The second form of the cerium(III) complex has been isolated according to the same protocol used for $[Ce(H_2TETP)(H_2O)(OH)].10H_2O$, except that the pH was maintained at 7 during the reaction. Under these conditions, the ligand species which predominates is the diprotonated H_2TETP^{2-} form, actually found in the crystalline state of the complex. The coordination scheme observed for these three complexes is similar, with the four functionalized chains of the ligand involved in the coordination polyhedron by only one of the two oxygen atoms of the carboxylate groups. The metal cations are eight-coordinated, the coordination sphere being completed either by four oxygen atoms assigned to water molecules in the case of gadolinium(III) and europium(III), or by three solvate water molecules and one oxygen atom from a disordered NO_3^- ion for the cerium(III) complex [Fig. 39(d)]. The different pH conditions employed during the synthesis may account for the distinct stoichiometries observed for these three complexes. Since the TETP macrocyclic cavity does not bind to the metal center, the cyclam skeleton adopts the same (3,4,3,4)-B quadrangular conformation as the free ligand. The torsion angles are not significantly modified upon complexation. Similar to the di-, tetra- and pentaprotonated forms of the free TETP ligand, both propionate arms linked to the protonated nitrogen atoms are extended outwards, whereas the two other functional groups are folded inwards and are involved in an intramolecular three-center hydrogen bond between the HN4–N4 donor and the O2 and N1 acceptors. In each of the two five-membered chelate rings, both adjacent substituents are located on the same side of the nitrogen atom mean plane, giving rise to a *trans*-IV configuration, since the molecules are centrosymmetric.

4.7. Carbamoyl derivatives

Few studies are devoted to cyclam derivatives containing amide functionalities. Structural information relative to the copper complex of the monoacetamide derivative **45** (1-carbamoylmethyl-4,8,11-trimethyl-1,4,8,11-tetraazacyclotetradecane) has been gained in solution by IR and absorption spectroscopy [79]. $[Cu(\mathbf{45})]^{2+}$ affords another example of a pH-dependent apical coordination of the single appended side-chain [79]. Axial interaction of the deprotonated amide group through its nitrogen atom has been evidenced by the shift of the $\nu_{C=O}$ stretch in D_2O from 1660 cm^{-1} (pH < 10) to 1580 cm^{-1} above pH 10 and by the bathochromic shift of the d–d band, typical for addition of a fifth axial ligand to a CuN_4 chromophore [204,276].

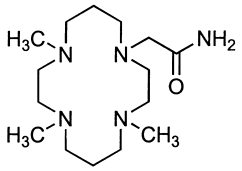

45

So far, only two structures of metal complexes have appeared in the literature, i.e. the nickel(II) complexes of ligand **46** (1,8-bis(2-carbamoylethyl)-4-(2-cyanoethyl)-1,4,8,11-tetraazacyclotetradecane) and of the tetrakispropionamide derivative **47**, abbreviated TETPA. In addition, Dahaoui-Gindrey et al. [277] solved the X-ray structure of the neutral and di-protonated forms of free TETPA.

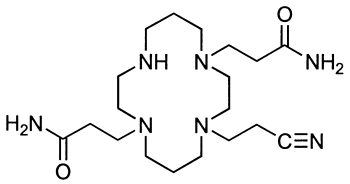

46

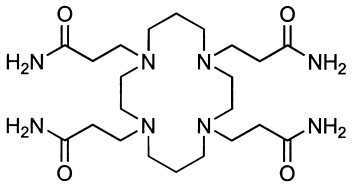

TETPA **47**

4.7.1. Structural characteristics of disubstituted carbamoyl metal complexes

X-ray quality crystals of [Ni(**46**)](ClO$_4$)$_2$ (Fig. 40) have been obtained by hydrolysis and monodealkylation in refluxing water of the corresponding nickel(II) complex of 1,4,8,11-tetrakis(2-cyanoethyl)-1,4,8,11-tetraazacyclotetradecane formed in situ [278]. Yields up to 51% have been reported for reaction times of 18–20 h. Besides [Ni(**46**)](ClO$_4$)$_2$, nickel cyclam and (1,8-bis(2-cyanoethyl)-1,4,8,11-tetraazacyclotetradecane)nickel(II) were isolated as side products in 5 and 15% yields. In [Ni(**46**)](ClO$_4$)$_2$, the nickel ion is hexacoordinated by the four macrocyclic nitrogen atoms and by both carbamoyl oxygen atoms in a *cis*-V arrangement. This configuration is achieved by folding the macrocycle along the N1–Ni–N8 diagonal which gives rise to two sets of three consecutive *gauche* bonds ($g^+g^+g^-$). The torsion angles follow the sequence 47.6, −58.1, 170.1, −72.0, 67.7, 66.1, −160.5, 53.9, −168.2, −179.4, −74.2, 70.3, 76.1 and −152.0 for τ_1–τ_{14}, respectively. The Ni–O distances are statistically equal [2.080(8) Å]. Among the tertiary amine–nickel distances, the Ni–N1 [2.130(8) Å] and Ni–N8 [2.121(8) Å] distances are contracted compared with Ni–N4 [2.174(8) Å] as a result of constrictions imposed by the carbamoylethyl chelate rings. The Ni–N11 bond [2.106(8) Å] is the shortest among the four Ni–N bonds, as expected for a secondary amine.

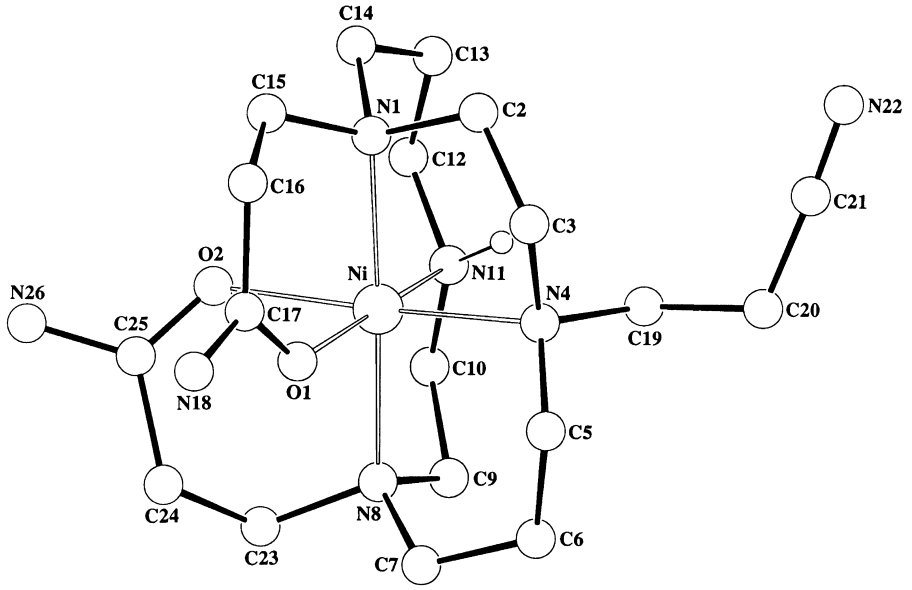

Fig. 40. Molecular view of the $[Ni(\mathbf{46})]^{2+}$ complex [278].

4.7.2. Tetrasubstituted carbamoyl derivatives

4.7.2.1. Protonation scheme of TETPA. The crystal structures of $TETPA.2H_2O$ and $[H_2TETPA](NO_3)_2.2H_2O$ are displayed in Fig. 41 [277]. While statistically equal C–N bond distances are observed for the neutral TETPA ligand [C–N = 1.465(3) Å], the C–N4 bond distances are on average higher than the C–N1 distances in H_2TETPA^{2+} [1.504(2) versus 1.471(6) Å, respectively]. Protonation of N4 was also confirmed by a residual peak of 0.78 $e^{-}Å^{-3}$ at 0.89 Å from N4 in the difference Fourier map. TETPA and H_2TETPA^{2+} exhibit both a (3,4,3,4)-B quadrangular conformation of the macrocyclic scaffold with a methylene group at each corner. The torsion angles within the tetraaza ring are comparable as well as the valence angles, except for N1–C2–C3 [115.8(1) and 113.4(2)° for TETPA and H_2TETPA^{2+}, respectively].

Although two of the four propionamide groups are extended outwards while the two others are folded inwards in both structures, their conformation is markedly different in TETPA and H_2TETPA^{2+}. Fig. 41 clearly shows the reversed conformation of the folded propionamide chains induced by the protonation in H_2TETPA^{2+} with respective C8–C9–C10–O1 [C8–C9–C10–N2] torsion angles of −156.1(2) and −44.2(3)° [22.6(2) and 135.9(2)°] for TETPA and H_2TETPA^{2+}. In TETPA, the N2 nitrogen atom is located 2.938(2) Å away from N4, giving rise to an intramolecular hydrogen bond [HN21···N4 = 2.14(2) Å, N2–HN21···N4 = 153(2)°], whereas a stronger intramolecular hydrogen bond occurs between the O1 oxygen atom and the HN4–N4 donor group [N4···O1 = 2.778(2) Å, HN4···O1 =

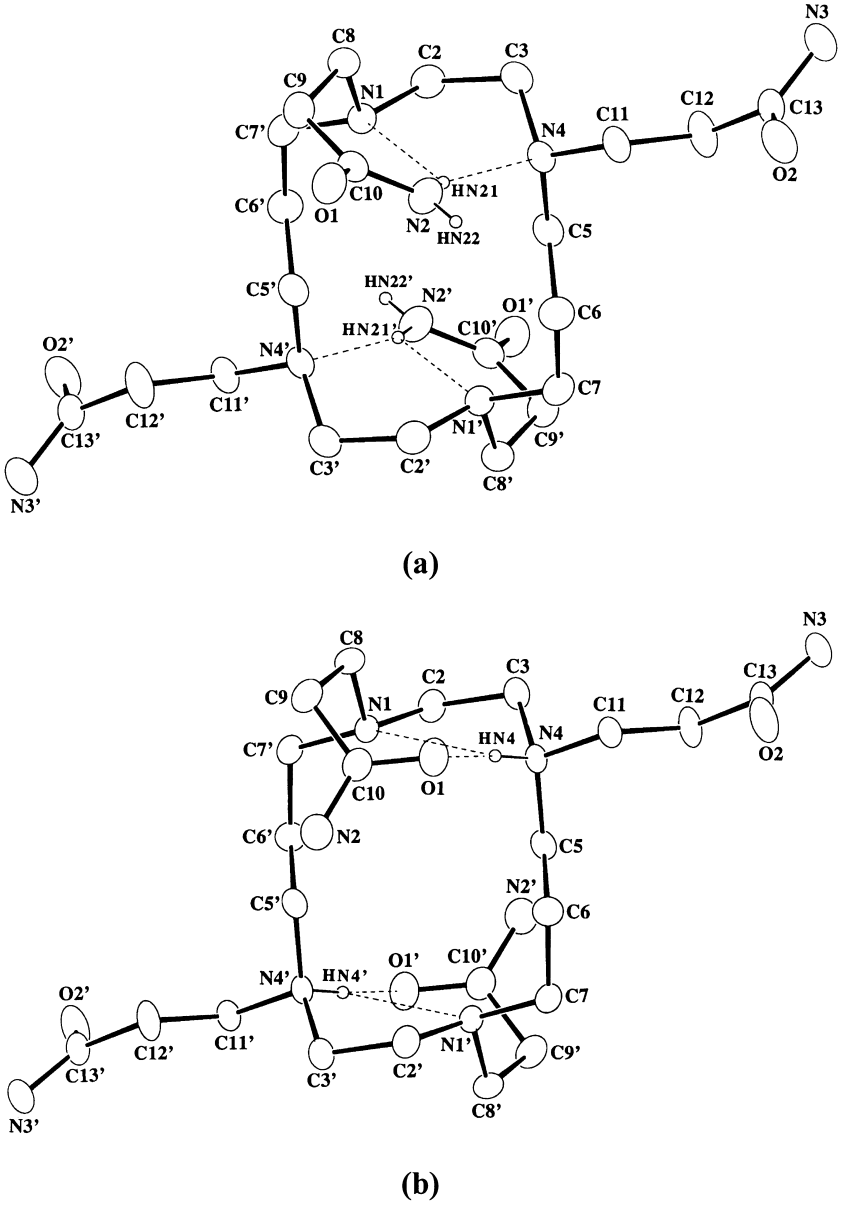

Fig. 41. ORTEP diagrams of (a) TETPA and (b) H_2TETPA^{2+} free ligand with 40% probability thermal ellipsoids for non-hydrogen atoms [277]. Intramolecular hydrogen bonds are indicated by dashed lines.

1.91(2) Å, N4–HN4···O1 = 163(2)°] in H_2TETPA^{2+}. This hydrogen-bonding pattern has an important effect on the conformation of the propionamide group: the C8–C9–C10 valence angle equals 111.3(1) and 117.0(1)°, and the

N1–C8–C9–C10 torsion angles are −56.1(2) and −77.6(2)° for H_2TETPA^{2+} and TETPA, respectively. In the neutral ligand, the proton HN21 is involved in a second intramolecular hydrogen bond with the N1 nitrogen acceptor atom [N2···N1 = 3.110(2) Å, HN21···N1 = 2.49(2) Å, N2–HN21···N1 = 129(1)°], giving rise to an almost symmetrical three-center hydrogen bond. In H_2TETPA^{2+}, the three-center hydrogen bond involving HN4, N1 and O1 [N4···N1 = 2.860(2) Å, HN4···N1 = 2.50(2) Å, N4–HN4···N1 = 104(2)°] is less symmetrical.

Fig. 41 also shows the influence of protonated amine sites on the conformation of the propionamide groups projecting outwards: the major differences occur for the N4–C11–C12 valence angles [116.4(1) and 112.6(2)° for TETPA and H_2TETPA^{2+}, respectively], as well as for the following torsion angles: C3–N4–C11–C12 (Δ = 8°), C5–N4–C11–C12 (Δ = 7°), N4–C11–C12–C13 (Δ = 8.4°), C11–C12–C13–N3 (Δ = 12.4°), and C11–C12–C13–O3 (Δ = 11.1°). These differences might be explained by a different crystal packing and the intermolecular hydrogen bond network which links together the H_2TETPA^{2+} molecules via the extended propionamide chains: this network does not occur for TETPA.

4.7.2.2. Structural characteristics of transition-metal complexes. The preparation of the TETPA nickel complex by hydrolysis of (1,4,8,11-tetrakis(2-cyanoethyl)-1,4,8,11-tetraazacyclotetradecane)nickel(II) has been briefly alluded to by Wainwright [279]. Later, Freeman et al. [278] pointed out some inconsistencies in Wainwright's structural assignment, and showed that a mixture of complexes is actually obtained, as mentioned in Section 4.7.1. In the same article, they proposed an unambiguous synthesis and structural characterization of $[Ni(TETPA)]^{2+}$. Two distinct stereoisomers are formed, depending on the reaction time. Refluxing a 1:1 mixture of $Ni(ClO_4)_2.6H_2O$ and TETPA in water for 2–3 min leads to α-$[Ni(TETPA)](ClO_4)_2$, a green high-spin five-coordinate complex, presumably of *trans*-I stereochemistry. The coordination sphere involves one of the carbamoyl oxygen atoms in addition to the four tertiary amine sites. Longer reaction times (1.5–2 h) afford a bright blue compound, designated as the β form by the authors, which was studied by X-ray diffraction after recrystallization in nitromethane. The octahedral coordination polyhedron consists of the four tertiary nitrogen atoms with Ni–N distances averaging 2.15(1) Å, and two axial oxygen atoms [Ni–O = 2.058(3) and 2.084(3) Å] which belong to carbamoyl groups attached in 1,4-positions. The four propionamide substituents in the β-$[Ni(TETPA)](C1O_4)_2.CH_3NO_2$ complex are arranged in a *trans*-III configuration and the macrocycle adopts an anangular conformation.

5. The use of molecular electrostatic potential in predicting the coordination mode

5.1. Molecular modeling and molecular electrostatic potential

Molecular electrostatic potential (MEP) which enables the prediction of molecular properties (atomic charges, bond orders, free valences, frontier electron densities,

Fukui functions), is a standard tool in quantum chemistry for the analysis of the spatial charge distribution effects on the shape and reactivity of molecules [280–285]. Unlike many other reactivity indices, the MEP is a real physical property which can either be determined experimentally by electron or X-ray diffraction [286–291] or calculated from the wave function [280]. In terms of electrostatics, the MEP is the potential created by the molecule around itself, and is felt by any approaching species. A spatial charge density distribution creates a potential $V(\boldsymbol{r})$:

$$V(\boldsymbol{r}) = \sum_i Z_i/|\boldsymbol{R}_i - \boldsymbol{r}| - \int \rho(\boldsymbol{r}')\, \mathrm{d}\boldsymbol{r}'/|\boldsymbol{r}' - \boldsymbol{r}|, \tag{4}$$

where Z_i is the charge on nucleus i located at $\boldsymbol{R}_i$ and $\rho(\boldsymbol{r}')$ is the electron density at $\boldsymbol{r}'$. This equation contains a summation over the point charges of the nuclei and an integration over the "continuous" negative electron density. The sign of $V(\boldsymbol{r})$ at any point of the molecular region reflects whether the nucleus (+) or electron density (−) is dominant. Calculation of the MEP is straightforward if the molecular wave function or $\rho(\boldsymbol{r}')$ is known. In addition to semi-empirical methods and ab initio calculations of $V(\boldsymbol{r})$ based on self-consistent field (SCF) or near-Hartree–Fock wave functions, there is increasing use of density functional theory (DFT). This approach is based on the Hohenberg–Kohn theorem [292], stating that all the electronic properties of a chemical system in its ground state, including energy, are determined by the electron density. An important feature of the DFT method is that it models the electron correlation. The MEP strongly depends on the conformation of the molecule, since each three-dimensional arrangement of atoms corresponds to a different spatial electron distribution. Thus, it is of fundamental importance to define first the molecular geometry before calculating the electronic properties. Molecular mechanics and dynamics are used to explore the energy hypersurface and to locate the local and global minima. This approach is then validated by experimental results: the geometry of the low-energy conformers is compared with X-ray crystallographic data. Experimental structural features like bond lengths, bond angles and torsion angles must be reproduced by the calculation.

One of the first applications of the MEP was to determine a reactivity map to predict the sites of electrophilic attack on a molecule. An approaching electrophile bearing a positive charge will initially be attracted to the negatively charged sites, and in particular to the points where $V(\boldsymbol{r})$ shows a local minimum. In the following, the MEP will be used to localize the more electronegative sites on the ligand susceptible to attract a positively charged metallic cation in order to rationalize the differences in the observed coordination modes for DOTA, TETA and TETP. However, it should be noted that this calculation does not take into account solvent effects nor changes such as polarization or geometrical distortion occurring when a metal begins to interact with the ligand. The MEP is a static representation of a given charge distribution and thus does not reflect the nature of an approaching species. Because of these inherent limitations, the MEP is most useful as a guide to study the early stages of a reaction where these effects are relatively minor. The strategy adopted to calculate the MEP of cyclen, cyclam, $DOTA^{4-}$, $TETA^{4-}$, $TETP^{4-}$, H_2TETP^{2-} and H_4TETP is described in Refs. [81,293].

5.2. Cyclen and cyclam

The MEP calculated for cyclen and cyclam (plotted in Fig. 42) clearly shows two negatively charged regions of nearly equivalent charge density located on two *trans* secondary amines [294]. The two other nitrogen atoms are surrounded by a much weaker negative electrostatic potential. Qualitatively, the calculated electronegativities faithfully reflect the protonation constant sequence established by potentiometry and NMR spectroscopy.

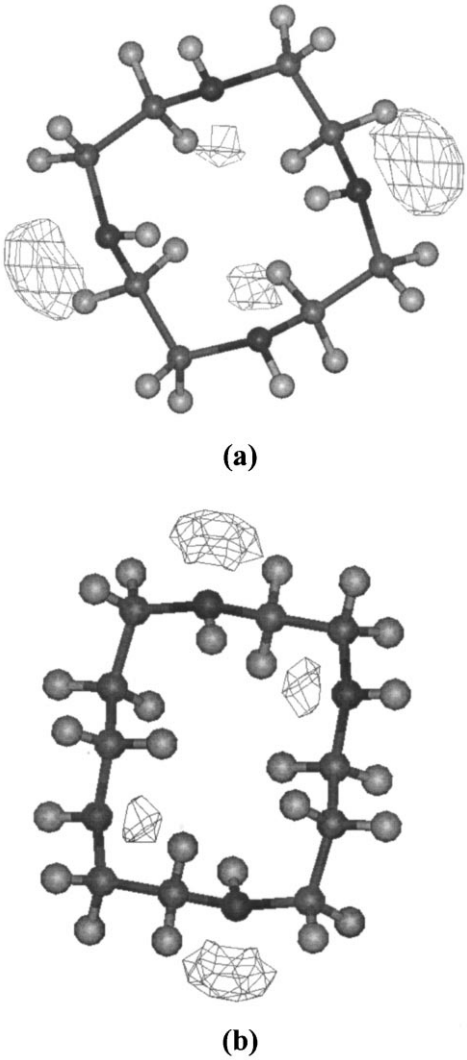

Fig. 42. MEP of (a) cyclen and (b) cyclam. Only the negative potential regions are represented at a contour level of −0.075 a.u. [294].

5.3. DOTA and TETA

In the absence of a crystal structure of the free DOTA ligand, molecular mechanics and molecular dynamics calculations were performed on the (3,3,3,3)-B conformer of the fully deprotonated ligand. The corresponding molecular potential map (Fig. 43) shows that negative surfaces are localized on the four deprotonated carboxylate groups and on one side of the macrocyclic cavity [81]. In agreement with other theoretical studies [255,295], all four nitrogen lone pairs are oriented on one side of the cycle in the most stable conformation of type I, explaining the calculated negative MEP above the central cavity. In contrast, the larger macrocyclic skeleton of TETA adopts a (3,4,3,4)-B most stable conformation, in which the lone pairs of the nitrogen atoms are oriented on both sides of the cycle in an alternate fashion (type-III configuration). The negative MEP surfaces in $TETA^{4-}$ correspond well to the position of the four extended carboxylate groups and the secondary amine lone pairs [81].

The shell-like structure characteristic of most DOTA and TETA complexes can be readily rationalized in terms of the MEP shown in Fig. 43 for $DOTA^{4-}$. They clearly indicate the increased tendency for a cation to bind to nitrogen atoms when moving from TETA to DOTA. The emission spectra of $[Gd(TETA)]^-$ indicates that the lanthanide is primarily coordinated via the carboxylate arms, since the characteristic metal-to-nitrogen band is weaker compared with that of

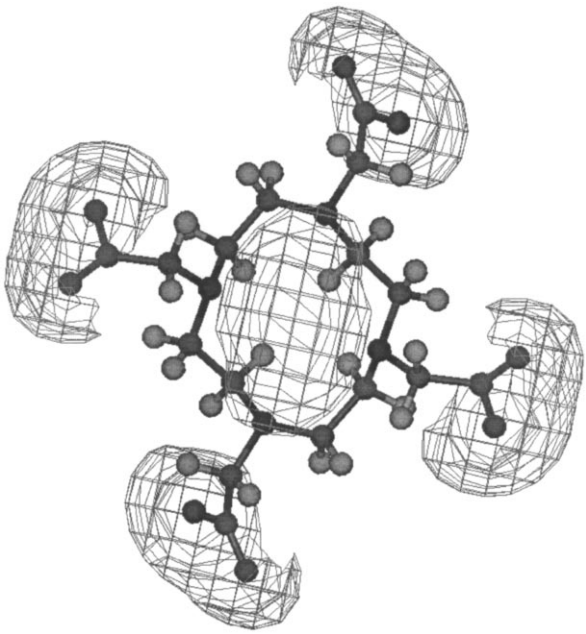

Fig. 43. MEP and molecular structure of $DOTA^{4-}$. Only the negative potential regions are represented at a contour level of -0.40 a.u. [81].

$[GdDOTA]^-$. As the ring size increases, the shell-like structure is retained in $[Tb(TETA)]^-$, as one might expect from the MEP, although the less strained macrocyclic TETA ligand wraps more efficiently around the central Tb^{3+} ion and adopts a biangular (7,7)-F conformation. The rearrangement of the (3,4,3,4)-B conformation into the non-diamond lattice biangular (7,7)-F geometry can be understood by the small strain energy difference and the small induced nuclear displacements [113]. However, a different coordination mode is encountered in $[Mg(H_2TETA)(H_2O)_4]$, which resembles that found in the crystal structure of $[Ce(TETP)]^-$.

5.4. TETP

In order to understand the peculiar coordination mode of TETP, the size of the macrocycle and the length of the appended substituents have to be taken into account. For a shell-type structure in which the metal is embedded in the center of the cavity, DOTA-type ligands generate only thermodynamically favorable five-membered chelate rings. Assuming that TETP adopts a similar topography upon encapsulation of a metal, the appended propionate arms would form four less-favorable six-membered chelate rings in addition to the two generated in the macrocycle. The favorable change in entropy expected for the formation of a cage-type (like $[Gd(DOTA)]^-$) versus an "open" structure, as found in TETP lanthanide complexes, is balanced by a unfavorable enthalpic contribution to the Gibbs free energy of complexation. With this in mind, the critical influence of the protonation state of the TETP ligand on the final coordination geometry is not unexpected. As shown below, the predisposition of the free ligand plays a key role in determining the structure of the complex. Provided that accurate ligand conformations are available, the calculated MEP can predict the complexation mode of the various protonated forms of $TETP^{4-}$.

The calculated electrostatic potential maps for the di- and the neutral tetraprotonated TETP ligand are presented in Fig. 44 [81]. In H_2TETP^{2-} (the predominant form between pH 5.5–10), all four carboxyethyl arms are deprotonated. Two of them, situated in *trans* positions, are folded and create a negative electrostatic field above and below the tetraazacyclotetradecane cycle which prevents a shell-like coordination mode. The remaining carboxylate groups have an extended conformation and point away from the cavity. These results lead to the prediction that each carboxylic group is predisposed to bind a different lanthanide ion if the reaction is carried out at pH values where the diprotonated form predominates. Comparison of the crystal structures of the free ligand H_2TETP^{2-} and of the corresponding cerium complex crystallized at pH 7, i.e. $[Ce(H_2TETP)(H_2O)_3(NO_3)].3H_2O$, fully supports this hypothesis, and most importantly, clearly shows the preorganization of the ligand (Ref. [273] and V. Dahaoui-Gindrey, C. Lecomte, F. Barbette, P. Pullumbi, C. Gros, R. Guilard, unpublished results).

Since two carboxylate arms in *trans* are protonated in H_4TETP, the ligand generates only two negatively charged electrostatic fields, which are located around both extended arms according to the MEP pictured in Fig. 44. Indeed, both protonated

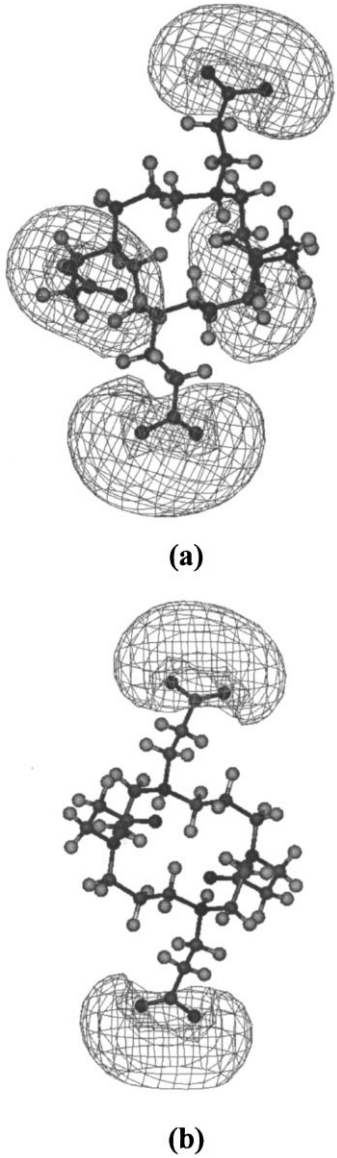

Fig. 44. MEP and molecular structure of (a) H_2TETP^{2-} and (b) H_4TETP (bottom). Only the negative potential regions are represented at a contour level of (a) -0.19 a.u. and (b) -0.05 a.u. [81].

groups in the crystal structure of the free tetraprotonated ligand are folded inwards and hydrogen-bonded. Thus, they do no longer create a negative MEP above and below the cavity [272]. Contrary to H_2TETP^{2-}, only the two extended arms of H_4TETP may coordinate to a metal center, giving rise to a different complexation mode. A second cerium(III) complex, $[Ce(H_2TETP)(H_2O)(OH)].10H_2O$, was iso-

lated during the complexation reaction carried out under slightly more acidic conditions (pH between 3.2 and 4.4) [81]. Its crystal structure confirms the conclusion drawn from the analysis of the MEP and shows that the preorganization of the TETP ligand to bind a Ce^{3+} cation is not restricted to the di-protonated species, but also occurs for the tetra-protonated form.

6. Conclusions

Several nomenclatures are commonly used to describe the polyazamacrocycle's conformations, each of which emphasizes different structural properties. However, neither of the two most widely used classifications proposed by Dale and Bosnich reaches a level of sophistication which accommodates in an univocal way the stereochemical features related to both the ligand and the metal. A major scope of this review is the unambiguous stereochemical description of the free and complexed ligands relying on a standardized notation.

A comprehensive survey of the structural data available for cyclen and cyclam derivatives possessing carboxylic and carbamoyl appended groups has pointed out the versatile modes of coordination. Prediction of the coordination scheme for this class of ligands is still largely a matter of speculation, and collection of more crystallographic data remains of interest for further progress. So far, the majority of the studies have focused on *N*-tetrasubstituted octadentate ligands (based on cyclen and to its complexes with metal ions) of biomedical relevance which favor coordination numbers of eight or more. These studies have outlined the influence of four major factors: (1) the size of the cavity, (2) the length of the appended arms, (3) the steric and electronic requirements inherent to the central cation, and (4) the reaction's pH conditions.

Much less attention has been paid to mono-, bi- and *N*-trisubstituted macrocycles, although they offer a wider range of coordination possibilities as compared to tetrasubstituted analogs. Furthermore, these ligands provide interesting new possibilities in the field of the treatment of waste water contaminated by toxic or radioactive metals and gas purification since they can be attached to an organic or inorganic solid support via relatively simple reactions. The industrial breakthrough of separation processes employing grafted functionalized macrocycles is related to their selectivity. In this respect, structural, thermodynamic and kinetic data are complementary and most useful information which will allow rational design by the molecular engineering of more efficient chelating agents.

Acknowledgements

Dr. Pluton Pullumbi (Centre de Recherche Claude Delorme, Société Air Liquide) is gratefully acknowledged for his contribution. We thank the CNRS, the Université de Bourgogne and the Université Henri Poincaré, Nancy I, for their financial support.

References

[1] J. van Alphen, Recl. Trav. Chim. Pays-Bas 56 (1937) 343.
[2] N.F. Curtis, J. Chem. Soc. (1960) 4409.
[3] M.C. Thompson, D.H. Busch, J. Am. Chem. Soc. 86 (1964) 3561.
[4] H. Stetter, K.H. Mayer, Chem. Ber. 94 (1961) 1410.
[5] B. Bosnich, C.K. Poon, M.L. Tobe, Inorg. Chem. 4 (1965) 1102.
[6] E.K. Barefield, Inorg. Chem. 11 (1972) 2273.
[7] E.K. Barefield, F. Wagner, K.D. Hodges, Inorg. Chem. 15 (1976) 1370.
[8] E.K. Barefield, F. Wagner, A.W. Herlinger, A.R. Dahl, S. Holt, Inorg. Synth. 16 (1976) 220.
[9] J.E. Richman, T.J. Atkins, J. Am. Chem. Soc. 96 (1974) 2268.
[10] G.R. Weisman, D.P. Reed, J. Org. Chem. 61 (1996) 5186.
[11] G.R. Weisman, D.P. Reed, J. Org. Chem. 62 (1997) 4548.
[12] O. Tempkin, P. Kapa, WO Patent no. 97/08157, 1997.
[13] L. Ciszewski, J. Amedio, P. Kapa, A. Kucerovy, G.T. Lee, WO Patent no. 97/05123, 1997.
[14] E. De Clercq, N. Yamamoto, R. Pauwels, M. Baba, D. Schols, H. Nakashima, J. Balzarini, Z.M. Debyser, B.A. Murrer, D. Schwartz, D. Thornton, G. Bridger, S. Fricker, G. Henson, M. Abrams, D. Picker, Proc. Natl. Acad. Sci. USA 89 (1992) 5286.
[15] E. De Clercq, Int. J. Immunother. 8 (1992) 115.
[16] E. De Clercq, N. Yamamoto, R. Pauwels, J. Balzarini, M. Witvrouw, K. De Vreese, Z. Debyser, B. Rosenwirth, P. Peichl, R. Datema, D. Thornton, R. Skerlj, F. Gaul, S. Padmanabhan, G. Bridger, G. Henson, M. Abrams, Antimicrob. Agents Chemother. 38 (1994) 668.
[17] G.J. Bridger, R.T. Skerlj, D. Thornton, S. Padmanabhan, S.A. Martellucci, G.W. Henson, M.J. Abrams, N. Yamamoto, K. De Vreese, R. Pauwels, E. De Clercq, J. Med. Chem. 38 (1995) 366.
[18] T. Koike, E. Kimura, J. Am. Chem. Soc. 113 (1991) 8935.
[19] E. Kimura, M. Shionoya, A. Hoshino, T. Ikeda, Y. Yamada, J. Am. Chem. Soc. 114 (1992) 10134.
[20] R.D. Hancock, in: A.P. Williams, C. Floriani, A.E. Merbach (Eds.), Perspectives in Inorganic Chemistry, VCH, Weinheim, 1992, p. 129.
[21] X. Zhang, R. van Eldik, Inorg. Chem. 34 (1995) 5606.
[22] A. Schrodt, A. Neubrand, R. van Eldik, Inorg. Chem. 36 (1997) 4579.
[23] Y. Nishida, N. Tanaka, S. Takahashi, Chem. Lett. (1993) 411.
[24] Y. Nishida, N. Tanaka, J. Chem. Soc., Dalton Trans. (1994) 2805.
[25] Y. Park, S. Kim, H. Na, J. Korean Chem. Soc. 37 (1993) 648.
[26] J.D. Koola, J.K. Kochi, Inorg. Chem. 26 (1987) 908.
[27] J.F. Kinneary, T.R. Wagler, C.J. Burrows, Tetrahedron Lett. 29 (1988) 877.
[28] W. Nam, R. Ho, J.S. Valentine, J. Am. Chem. Soc. 113 (1991) 7052.
[29] W. Nam, J.S. Valentine, J. Am. Chem. Soc. 115 (1993) 1772.
[30] J.S. Valentine, W. Nam, R.Y.N. Ho, in: D.H.R. Barton (Ed.), The Activation of Dioxygen and Homogeneous Catalytic Oxidation, Plenum, New York, 1993, p. 183.
[31] W. Nam, H.J. Kim, S.H. Kim, R.Y.N. Ho, J.S. Valentine, Inorg. Chem. 35 (1996) 1045.
[32] L.T. Kist, M.J.F. Trujillo, B. Szpoganicz, M.A. Manez, M.G. Basallote, Polyhedron 16 (1997) 3827.
[33] T. Geiger, F.C. Anson, J. Am. Chem. Soc. 103 (1981) 7489.
[34] J. Ouyang, F.C. Anson, J. Electroanal. Chem. 271 (1989) 331.
[35] J. Premkumar, R. Ramaraj, Radiat. Phys. Chem. 49 (1997) 115.
[36] M. Beley, J.P. Collin, R. Ruppert, J.P. Sauvage, J. Am. Chem. Soc. 108 (1986) 7461.
[37] S. Matsuoka, K. Yamamoto, T. Ogata, M. Kusaba, N. Nakashima, E. Fujita, S. Yanagida, J. Am. Chem. Soc. 115 (1993) 601.
[38] M.L. Bowers, F.C. Anson, S.W. Feldberg, J. Electroanal. Chem. 216 (1987) 249.
[39] I. Taniguchi, N. Nakashima, K. Yasukouchi, J. Chem. Soc., Chem. Commun. (1986) 1814.
[40] I. Taniguchi, N. Nakashima, K. Matsushita, K. Yasukouchi, J. Electroanal. Chem. 224 (1987) 199.
[41] H. Li, W.C. Anderson, J.Q. Chambers, D.T. Hobbs, Inorg. Chem. 28 (1989) 863.
[42] L. Ma, B. Zhang, H. Li, J.Q. Chambers, J. Electroanal. Chem. 362 (1993) 201.
[43] L. Ma, H. Li, Electroanalysis 7 (1995) 756.

[44] W. Nam, S.J. Baek, K.A. Lee, B.T. Ahn, J.G. Muller, C.J. Burrows, J.S. Valentine, Inorg. Chem. 35 (1996) 6632.
[45] B. Bosnich, C.K. Poon, M.L. Tobe, Inorg. Chem. 5 (1966) 1514.
[46] M. Kodama, E. Kimura, J. Chem. Soc., Dalton Trans. (1980) 327.
[47] C. Wong, J.A. Switzer, K.P. Balakrishnan, J.F. Endicott, J. Am. Chem. Soc. 102 (1980) 5511.
[48] C. Wong, J.F. Endicott, Inorg. Chem. 20 (1981) 2233.
[49] R. Machida, E. Kimura, M. Kodama, Inorg. Chem. 22 (1983) 2055.
[50] K. Kumar, J.F. Endicott, Inorg. Chem. 23 (1984) 2447.
[51] N. Shinohara, K. Ishii, M. Hirose, J. Chem. Soc., Chem. Commun. (1990) 700.
[52] T. Tsuda, T. Fujiwara, J. Chem. Soc., Chem. Commun. (1992) 1659.
[53] T. Tsuda, T. Fujiwara, J. Chem. Soc., Chem. Commun. (1993) 428.
[54] M. Zhang, R. van Eldik, J.H. Espenson, A. Bakac, Inorg. Chem. 33 (1994) 130.
[55] C.A. Kelly, Q.G. Mulazzani, E.L. Blinn, M.A.J. Rodgers, Inorg. Chem. 35 (1996) 5122.
[56] L. Percelay, V. Louvet, H. Handel, P. Appriou, Anal. Chim. Acta 169 (1985) 325.
[57] L. Percelay, P. Appriou, H. Handel, R. Guglielmetti, Anal. Chim. Acta 209 (1988) 249.
[58] S. Blain, P. Appriou, H. Chaumeil, H. Handel, Anal. Chim. Acta 232 (1990) 331.
[59] J.L. Veuthey, M.A. Bagnoud, W. Haerdi, Int. J. Environ. Anal. Chem. 26 (1986) 157.
[60] M.A. Bagnoud, W. Haerdi, J.L. Veuthey, Chromatographia 29 (1990) 495.
[61] V. Louvet, P. Appriou, H. Handel, Tetrahedron Lett. 23 (1982) 2445.
[62] W. Szczepaniak, K. Kuczynski, React. Polym. 3 (1985) 101.
[63] V. Louvet, H. Handel, P. Appriou, R. Guglielmetti, Eur. Polym. J. 23 (1987) 585.
[64] V. Nicolaus, D. Wöhrle, Angew. Makromol. Chem. 198 (1992) 179.
[65] R.B. Lauffer, Chem. Rev. 87 (1987) 901.
[66] M.F. Tweedle, in: J.C.G. Bünzli, G.R. Choppin (Eds.), Lanthanide Probes in Life, Chemical and Earth Sciences, Elsevier, Amsterdam, 1989, p. 127.
[67] D. Parker, Chem. Soc. Rev. 19 (1990) 271.
[68] S. Jurisson, D. Berning, W. Jia, D. Ma, Chem. Rev. 93 (1993) 1137.
[69] V. Alexander, Chem. Rev. 95 (1995) 273.
[70] R.M. Izatt, R.L. Bruening, B.J. Tarbet, L.D. Griffin, M.L. Bruening, K.E. Krakowiak, J.S. Bradshaw, Pure Appl. Chem. 62 (1990) 1115.
[71] R. Guilard, H. Chollet, P. Guiberteau, P. Cocolios, FR Patent no. 2725382, 1997.
[72] M.F. Loncin, J.F. Desreux, E. Merciny, Inorg. Chem. 25 (1986) 2646.
[73] R.M. Smith, A.E. Martell, R.J. Motekaitis, NIST Critically Selected Stability Constants of Metal Complexes Database, NIST Standard Reference Data no. 46, Gaithersburg, MD, 1997.
[74] D. Doucet, M. Meyer, B. Bonnemain, D. Doyon, J.M. Caille, Enhanced Magnetic Resonance Imaging, Mosky Co, St. Louis, 1989.
[75] M. Meyer, M. Schaefer, B. Bonnemain, Invest. Radiol. 23 (1988) 232.
[76] R.D. Hancock, A.E. Martell, Chem. Rev. 89 (1989) 1875.
[77] A.E. Martell, R.D. Hancock, Metal Complexes in Aqueous Solutions, Plenum Press, New York, 1996.
[78] R.D. Hancock, H. Maumela, A.S. Desousa, Coord. Chem. Rev. 148 (1996) 315.
[79] T.A. Kaden, Top. Curr. Chem. 121 (1984) 157.
[80] A. Riesen, M. Zehnder, T. Kaden, Helv. Chim. Acta 69 (1986) 2067.
[81] C. Lecomte, V. Dahaoui-Gindrey, H. Chollet, C. Gros, A.K. Mishra, F. Barbette, P. Pullumbi, R. Guilard, Inorg. Chem. 36 (1997) 3827.
[82] P.V. Bernhardt, G.A. Lawrance, Coord. Chem. Rev. 104 (1990) 297.
[83] J.S. Bradshaw, K.E. Krakowiak, R.M. Izatt, Aza-Crown Macrocycles, Wiley, New York, 1993.
[84] L.F. Lindoy, The Chemistry of Macrocyclic Ligand Complexes, Cambridge University Press, Cambridge, 1989.
[85] K.P. Wainwright, Coord. Chem. Rev. 166 (1997) 35.
[86] R.D. Shannon, Acta Crystallogr. A 32 (1976) 751.
[87] C.K. Johnson, ORTEP, ORNL Report 3794, 2nd revision, Oak Ridge National Laboratory, Oak Ridge, TN, 1970.
[88] J. Dale, Acta Chem. Scand. 27 (1973) 1115.

[89] J. Dale, Top. Stereochem. 9 (1976) 199.
[90] J. Dale, Isr. J. Chem. 20 (1980) 3.
[91] W. Klyne, V. Prelog, Experientia 16 (1960) 521.
[92] K.B. Wiberg, J. Am. Chem. Soc. 87 (1965) 1070.
[93] M. Bixon, S. Lifson, Tetrahedron 23 (1967) 769.
[94] N.L. Allinger, M.T. Tribble, M.A. Miller, D.H. Wertz, J. Am, Chem. Soc. 93 (1971) 1637.
[95] E.M. Engler, J.D. Andose, P. von R Schleyer, J. Am. Chem. Soc. 95 (1973) 8005.
[96] F.A.L. Anet, T.N. Rawdah, J. Am. Chem. Soc. 100 (1978) 7166.
[97] E.J. Corey, J.C. Bailar, Jr, J. Am. Chem. Soc. 81 (1959) 2620.
[98] J.D. Dunitz, H.M.M. Shearer, Helv. Chim. Acta 43 (1960) 18.
[99] H. Fuhrer, H.H. Günthard, Helv. Chim. Acta 48 (1965) 236.
[100] F.A.L. Anet, A.K. Cheng, J.J. Wagner, J. Am. Chem. Soc. 94 (1972) 9250.
[101] G. Samuel, R. Weiss, Tetrahedron 26 (1970) 3951.
[102] J. Dehli, P. Groth, Acta Chem. Scand. 23 (1969) 587.
[103] L.M. Trefonas, J. Couvillion, J. Am. Chem. Soc. 85 (1963) 3184.
[104] J.D. Dunitz, H.P. Weber, Helv. Chim. Acta 47 (1964) 1138.
[105] T. Sakurai, K. Kobayashi, K. Tsuboyama, S. Tsuboyama, Acta Crystallogr. B 34 (1978) 1144.
[106] M.A. Neuman, E.C. Steiner, F.P. van Remoortere, F.P. Boer, Inorg. Chem. 14 (1975) 734.
[107] P. Groth, Acta Chem. Scand. A 32 (1978) 279.
[108] F.A.L. Anet, J. Krane, J. Dale, K. Daasvatn, P.O. Kristiansen, Acta Chem. Scand. 27 (1973) 3395.
[109] G. Borgen, J. Dale, K. Daasvatn, J. Krane, Acta Chem. Scand. B 34 (1980) 249.
[110] P.R. Raithby, G.P. Shields, F.H. Allen, Acta Crystallogr. B 53 (1997) 241.
[111] F.P. van Remoortere, F.P. Boer, Inorg. Chem. 13 (1974) 2071.
[112] F.P. Boer, M.A. Neuman, F.P. van Remoortere, E.C. Steiner, Inorg. Chem. 13 (1974) 2826.
[113] M.J. Bovill, D.J. Chadwick, I.O. Sutherland, D. Watkin, J. Chem. Soc., Perkin Trans. 2 (1980) 1529.
[114] P. Groth, Acta Chem. Scand. A 30 (1976) 155.
[115] G. Borgen, J. Dale, J. Chem. Soc., Chem. Commun. (1970) 1340.
[116] J. Dale, J. Chem. Soc. (1963) 93.
[117] J.D. Dunitz, E.F. Meyer, Helv. Chim. Acta 48 (1965) 1441.
[118] C.J. Brown, J. Chem. Soc. (1966) 1108.
[119] P. Groth, Acta Chem. Scand. A 32 (1978) 91.
[120] G. Borgen, J. Dale, G. Teien, Acta Chem. Scand. B 33 (1979) 15.
[121] J.H. Reibenspies, Acta Crystallogr. C 48 (1992) 1717.
[122] J.H. Reibenspies, O.P. Anderson, Acta Crystallogr. C 46 (1990) 163.
[123] J.M. Weeks, M.R. Taylor, K.P. Wainwright, J. Chem. Soc., Dalton Trans. (1997) 317.
[124] J. Huskens, D.A. Torres, Z. Kovacs, J.P. André, C.F.G.C. Geraldes, A.D. Sherry, Inorg. Chem. 36 (1997) 1495.
[125] K. Kumar, C.A. Chang, L.C. Francesconi, D.D. Dischino, M.F. Malley, J.Z. Gougoutas, M.F. Tweedle, Inorg. Chem. 33 (1994) 3567.
[126] H.Z. Cai, T.A. Kaden, Helv. Chim. Acta 77 (1994) 383.
[127] C.A. Chang, J. Chem. Soc., Dalton Trans. (1996) 2347.
[128] S.I. Kang, R.S. Ranganathan, J.E. Emswiler, K. Kumar, J.Z. Gougoutas, M.F. Malley, M.F. Tweedle, Inorg. Chem. 32 (1993) 2912.
[129] S. Aime, P.L. Anelli, M. Botta, F. Fedeli, M. Grandi, P. Paoli, F. Uggeri, Inorg. Chem. 31 (1992) 2422.
[130] E. Toth, R. Kiraly, J. Platzek, B. Radüchel, E. Brücher, Inorg. Chim. Acta 249 (1996) 191.
[131] L. Burai, I. Fabian, R. Kiraly, E. Szilagyi, E. Brücher, J. Chem. Soc., Dalton Trans. (1998) 243.
[132] U. Brunner, M. Neuburger, M. Zehnder, T.A. Kaden, Supramol. Chem. 2 (1993) 103.
[133] R.D. Hancock, R.J. Motekaitis, J. Mashishi, I. Cukrowski, J.H. Reibenspies, A.E. Martell, J. Chem. Soc., Perkin Trans. 2 (1996) 1925.
[134] J.F. Desreux, E. Merciny, M.F. Loncin, Inorg. Chem. 20 (1981) 987.
[135] B. Perlmutter-Hayman, Acc. Chem. Res. 19 (1986) 90.
[136] S. Hannongbua, J. Phys. Chem. 100 (1996) 17655.
[137] G.A. Jeffrey, W. Saenger, Hydrogen Bonding in Biological Structures, Springer, New York, 1991.

[138] J.R. Ascenso, R. Delgado, J.J.R. Frausto da Silva, J. Chem. Soc., Perkin Trans. 2 (1985) 781.
[139] C.F.G.C. Geraldes, A.D. Sherry, M. Paula, M.P.M. Marques, M.C. Alpoim, S. Cortes, J. Chem. Soc., Perkin Trans. 2 (1991) 137.
[140] M.F.C. Ladd, D.C. Povey, B.C. Stace, J. Cryst. Mol. Struct. 4 (1974) 313.
[141] S.P. Kasprzyk, R.G. Wilkins, Inorg. Chem. 21 (1982) 3349.
[142] T.A. Kaden, Pure Appl. Chem. 65 (1993) 1477.
[143] T.A. Del Donno, N. Matsumoto, D.H. Busch, N.W. Alcock, J. Chem. Soc., Dalton Trans. (1990) 257.
[144] Y. Iitaka, M. Shina, E. Kimura, Inorg. Chem. 13 (1974) 2886.
[145] J.H. Loehlin, E.B. Fleisher, Acta Crystallogr. B 32 (1976) 3063.
[146] N. Matsumoto, A. Hirano, T. Hara, A. Ohyoshi, J. Chem. Soc., Dalton Trans. (1983) 2405.
[147] K. Kumar, M.F. Tweedle, M.F. Malley, J.Z. Gougoutas, Inorg. Chem. 34 (1995) 6472.
[148] C.A. Chang, L.C. Francesconi, M.F. Malley, K. Kumar, J.Z. Gougoutas, M.F. Tweedle, D.W. Lee, L.J. Wilson, Inorg. Chem. 32 (1993) 3501.
[149] A. Riesen, T.A. Kaden, W. Ritter, H.R. Mäcke, J. Chem. Soc., Chem. Commun. (1989) 460.
[150] A. Riesen, M. Zehnder, T.A. Kaden, Acta Crystallogr. C 47 (1991) 531.
[151] O.P. Anderson, J.H. Reibenspies, Acta Crystallogr. C 52 (1996) 792.
[152] M.P.M. Marques, C.F.G.C. Geraldes, A.D. Sherry, A.E. Merbach, H. Powell, D. Pubanz, S. Aime, M. Botta, J. Alloys Compounds 225 (1995) 303.
[153] J.F. Desreux, in: J.C.G. Bünzli, G.R. Choppin (Eds.), Lanthanide Probes in Life, Chemical and Earth Sciences, Elsevier, Amsterdam, 1989, p. 43.
[154] X. Wang, T. Jin, V. Comblin, A. Lopez-Mut, E. Merciny, J.F. Desreux, Inorg. Chem. 31 (1992) 1095.
[155] K. Kumar, M.F. Tweedle, Inorg. Chem. 32 (1993) 4193.
[156] K. Kumar, T. Jin, X. Wang, J.F. Desreux, M.F. Tweedle, Inorg. Chem. 33 (1994) 3823.
[157] S.L. Wu, W.D. Horrocks, Inorg. Chem. 34 (1995) 3724.
[158] D.D. Dischino, E.J. Delaney, J.E. Emswiler, G.T. Gaughan, J.S. Prasad, S.K. Srivastava, M.F. Tweedle, Inorg. Chem. 30 (1991) 1265.
[159] K. Kumar, C.A. Chang, M.F. Tweedle, Inorg. Chem. 32 (1993) 587.
[160] I. Lazar, D.C. Hrncir, K. Won-Dae, G.E. Kiefer, A.D. Sherry, Inorg. Chem. 31 (1992) 4422.
[161] S. Tsuboyarna, K. Kobayashi, T. Sakurai, K. Tsuboyama, Acta Crystallogr. C 40 (1984) 1178.
[162] M. Ciampolini, M. Micheloni, F. Vizza, F. Zanobini, S. Chimichi, P. Dapporto, J. Chem. Soc., Dalton Trans. (1986) 505.
[163] A.D. Sherry, R.D. Brown, C.F.G.C. Geraldes, S.H. Koenig, K.T. Kuan, M. Spiller, Inorg. Chem. 28 (1989) 620.
[164] M. Li, P.R. Selvin, J. Am. Chem. Soc. 117 (1995) 8132.
[165] J. Platzek, P. Blaszkiewicz, H. Gries, P. Luger, G. Michl, A. Müller-Fahrnow, B. Radüchel, D. Sülzle, Inorg. Chem. 36 (1997) 6086.
[166] K. Kumar, M.F. Tweedle, Pure Appl. Chem. 65 (1993) 515.
[167] R.M. Izatt, K. Pawlak, J.S. Bradshaw, R.L. Bruening, Chem. Rev. 91 (1991) 1721.
[168] R.M. Izatt, K. Pawlak, J.S. Bradshaw, R.L. Bruening, Chem. Rev. 95 (1995) 2529.
[169] A. Riesen, M. Zehnder, T.A. Kaden, J. Chem. Soc., Chem. Commun. (1985) 1336.
[170] A. Riesen, M. Zehnder, T. Kaden, Helv. Chim. Acta 69 (1986) 2074.
[171] J.N. van Niekerk, F.R.L. Schoening, Acta Crystallogr. 6 (1953) 227.
[172] R. Delgado, J.J.R. Frausto da Silva, Talanta 29 (1982) 815.
[173] S. Aime, M. Botta, M. Fasano, M.P.M. Marques, C.F.G.C. Geraldes, D. Pubanz, A.E. Merbach, Inorg. Chem. 36 (1997) 2059.
[174] D. Parker, K. Pulukkody, F.C. Smith, A. Batsanov, J.A.K. Howard, J. Chem. Soc., Dalton Trans. (1994) 689.
[175] V. Jacques, J.F. Desreux, J. Alloys Compounds 213–214 (1994) 286.
[176] S. Aime, A. Barge, F. Benetollo, G. Bombieri, M. Botta, F. Uggeri, Inorg. Chem. 36 (1997) 4287.
[177] M.R. Spirlet, J. Rebizant, J.F. Desreux, M.F. Loncin, Inorg. Chem. 23 (1984) 359.
[178] G. Bombieri, J. Alloys Compounds 249 (1997) 76.

[179] J.P. Dudbost, J.M. Leger, M.H. Langlois, D. Meyer, M. Schaefer, CR Acad. Sci. Paris Ser. 2 312 (1991) 349.
[180] S. Aime, A. Barge, M. Botta, M. Fasano, J.D. Ayala, G. Bombieri, Inorg. Chim. Acta 246 (1996) 423.
[181] K. Micskei, L. Helm, E. Brücher, A.E. Merbach, Inorg. Chem. 32 (1993) 3844.
[182] A.D. Sherry, C.F.G.C. Geraldes, in: J.C.G. Bünzli, G.R. Choppin (Eds.), Lanthanide Probes in Life, Chemical and Earth Sciences, Elsevier, Amsterdam, 1989, p. 93.
[183] C.C. Bryden, C.N. Reilley, J.F. Desreux, Anal. Chem. 53 (1981) 1418.
[184] M.D. Kemple, B.D. Ray, K.B. Lipkowitz, F.G. Prendergast, B.D.N. Rao, J. Am. Chem. Soc. 110 (1988) 8275.
[185] S. Aime, M. Botta, G. Ermondi, E. Terreno, P.L. Anelli, F. Fedeli, F. Uggeri, Inorg. Chem. 35 (1996) 2726.
[186] S. Aime, L. Barbero, M. Botta, G. Ermondi, J. Chem. Soc., Dalton Trans. (1992) 225.
[187] J.C.G. Bünzli, in J.C.G. Bünzli, G.R. Choppin (Eds.), Lanthanide Probes in Life, Chemical and Earth Sciences, Elsevier, Amsterdam, 1989, p. 219.
[188] W.D. Horrocks, D.R. Sudnick, J. Am. Chem. Soc. 101 (1979) 334.
[189] R.S. Dickins, D. Parker, A.S. Sousa, J.A.G. Williams, J. Chem. Soc., Chem. Commun. (1996) 697.
[190] J.L. Kropp, M.W. Windsor, J. Chem. Phys. 39 (1963) 2769.
[191] J.L. Kropp, M.W. Windsor, J. Chem. Phys. 42 (1965) 1599.
[192] J.L. Kropp, M.W. Windsor, J. Chem. Phys. 45 (1966) 761.
[193] Y. Haas, G. Stein, Chem. Phys. Lett. 11 (1971) 143.
[194] Y. Haas, G. Stein, J. Phys. Chem. 75 (1971) 3677.
[195] C.C. Bryden, C.N. Reilley, Anal. Chem. 54 (1982) 610.
[196] M. Albin, W.D. Horrocks, F.J. Liotta, Chem. Phys. Lett. 85 (1982) 61.
[197] H.G. Brittain, J.F. Desreux, Inorg. Chem. 23 (1984) 4459.
[198] S. Aime, M. Botta, G. Ermondi, Inorg. Chem. 31 (1992) 4291.
[199] S. Hoeft, K. Roth, Chem. Ber. 126 (1993) 869.
[200] J.F. Desreux, Inorg. Chem. 19 (1980) 1319.
[201] V. Jacques, J.F. Desreux, Inorg. Chem. 33 (1994) 4048.
[202] C.J. Broan, J.P.L. Cox, A.S. Craig, R. Kataky, D. Parker, A. Harrison, A.M. Randall, G. Ferguson, J. Chem. Soc., Perkin Trans. 2 (1991) 87.
[203] S. Aime, M. Botta, G. Ermondi, F. Fedeli, F. Uggeri, Inorg. Chem. 31 (1992) 1100.
[204] E.J. Billo, Inorg. Nucl. Chem. Lett. 10 (1974) 613.
[205] R.D. Hancock, in: A.P. Williams, C. Floriani, A.E. Merbach (Eds.), Perspectives in Inorganic Chemistry, VCH, Weinheim, 1992, p. 129.
[206] R.D. Hancock, A.E. Martell, Adv. Inorg. Chem. 42 (1995) 89.
[207] H. Maumela, R.D. Hancock, L. Carlton, J.H. Reibenspies, K.P. Wainwright, J. Am. Chem. Soc. 117 (1995) 6698.
[208] S. Amin, J.R. Morrow, C.H. Lake, M.R. Churchill, Angew. Chem., Int. Ed. Engl. 33 (1994) 773.
[209] S. Amin, D.A. Voss, W.D. Horrocks, C.H. Lake, M.R. Churchill, J.R. Morrow, Inorg. Chem. 34 (1995) 3294.
[210] L. Carlton, R.D. Hancock, H. Maumela, K.P. Wainwright, J. Chem. Soc., Chem. Commun. (1994) 1007.
[211] J.C. Bailar, J. Inorg. Nucl. Chem. 8 (1958) 165.
[212] D. Parker, J.A. Williams, J. Chem. Soc., Dalton Trans. (1996) 3613.
[213] R.S. Dickins, J.A.K. Howard, C.W. Lehmann, J. Moloney, D. Parker, R.D. Peacock, Angew. Chem., Int. Ed. Engl. 36 (1997) 521.
[214] R.S. Dickins, J.A.K. Howard, J.M. Moloney, D. Parker, R.D. Peacock, G. Siligardi, Chem. Commun. (1997) 1747.
[215] A. Beeby, R.S. Dickins, S. Faulkner, D. Parker, J.A.G. Williams, Chem. Commun. (1997) 1401.
[216] D. Parker, J.A.G. Williams, J. Chem. Soc., Perkin Trans. 2 (1995) 1305.
[217] A. Beeby, D. Parker, J.A.G. Williams, J. Chem. Soc., Perkin Trans. 2 (1996) 1565.
[218] D. Parker, J.A.G. Williams, J. Chem. Soc., Perkin Trans. 2 (1996) 1581.
[219] D. Parker, K. Senanayake, J.A.G. Williams, J. Chem. Soc., Chem. Commun. (1997) 1777.

[220] D. Parker, J.A.G. Williams, J. Chem. Soc., Chem. Commun. (1998) 245.
[221] H. Tsukube, Y. Mizutani, S. Shinoda, M. Tadokoro, K. Hori, Tetrahedron Lett. 38 (1997) 5021.
[222] J.H. Forsberg, R.M. Delaney, Q. Zhao, G. Harakas, R. Chandran, Inorg. Chem. 34 (1995) 3705.
[223] N.L. Allinger, J. Am. Chem. Soc. 99 (1977) 8127.
[224] J.R. Morrow, S. Amin, C.H. Lake, M.R. Churchill, Inorg. Chem. 32 (1993) 4566.
[225] G.H. Robinson, S.A. Sangokoya, W.T. Pennington, M.F. Self, R.D. Rogers, J. Coord. Chem. 19 (1989) 287.
[226] C. Nave, M.R. Truter, J. Chem. Soc., Dalton Trans. (1974) 2351.
[227] S. Subramanian, M.J. Zaworotko, Can. J. Chem. 71 (1993) 433.
[228] S. Subramanian, M.J. Zaworotko, J. Chem. Soc., Chem. Commun. (1993) 952.
[229] M. Studer, A. Riesen, T.A. Kaden, Helv. Chim. Acta 72 (1989) 1253.
[230] G. Bandoli, A. Dolmella, S. Gatto, J. Cryst. Spectrosc. Res. 23 (1993) 755.
[231] I.K. Becker, R. Mattes, Z. Anorg. Allg. Chem. 622 (1996) 105.
[232] S. Subramanian, M.J. Zaworotko, Can. J. Chem. 73 (1995) 414.
[233] J.M. Harrowfield, H. Miyamae, T.M. Shand, B.W. Skelton, A.A. Soudi, A.H. White, Aust. J. Chem. 49 (1996) 1051.
[234] A.J. Blake, J.A. Greig, M. Schröder, Acta Crystallogr. C 46 (1990) 322.
[235] M. Micheloni, A. Sabbatini, P. Paoletti, J. Chem. Soc., Perkin Trans. 2 (1978) 828.
[236] V.J. Thöm, G.D. Hosken, R.D. Hancock, Inorg. Chem. 24 (1985) 3378.
[237] M. Studer, T.A. Kaden, Helv. Chim. Acta 69 (1986) 2081.
[238] R.J. Motekaitis, B.E. Rogers, D.E. Reichert, A.E. Martell, M.J. Welch, Inorg. Chem. 35 (1996) 3821.
[239] M. Studer, A. Riesen, T.A. Kaden, Acta Crystallogr. C 46 (1990) 741.
[240] E.K. Barefield, K.A. Foster, G.M. Freeman, K.D. Hodges, Inorg. Chem. 25 (1986) 4663.
[241] D. Tschudin, A. Basak, T.A. Kaden, Helv. Chim. Acta 71 (1988) 100.
[242] J. Xu, S. Ni, Y. Lin, Inorg. Chem. 27 (1988) 4651.
[243] Y. Lin, S. Ni, J. Xu, Jiegou Huaxue 4 (1985) 229.
[244] K. Panneerselvam, T. Lu, T. Chi, C. Chung, Y. Chen, K. Kwan, Acta Crystallogr. C 54 (1998) 25.
[245] R. Clay, J. Murray-Rust, P. Murray-Rust, J. Chem. Soc., Dalton Trans. (1979) 1135.
[246] Y. Lin, S. Ni, J. Xu, Jiegou Huaxue 5 (1986) 5.
[247] Y. Lin, S. Ni, J. Xu, Jiegou Huaxue 7 (1988) 107.
[248] I.M. Helps, D. Parker, J. Chapman, G. Ferguson, J. Chem. Soc., Chem. Commun. (1988) 1094.
[249] J. Chapman, G. Ferguson, J.F. Gallagher, M.C. Jennings, D. Parker, J. Chem. Soc., Dalton Trans. (1992) 345.
[250] J. Xu, S. Ni, Y. Lin, Inorg. Chim. Acta 111 (1986) 61.
[251] V.K. Belsky, N.R. Streltsova, E.N. Kuzmina, A.Y. Nazarenko, Polyhedron 12 (1993) 831.
[252] L. Chen, L.K. Thompson, J.N. Bridson, J. Xu, S. Ni, R. Guo, Can. J. Chem. 71 (1993) 1805.
[253] D.C. Ware, D.M. Tonei, L.J. Baker, P.J. Brothers, G.R. Clark, Chem. Commun. (1996) 1303.
[254] Y. Lin, X. Ye, B. Hao, L. Song, J. Xu, S. Ni, Jiegou Huaxue 15 (1996) 362.
[255] V.J. Thöm, C.C. Fox, J.C.A. Boeyens, R.D. Hancock, J. Am. Chem. Soc. 106 (1984) 5947.
[256] R.D. Hancock, Prog. Inorg. Chem. 37 (1989) 187.
[257] R.D. Hancock, Acc. Chem. Res. 23 (1990) 253.
[258] Y. Lin, L. Chen, S. Ni, J. Xu, Jiegou Huaxue 14 (1995) 44.
[259] M.R. Maurya, E.J. Zaluzec, S.F. Pavkovic, A.W. Herlinger, Inorg. Chem. 30 (1991) 3657.
[260] M.R. Spirlet, J. Rebizant, P.P. Barthélemy, J.F. Desreux, J. Chem. Soc., Dalton Trans. (1991) 2477.
[261] H. Häfliger, T.A. Kaden, Helv. Chim. Acta 62 (1979) 683.
[262] H. Stetter, W. Frank, Angew. Chem., Int. Ed. Engl. 15 (1976) 686.
[263] A. Riesen, M. Zehnder, T.A. Kaden, Acta Crystallogr. C 44 (1988) 1740.
[264] M.K. Moi, M. Yanuck, S.V. Deshpande, H. Hope, S.J. DeNardo, C.F. Meares, Inorg. Chem. 26 (1987) 3458.
[265] C.M. Madeyski, J.P. Michael, R.D. Hancock, Inorg. Chem. 23 (1984) 1487.
[266] E. Kimura, T. Koike, M. Yamaoka, M. Kodama, J. Chem. Soc., Chem. Commun. (1985) 1341.
[267] M. Ali, I. Zilbermann, H. Cohen, A.I. Shames, D. Meyerstein, Inorg. Chem. 35 (1996) 5127.
[268] M.R. Spirlet, J. Rebizant, M.F. Loncin, J.F. Desreux, Inorg. Chem. 23 (1984) 4278.

[269] CRC Handbook of Chemistry and Physics, CRC Press, Boca Raton, FL, 1983/1984.
[270] J.F. Desreux, M.F. Loncin, Inorg. Chem. 25 (1986) 69.
[271] D.L. Kepert, Inorganic Chemistry Concepts, vol. 6, Springer, Heidelberg, 1982.
[272] V. Dahaoui-Gindrey, C. Lecomte, H. Chollet, A.K. Mishra, C. Mehadji, R. Guilard, New J. Chem. 19 (1995) 839.
[273] V. Dahaoui-Gindrey, S. Dahaoui, C. Lecomte, F. Barbette, R. Guilard, Acta Crystallogr. C 53 (1997) 1797.
[274] V. Bulach, D. Mandon, J. Fischer, R. Weiss, Inorg. Chim. Acta 210 (1993) 7.
[275] G.A. Jeffrey, J. Mitra, Acta Crystallogr. B 39 (1983) 469.
[276] A. Kurganov, V.A. Davankov, Inorg. Nucl. Chem. Lett. 12 (1976) 743.
[277] V. Dahaoui-Gindrey, C. Lecomte, C. Gros, A.K. Mishra, R. Guilard, New J. Chem. 19 (1995) 831.
[278] G.M. Freeman, E.K. Barefield, D.G. van Derveer, Inorg. Chem. 23 (1984) 3092.
[279] K.P. Wainwright, J. Chem. Soc., Dalton Trans. (1980) 2117.
[280] P. Politzer, D.G. Truhlar, Plenum, New York 1981.
[281] J. Tomasi, R. Bonaccorsi, R. Cammi, in: Z. Maksic (Ed.), Theoretical Models of Chemical Bonding, vol. 4, Springer, New York, 1991, p. 229.
[282] J.S. Murray, T. Brinck, M.E. Grice, P. Politzer, J. Mol. Struct. 256 (1992) 29.
[283] J. Korchowiec, H. Gerwens, K. Jug, Chem. Phys. Lett. 222 (1994) 58.
[284] P.C. Mishra, A. Kumar, Top. Curr. Chem. 174 (1995) 27.
[285] G. Naray-Szabo, G.G. Ferenczy, Chem. Rev. 95 (1995) 829.
[286] N.E. Ghermani, N. Bouhmaida, C. Lecomte, Acta Crystallogr. A 49 (1993) 781.
[287] N.E. Ghermani, C. Lecomte, N. Bouhmaida, Z. Naturforsch. A 48 (1993) 91.
[288] N.E. Ghermani, N. Bouhmaida, C. Lecomte, A.L. Papet, A. Marsura, J. Phys. Chem. 98 (1994) 6287.
[289] C. Lecomte, Adv. Mol. Struct. Res. 1 (1995) 261.
[290] N. Bouhmaida, N.E. Ghermani, C. Lecomte, A. Thalal, Acta Crystallogr. A 53 (1997) 556.
[291] G. Royal, V. Dahaoui-Gindrey, S. Dahaoui, A. Tabard, R. Guilard, P. Pullumbi, C. Lecomte, Eur. J. Org. Chem. (1998) 1971.
[292] P. Hohenberg, W. Kohn, Phys. Rev. B 136 (1964) 864.
[293] C. Mellot, J. Lignières, P. Pullumbi, R. Guilard, Rev. Inst. Fr. Petrole 51 (1996) 81.
[294] S. Brandès, S. Lacour, F. Denat, P. Pullumbi, R. Guilard, J. Chem. Soc., Perkin Trans. 1 (1998) 639.
[295] K.R. Adam, M. Antolovich, L.G. Brigden, L.F. Lindoy, J. Am. Chem. Soc. 113 (1991) 3346.